PARITY MEASUREMENTS IN OPTICAL INTERFEROMETRY AND TESTS OF QUANTUM MECHANICS

By

Adil Benmoussa

A dissertation submitted to the Graduate Faculty in Physics in partial fulfillment of the requirements for the degree of

DOCTOR OF PHILOSOPHY

at

THE CITY UNIVERSITY OF NEW YORK

2005

INFORMATION TO USERS

The quality of this reproduction is dependent upon the quality of the copy submitted. Broken or indistinct print, colored or poor quality illustrations and photographs, print bleed-through, substandard margins, and improper alignment can adversely affect reproduction.

In the unlikely event that the author did not send a complete manuscript and there are missing pages, these will be noted. Also, if unauthorized copyright material had to be removed, a note will indicate the deletion.

ProQuest Information and Learning Company
300 North Zeeb Road
P.O. Box 1346
Ann Arbor, MI 48106-1346

This manuscript has been read and accepted for the Graduate Faculty in Physics in satisfaction of the dissertation requirement for the degree of Doctor of Philosphy.

April 8, 2005
Date

Professor C Christopher Gerry
Chair of Examining Committee

4/8/2005
Date

Professor Sultan Catto
Executive Officer

Professor Mark Hillery

Professor Janŏs Bergou

Professor Ramzi Khuri
Supervisory Committee

THE CITY UNIVERSITY OF NEW YORK

Abstract

PARITY MEASUREMENTS IN OPTICAL INTERFEROMETRY AND TESTS OF QUANTUM MECHANICS

by

Adil Benmoussa

Advisor: Christopher C Gerry

We study the use of parity in context of high resolution interferometry. Maximally entangled states play a crucial role in the applications of the Heisenberg-limited interferometry; it enhances the sensitivity of the detection of the gravitational waves. Interferometry with maximally entangled states cannot be performed by simply subtracting the output photocounts as in standard quantum interferometry. Instead, one must perform parity measurements on only one of the output beams. We use the same technique to show that with twin Fock input states in a Mach-Zehnder interferometer, the phase sensitivity approaches the Heisenberg limit for large photon number. Then we study the generations of maximally entangled states and states of superposition of maximally entangled states using nonlinear interferometry. Nonlinear interferometers are Mach-Zehnder interferometers with Kerr media in either one or both arms. We refer to these devices, respectively, as the asymmetric and symmetric nonlinear interferometers. In the asymmetric case, with one input mode in the vacuum, it is possible to generate maximally entangled states or superpositions of such states. We consider the device as a resource of entangled states for applications to Heisenberg-limited interferometry. We also consider the nonlinear four-wave mixer as a resource for superpositions of only even input states. Considering both even coherent states and squeezed vacuum states as inputs, we study their applications to high resolution interferometry.

We then study parity measurements. We show that the symmetric nonlinear

interferometer, with the vacuum state in one input mode, may be used to perform parity measurements. The same device is shown to produce, with an input coherent state and upon projective measurements, even or odd coherent states, examples of the Schrödinger cat states. We also study quantum non-demolition parity measurements using cross-Kerr medium. We show that one can determine parity of a state without destroying it, using cross-Kerr medium along with homodying measurements. With the same technique we can construct some Schrödinger cat states.

We also study parity measurements to test quantum mechanics against the local realistic theories. To that end, we propose an optical realization of the Greenberger, Horne, Zeilinger (GHZ) state. The optical GHZ states in this case are three-mode entangled coherent states and the relevant observable used to perform test of quantum mechanics against local realistic theories is photon number parity. The amplitudes of the coherent states need by mescoscopic if significant losses are involved by may be macroscopic if losses are minimal. We propose a method of generating the required GHZ state that amounts to an extension of a proposal previously discussed by C.C. Gerry (Phys. Rev A 59, 4095 (1999)) for generating macroscopic superposition states of traveling wave fields.

Acknowledgements

First and foremost, I would like to thank my supervisor, Professor Christopher C Gerry, for his patient guidance throughout both my undergraduate and my Ph.D. studies, and his tremendous help in providing many valuable comments and suggestions while drafting this thesis.

My thanks go to Professor Sultan Catto for all his help as the executive officer at the Physics Department. My special thanks and appreciation go to Professor Mark Hillery for teaching me quantum mechanics and quantum information. My thanks go to Professor Janŏs Bergou and Professor Ramzi Khuri for their help as members of my thesis committee. Also I would like to thank Dr. Rich Campos.

I would like to thank my parents for their support. I am also grateful to my wife for her patience and encouragements during all the period of my graduate studies. Finally, I would like to express my appreciation to PSCUNY, AGEP, LSAMP, CUNY GK-12 Fellowship project, and MAGNET Dissertation Fellowship for their financial support.

Table of Contents

List of Figures

Chapter 1

Introduction

In this thesis, we study the use of parity measurements and its applications. In the context of a single-mode field the parity operator has the form $(-1)^{\hat{N}}$, where $\hat{N}$ is the number operator for that mode. This operator is bounded and oscillates rapidly between -1 and 1, and has no classical counterpart. The parity of the electromagnetic fields, as well as other systems, is a useful observable for various applications of a fundamental and practical importance.

One of the potential uses of parity is in the area of high-resolution quantum optical interferometry. Interferometer usage ranges from measuring density in a fluid to detecting gravity waves. Gravitational waves interactions with terrestrial detectors are of the order of 10^{-19} cm. Small fluctuations disturb the accuracy of the measurements and can obscure the whole signal. With a laser beam of average photon number $\bar{N}$, one can detect phase shifts with an uncertainty up to $\Delta\varphi_{SQL} = 1/\sqrt{\bar{N}}$, which is the standard quantum limit, in an ordinary Mach-Zehnder interferometer. Using nonclassical light, we can improve the sensitivity of the interferometer up to $\Delta\varphi_{HL} = 1/\bar{N}$, which is the so-called Heisenberg quantum limit, the ultimate limit

allowed by quantum mechanics assuming that the phase shifts are linear. Caves suggested a scheme using squeezed light that could improve the sensitivity to $e^{-r}/\bar{N}$, where r is the squeezing parameter. In the present work we study new approaches using maximally entangled states, superposition of maximally entangled states and twin Fock states, along with parity measurements to obtain Heisenberg-limited sensitivities.

Construction of the maximally entangled states is interesting in its own right. Maximally entangled states of arbitrary numbers of photons are not easy to construct with linear optics only. With the state reduction technique, it is possible to construct maximally entangled states for low photon numbers, but it becomes more problematic for larger numbers of photon. Nonlinear optics is very promising when it comes for the preparation of nonclassical light. In this thesis we focus our attention mainly on the use of the nonlinear optics with or without state reduction to construct the desired states.

In a modified version of Mach-Zehnder interferometer with a Kerr medium in one arm, which we refer to as the asymmetric nonlinear interferometer, we can produce, *deterministically*, the maximally entangled states for any photon number state should we have Fock states available.

Currently, we do not have Fock states available for arbitrary numbers of photons. As an alternative, we can try using coherent states, which are available from stabilized lasers. As a matter of fact, using numerical computation we show that the uncertainty of the phase shift reaches the Heisenberg quantum limit for just an input coherent state in the asymmetric interferometer before it is injected in the main interferometer.

In a different setup, we propose a scheme involving nonlinear four-wave mixing in a

modified version of a Mach-Zehnder interferometer to construct maximally entangled states. The suggested scheme requests even numbered photon input states, so we consider as inputs the even coherent states and the squeezed vacuum states. The states right after the four-wave mixer are superposition of maximally entangled states, in both cases. We show that the phase uncertainty reaches the Heisenberg limit of sensitivity.

In another setup, we consider the twin Fock states as input states for a Mach-Zehnder Interferometer. Holland and Burnett studied the uncertainties in optical phase measurements obtained in Mach-Zehnder interferometer under the assumption of twin Fock states input. By studying the phase-difference distribution for the states inside the Mach-Zehnder interferometer, these authors concluded that the uncertainty in the measurement of the phase difference approaches the Heisenberg limit asymptotically as the number of the injected photons passing through the interferometer becomes large. Their approach was based on measuring the photocounting. In the present work we take a different approach by measuring the parity operator at one of the output beam.

These proposals for the use of parity measurements of the parity of optical fields obviously demand a convenient way for its measurement. Parity measurements can be done, in principle, by counting the photon number and raise (-1) to that power. This method requires efficient detectors that distinguish the photoncount at a single photon. Noting that parity measurements can be done without knowing exactly what is the photon number, it suffices to determine either the photon number is odd or even. All we need is to resolve the parity. To that end, we consider a symmetric nonlinear interferometer, a device suited for resolving the parity of the signal light

without the requirement of detectors of 100% efficiency. Another possible approach to the measurement of parity is that of quantum non-demolition. This approach utilizes a two-mode cross-Kerr interaction. Both nonlinear interferometer and cross-Kerr interaction require a large nonlinear susceptibility.

We also use the parity measurement for tests of the local realistic theories against quantum mechanics. To that goal, we propose a method for generating an optical meso/ macro-scopic traveling-wave Greenberger-Horne-Zeilinger states. The proposal is an extension of a method studied by Gerry. Taken into account the interactions of the environment, we show that these states are still capable of demonstrating the clash between local realistic theories and quantum mechanics.

The organization of this thesis is as follows. In Chap. 2 we review standard quantum interferometry. We start with interferometric measurement in a regular Mach-Zehnder interferometer with a coherent state as an input state in one mode and the other input is left with the vacuum and obtain the standard quantum limit for the phase shift uncertainty. Then we show an improvement in the phase shift uncertainty measurement using a squeezed vacuum instead of the vacuum. Also we study the phase shift distribution inside the interferometer and compare it to its counterpart in the standard quantum limit. In Chap. 3 we study interferometry using maximally entangled states inside a Mach-Zehnder interferometer, and we show that the phase uncertainty reaches the Heisenberg limit of uncertainty if parity is the measured observable. Then we extend our discussion to include certain superposition states of maximally entangled states. Next, in Chap. 4, we suggest schemes to construct maximally entangled states and states of superposition of maximally entangled states. In Chap. 5 we examine the use of twin Fock states as input states for

a Mach-Zehnder interferometer. Again using parity as the observable, we show how this states also improve the phase shift uncertainty measurements to the ultimate phase sensitivity. In Chap. 6 we consider possible schemes for measurement of parity. First we consider the symmetric nonlinear interferometer as an alternative to precise detection of photon numbers. Then we consider quantum measurements of parity using a cross-Kerr medium. Next in Chap. 7, we propose an optical realization of the GHZ state to perform test of quantum mechanics against realistic theories using the photon number parity as the relevant observable quantity. We conclude our thesis in Chap. 8 and in Appendix A we review the beam splitter transformations using the angular momentum Schwinger realization. Appendix B is a brief review of the quantum phase operator. Finally, in Appendix C we derive the expectation value of the parity operator as function of time taking into account the dissipative interactions of the environment using the master equation approach.

Chapter 2

Standard Quantum Interferometry

In this chapter we review standard quantum limited interferometry mainly using coherent light. Coherent states of light are the most classical-like of all quantum states of light and still on the quantum classical border. First, we describe briefly the Mach-Zehnder interferometer (MZI) and calculate the phase shift uncertainty. It is well known that there is an association between the phase distribution and the phase sensitivity [1], so we describe the phase shift distribution inside the interferometer. Nonclassical light can improve the sensitivity of the inteferomter [2]. For instance, squeezed vacuum state can improve the phase shift sensitivity when injected simultaneously with coherent state in the inputs of an MZI, as we shall see in details in the second section.

2.1 Standard Quantum Interferometry

An MZI consists of two beam splitters and a phase shifter (PS). In Fig. 2.1 we depict a schematic of an MZI, where BS1 and BS2 refer to the two 50:50 beam splitters of $\hat{J}_1$ type. Using the Schwinger realization discussed in Appendix A, the unitary transformation associated with BS1 and BS2 can be described with operators of the

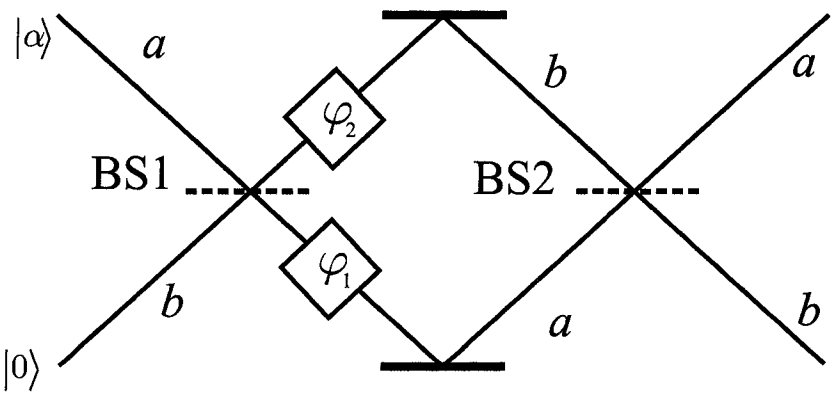

Figure 2.1: Mach-Zehnder interferometer: light is injected at the input ports, photomixes at the beam splitter BS1, experiences a phase shift φ, and meets again at the beam splitter BS2 before it exits at the output ports. Here the input state is $|\text{in}\rangle = |\alpha\rangle_a|0\rangle_b$, a coherent state is injected at the input port a and vacuum in the input port b.

form

$$\hat{U}_{\text{BS1}} = \hat{U}_{\text{BS2}} = \exp\left(i\pi\hat{J}_1/2\right), \tag{2.1.1}$$

where

$$\hat{J}_1 = (\hat{a}^\dagger\hat{b} + \hat{a}\hat{b}^\dagger)/2, \tag{2.1.2}$$

as defined in Appendix A, where $\hat{a}$ is the creation operator associated with the arm a, and $\hat{b}$ with arm b.

We are interested in measuring an observable that is sensible to the phase difference φ between the two arms, where it is clear that $\varphi = \varphi_2 - \varphi_1$. In the standard interferometry, one does phase measurements by photocounting the output beams, subtracting, and averaging. This method amounts to measuring $\left\langle \hat{J}_3 \right\rangle_{\text{out}}$, where $\hat{J}_3$ is defined in Eq. A.0.17. For the simplest case, let us assume that we inject a coherent

state $|\alpha\rangle_a$, of average photon number $\bar{N} = |\alpha|^2$, in the a mode and leave the b mode with the vacuum as displayed in Fig. 2.1. The two-mode input state is of the form

$$|\text{in}\rangle = |\alpha\rangle_a|0\rangle_b, \tag{2.1.3}$$

where a and b refer to the modes. It is convenient to rewrite the input state in Eq. 2.1.3 as

$$|\text{in}\rangle = \hat{D}_a(\alpha)|0\rangle_a|0\rangle_b, \tag{2.1.4}$$

where

$$\hat{D}_a(\alpha) = e^{\alpha\hat{a}^\dagger - \alpha^*\hat{a}}, \tag{2.1.5}$$

is the Glauber displacement operator. The beam splitter BS1 causes the transformation

$$\begin{aligned}
\hat{U}_{\text{BS1}}|\text{in}\rangle &= \exp\left(i\pi\hat{J}_1/2\right)\hat{D}(\alpha,\hat{a})|0\rangle_a|0\rangle_b \\
&= \exp\left(i\pi\hat{J}_1/2\right)\hat{D}(\alpha,\hat{a})\exp\left(-i\pi\hat{J}_1/2\right)\exp\left(i\pi\hat{J}_1/2\right)|0\rangle_a|0\rangle_b \\
&= \hat{D}_a\left(\frac{\alpha}{\sqrt{2}}\right)\hat{D}_b\left(\frac{i\alpha}{\sqrt{2}}\right)|0\rangle_a|0\rangle_b \qquad (2.1.6) \\
&= \left|\frac{\alpha}{\sqrt{2}}\right\rangle_a\left|\frac{i\alpha}{\sqrt{2}}\right\rangle_b, \qquad (2.1.7)
\end{aligned}$$

where Eq. A.0.28 has been used to derive Eq. 2.1.6. State in Eq. 2.1.7 is a two-mode separable state. This is another indication of the fact that coherent states are nearly classical. In fact, coherent states are classical-like quantum states; they are the most classical of all pure states of light. Notice that mode b picks a phase shift, i, and that is due to the type of the beam splitter, BS1. Boxes containing φ_1 and φ_2 represent phase shifts at arms a and b, respectively. The unitary transformation associated

with these phase shifts is described by the following unitary operator

$$\hat{U}_{\rm PS} = \exp\left(i\varphi_1 \hat{a}^\dagger \hat{a}\right) \exp\left(i\varphi_2 \hat{b}^\dagger \hat{b}\right). \tag{2.1.8}$$

The phase shift right before BS2 results in

$$\hat{U}_{\rm PS}\hat{U}_{\rm BS1}|{\rm in}\rangle = \exp\left(i\varphi_1 \hat{a}^\dagger \hat{a}\right) \exp\left(i\varphi_2 \hat{b}^\dagger \hat{b}\right) \left|\frac{\alpha}{\sqrt{2}}\right\rangle_a \left|\frac{i\alpha}{\sqrt{2}}\right\rangle_b \tag{2.1.9}$$

$$= \left|\frac{\alpha e^{i\varphi_1}}{\sqrt{2}}\right\rangle_a \left|\frac{i\alpha e^{i\varphi_2}}{\sqrt{2}}\right\rangle_b, \tag{2.1.10}$$

After the beam splitter BS2 we obtain the output state

$$|{\rm out}\rangle = \hat{U}_{\rm MZI}|{\rm in}\rangle \tag{2.1.11}$$

$$= \hat{U}_{\rm BS2}\hat{U}_{\rm PS}\hat{U}_{\rm BS1}|{\rm in}\rangle \tag{2.1.12}$$

$$= \left|\frac{\alpha(e^{i\varphi_1} - e^{i\varphi_2})}{2}\right\rangle_a \left|\frac{\alpha(e^{i\varphi_1} + e^{i\varphi_2})}{2}\right\rangle_b \tag{2.1.13}$$

$$= \left|\frac{\alpha e^{i\varphi_1}(1 - e^{i\varphi})}{2}\right\rangle_a \left|\frac{\alpha e^{i\varphi_1}(1 + e^{i\varphi})}{2}\right\rangle_b, \tag{2.1.14}$$

where $\varphi = \varphi_2 - \varphi_1$. The state in Eq. 2.1.14 is a separable two-mode state; there is no entanglement involved and this is what one expects in the case of classical light. As we have mentioned above, our goal is to measure a quantity that is sensitive to the phase difference inside the interferometer. It is customary in the standard interferometry to measure $\left\langle \hat{J}_3 \right\rangle_{\rm out}$. Following this method, we obtain

$$\left\langle \hat{J}_3 \right\rangle_{\rm out} = \frac{1}{2}\langle {\rm out}| \left(\hat{a}^\dagger \hat{a} - \hat{b}^\dagger \hat{b}\right) |{\rm out}\rangle \tag{2.1.15}$$

$$= -\frac{|\alpha|^2}{2}\cos\varphi, \tag{2.1.16}$$

for the output state described in Eq. 2.1.14, where we have used the fact that coherent states are eigenvalues of the annihilation operator

$$\hat{a}|\alpha\rangle = \alpha|\alpha\rangle. \tag{2.1.17}$$

Using the same property we can compute

$$\left\langle \hat{J}_3^2 \right\rangle_{\text{out}} = \frac{1}{4}\langle \text{out}| \left(\hat{a}^\dagger \hat{a} - \hat{b}^\dagger \hat{b}\right)^2 |\text{out}\rangle \tag{2.1.18}$$

$$= \frac{1}{4}\langle \text{out}| \left(\hat{a}^{\dagger 2}\hat{a}^2 + \hat{b}^{\dagger 2}\hat{b}^2 + \hat{a}^\dagger \hat{a} + \hat{b}^\dagger \hat{b} - 2\hat{a}^\dagger \hat{a}\hat{b}^\dagger \hat{b}\right) |\text{out}\rangle \tag{2.1.19}$$

$$= \frac{1}{4}\left(|\alpha|^4 \cos^2\varphi + |\alpha|^2\right) \tag{2.1.20}$$

to determine the variance

$$\left\langle \left(\Delta \hat{J}_3\right)^2 \right\rangle_{\text{out}} = \frac{|\alpha|^2}{4}. \tag{2.1.21}$$

Using error propagation analysis we can determine the phase difference sensitivity $\Delta\varphi$, and for this case it turns out to be

$$\Delta\varphi = \frac{\Delta \hat{J}_3}{\left|\partial \left\langle \hat{J}_3 \right\rangle_{\text{out}} / \partial\varphi\right|} \tag{2.1.22}$$

$$= \frac{1}{|\alpha||\sin\varphi|} \tag{2.1.23}$$

$$= \frac{1}{\sqrt{\bar{N}}|\sin\varphi|} \tag{2.1.24}$$

As $\varphi \to \pi/2$, we get the minimum uncertainty allowed for a given $\bar{N}$:

$$\Delta\varphi = \frac{1}{\sqrt{\bar{N}}} \equiv \Delta_{SQL}, \tag{2.1.25}$$

which is defined as the standard quantum limit (SQL). Besides a low phase difference uncertainty, it is important to have a high signal-to-noise ratio (SNR). The SNR ratio is defined for any operator $\hat{O}$ [3] as

$$SNR = \frac{\left|\left\langle \hat{O} \right\rangle\right|}{\Delta\hat{O}}. \tag{2.1.26}$$

For the standard quantum limit case we have

$$SNR = \frac{\left|\left\langle \hat{J}_3 \right\rangle\right|}{\Delta \hat{J}_3} \tag{2.1.27}$$

$$= \bar{N}|\cos\varphi|. \tag{2.1.28}$$

It is obvious that as $\varphi \to \pi/2$ the $SNR \to 0$. This is a very low SNR. Thus we need to look for another method which yields a higher SNR and a low $\Delta\varphi$.

Let's leave aside for now the issue of the SNR and examine the phase difference distribution inside the interferometer. Han [1] has shown that the nature of the phase difference distribution inside the interferometer, especially the width of peaks of the distribution, are strongly correlated with the uncertainty in measures of the phase difference.

To illustrate the properties of the phase difference inside the interferometer for the case of the SQL, we review the phase distribution first. For a general two-mode state $|\psi(\varphi)\rangle_{a,b}$ the phase distribution is defined by

$$\mathcal{P}(\phi_a, \phi_b|\varphi) = \frac{1}{(2\pi)^2} \left|\langle\phi_a| \langle\phi_b| \psi(\varphi)\rangle_{a,b}\right|^2, \tag{2.1.29}$$

where $|\phi_a\rangle$ and $|\phi_b\rangle$ are the phase states defined in Appendix B, where it is clear that the indices a and b refer to the modes. The phase-difference distribution is obtained by integration over the sum of the phases,

$$\mathcal{D}(\theta|\varphi) = \int_0^{2\pi} d\phi_s \mathcal{P}((\phi_s - \theta)/2, (\phi_s + \theta)/2|\varphi), \tag{2.1.30}$$

where $\phi_s, \theta = \phi_2 \pm \phi_1$. In Figs. 2.2, we plot the phase-difference distributions inside the MZI for input coherent states with photon number average for (a) $\bar{N}_{CS} = |\alpha|^2 = 5$ and (b) $\bar{N}_{CS} = |\alpha|^2 = 10$ while keeping the phase difference constant at $\varphi = 0$. These figures display one peak centered at the origin, which what one would expect for an interferometer with zero phase shift $\varphi = 0$ injected with classical-like light. It is evident that the greater the average photon number gets the narrower the peak becomes. Later we shall describe the phase distribution for the case of an input squeezed vacuum state.

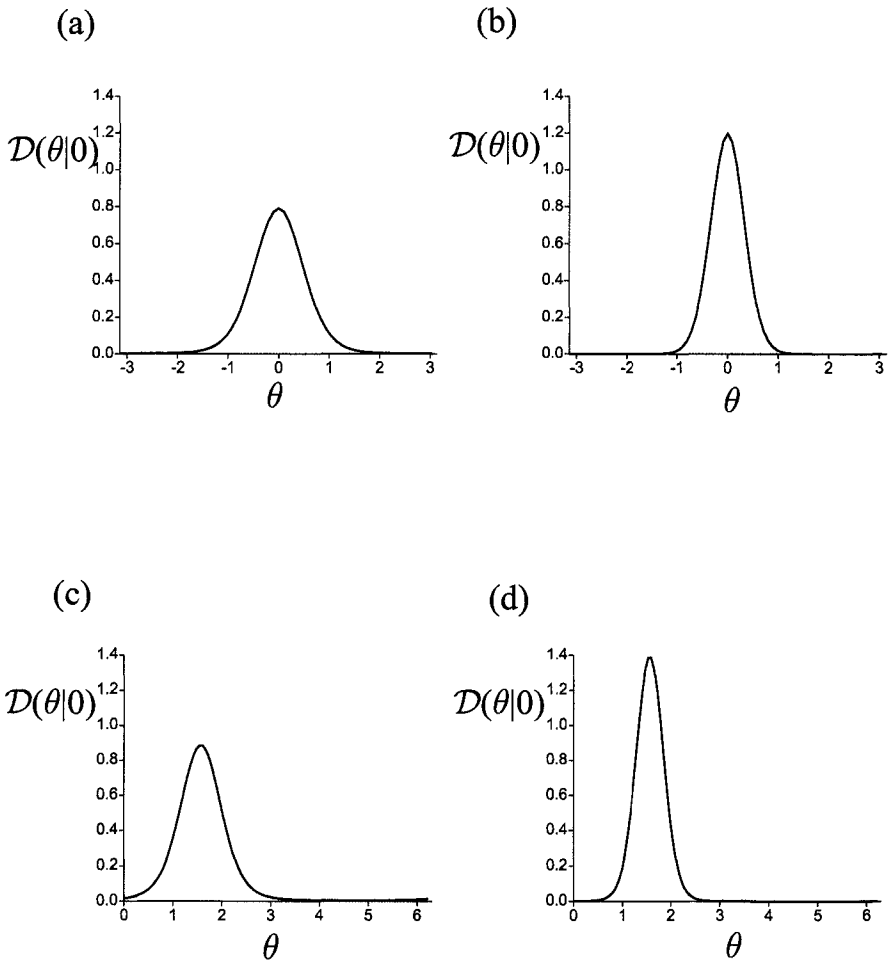

Figure 2.2: Phase difference distribution $\mathcal{D}(\theta|0)$ inside the MZI for the input coherent states for (a) $|\alpha|^2 = 5$, (b) $|\alpha|^2 = 10$ in mode a and vacuum in mode b. In (c) and (d) we plot $\mathcal{D}(\theta|0)$ keeping mode a the same as in (a) and (b), respectively, but a squeezed vacuum input state $|\xi\rangle$ in mode b with $|\xi| = 0.2$.

2.2 Interferometry with Squeezed Light

As an example of how a nonclassical state of light can improve the phase difference sensitivity, we consider here the replacement of the vacuum state by a squeezed vacuum, as was first done by Caves [4]. Before we calculate the phase shift uncertainty in this new setup, we compare the phase difference distributions in both situations. In Figs. 2.2, we plot the phase difference distribution with the new input state for (c) $|\alpha|^2 = 5$, and (d) $|\alpha|^2 = 10$ and $|\xi| = 0.2$. It is obvious that the injection of the squeezed vacuum state in the mode b makes the distribution narrower as one can see by comparing the distributions in Fig. 2.2 c and d to those in a and b. This narrowness is a good indication for the phase sensitivity. Notice that we choose a small value of ξ in order not to change significantly the average photon number inside the interferometer, and for other consideration that we discuss below. It should be clear that the change of the phase distribution is due mainly to the simultaneous injection of the squeeze vacuum and the coherent state in input ports b and a, respectively.

Now we want to obtain $\left\langle \hat{J}_3 \right\rangle_{\text{out}}$, so we proceed as follows [5]:

$$\hat{U}^{\dagger}_{\text{MZI}} \hat{J}_3 \hat{U}_{\text{MZI}} = \hat{U}^{\dagger}_{\text{BS1}} \hat{U}^{\dagger}_{\text{PS}} \hat{U}^{\dagger}_{\text{BS2}} \hat{J}_3 \hat{U}_{\text{BS2}} \hat{U}_{\text{PS}} \hat{U}_{\text{BS1}} \tag{2.2.1}$$

$$= \hat{U}^{\dagger}_{\text{BS1}} \hat{U}^{\dagger}_{\text{PS}} \hat{J}_2 \hat{U}_{\text{PS}} \hat{U}_{\text{BS1}} \tag{2.2.2}$$

$$= \hat{U}_{\text{BS1}} \left(-\sin\varphi \hat{J}_1 + \cos\varphi \hat{J}_2 \right) \hat{U}_{\text{BS1}} \tag{2.2.3}$$

$$= -\sin\varphi \hat{J}_1 + \cos\varphi \hat{J}_3, \tag{2.2.4}$$

where U_{BS1}, U_{BS2}, U_{PS}, and $\hat{U}_{\text{MZI}} = \hat{U}_{\text{BS2}} \hat{U}_{\text{PS}} \hat{U}_{\text{BS1}}$ are the unitary transformations associated with BS1, BS2, the phase shifter and the MZI, respectively. Also we have dropped an irrelevant phase factor $\exp\left[i(\varphi_1 + \varphi_2)\hat{N}/2 \right]$. Properties of the angular momentum operators have been used to derive Eq. 2.2.4, (see Appendix A for more

details). Finally, at the output of the MZI we have

$$\langle \text{out}|\hat{J}_3|\text{out}\rangle = \langle \text{in}|\hat{U}^{\dagger}_{\text{MZI}}\hat{J}_3\hat{U}_{\text{MZI}}|\text{in}\rangle \tag{2.2.5}$$

$$= -\sin\varphi\langle \text{in}|\hat{J}_1|\text{in}\rangle + \cos\varphi\langle \text{in}|\hat{J}_3|\text{in}\rangle \tag{2.2.6}$$

The same way one can easily prove that [5]

$$\langle \text{out}|\hat{J}_3^2|\text{out}\rangle = \sin^2\varphi\langle \text{in}|\hat{J}_1^2|\text{in}\rangle + \cos^2\varphi\langle \text{in}|\hat{J}_3^2|\text{in}\rangle - \cos\varphi\sin\varphi\langle \text{in}|\left(\hat{J}_3\hat{J}_1 + \hat{J}_1\hat{J}_3\right)|\text{in}\rangle \tag{2.2.7}$$

So far we have not specified $|\text{in}\rangle$. For a coherent input state injected in port a and a squeezed vacuum state in port b, we have

$$|\text{in}\rangle = |\alpha\rangle_a|\xi\rangle_b, \tag{2.2.8}$$

where $|\xi\rangle$ is the squeezed vacuum defined as

$$|\xi\rangle = \hat{S}(\xi)|0\rangle \tag{2.2.9}$$

$$= \exp\left(\frac{1}{2}\xi^*\hat{a}^2 - \frac{1}{2}\xi\hat{a}^{\dagger 2}\right)|0\rangle \tag{2.2.10}$$

$\hat{S}(\xi)$ is known as the squeeze operator, $\xi = re^{2i\phi}$, r is the squeeze parameter, and ϕ is the phase of the pump field. Using the following identity of the unitary squeeze operator [4]

$$\hat{S}^{\dagger}(\xi)\hat{a}\hat{S}(\xi) = \cosh r\hat{a} - e^{-2i\phi}\sinh r\hat{a}^{\dagger} \tag{2.2.11}$$

one can easily prove that

$$\langle \text{in}|\hat{J}_3|\text{in}\rangle = \frac{1}{2}\left(|\alpha|^2 - \sinh^2 r\right) \tag{2.2.12}$$

$$\langle \text{in}|\hat{J}_1|\text{in}\rangle = \langle \text{in}|\hat{J}_1\hat{J}_3|\text{in}\rangle = 0 \tag{2.2.13}$$

$$\langle \text{in}|\hat{J}_3^2|\text{in}\rangle = \frac{1}{4}\left(|\alpha|^4 + |\alpha|^2 + \sinh^2 r + \sinh^4 r - 2|\alpha|^2\sinh^2 r\right) \tag{2.2.14}$$

$$\langle \text{in}|\hat{J}_1^2|\text{in}\rangle = \frac{1}{4}\left[-\left(\alpha^{*2} + \alpha^2\right)\sinh r\cosh r + |\alpha|^2 + 2|\alpha|^2\sinh^2 r + \sinh^2 r\right] \tag{2.2.15}$$

which themselves lead to

$$\left\langle \left(\Delta \hat{J}_3\right)^2 \right\rangle_{\text{out}} = \frac{1}{4}\left[-\left(\alpha^{*2}+\alpha^2\right)\sinh r\cosh r\sin^2\varphi + |\alpha|^2 + 2|\alpha|^2\sinh^2 r\sin^2\varphi + \sinh^2 r\right] \tag{2.2.16}$$

$$\langle \text{out}|\hat{J}_3|\text{out}\rangle = \frac{1}{2}\left(|\alpha|^2 - \sinh^2 r\right)\cos\varphi \tag{2.2.17}$$

For $\varphi \to \pi/2$ and $|\alpha|^2 \gg \sinh^2 r$ we will have

$$\Delta\varphi = \frac{\Delta \hat{J}_3}{\left|\partial \left\langle \hat{J}_3 \right\rangle / \partial\varphi\right|} \tag{2.2.18}$$

$$= \frac{e^{-r}}{|\alpha|} \tag{2.2.19}$$

$$= \frac{e^{-r}}{\sqrt{\bar{N}}} = e^{-r}\Delta_{SQL}, \tag{2.2.20}$$

where it is clear that $\bar{N} = |\alpha|^2$ in this case. This is an improvement by a factor of e^{-r} over the standard quantum limit.

Such an improvement has been already achieved in experiments carried by Xiao *et al.* [6]. This is still not the best precision we can get with an interferometer. For the sake of comparison, we plot in Fig. 2.3 the phase uncertainty in Eq. 2.2.19 (solid line) along with the standard quantum (dot-dashed line) and the Heisenberg (dashed line) limits. It is clear that the line of the phase uncertainty is below the line of the SQL. In next chapter we will show how we can reach the Heisenberg level of uncertainty by using different states.

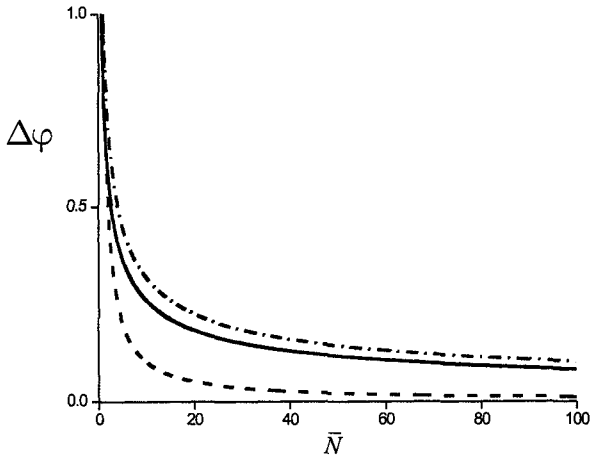

Figure 2.3: The phase uncertainty $\Delta\varphi$ versus the average photon number $\bar{N}$. The solid line is our $\Delta\varphi$ obtained from Eq. 2.2.19 for $r = 0.2$, the dashed line for the Heisenberg limit $\Delta\varphi_{HL} = 1/\bar{N}$, and the dot-dashed line is for the standard quantum limit $\Delta\varphi_{SQL} = 1/\sqrt{\bar{N}}$.

Chapter 3

Interferometry with Maximally Entangled States

Two-mode Maximally entangled states (MES) are states of the form

$$|N :: 0\rangle_{a,b}^{\Phi} \equiv \frac{1}{\sqrt{2}} \left(|N\rangle_a |0\rangle_b + e^{i\Phi} |0\rangle_a |N\rangle_b \right), \tag{3.0.1}$$

also called the NOON states, where a and b represent the two modes. Notation on the left hand side of Eq. 3.0.1 has been introduced by Kok *et al.* [7]. In general, a state of M photons entangled with N photons is denoted

$$|M :: N\rangle_{a,b}^{\Phi_{MN}} \equiv \frac{1}{\sqrt{2}} \left(|M\rangle_a |N\rangle_b + e^{i\Phi_{MN}} |N\rangle_a |M\rangle_b \right). \tag{3.0.2}$$

As we showed in Chapter 2, in standard interferometry phase measurements are performed by subtracting the photocounts on the output beams and averaging, which amounts to obtaining $\left\langle \hat{J}_3 \right\rangle_{\text{out}}$. However, such a procedure does not work for the case where we have MES inside an MZI because $\left\langle \hat{J}_3 \right\rangle_{\text{out}} = 0$, i.e., it is insensitive to the phase shift. Thus we need to find an appropriate observable that is sensitive to the phase difference and at the same time yields Heisenberg-limited sensitivities and has a high SNR. One possibility is to measure $\hat{J}_3^2$. This was proposed in [8] but though it displayed Heisenberg-limited sensitivity it has a restricted SNR. Let assume we

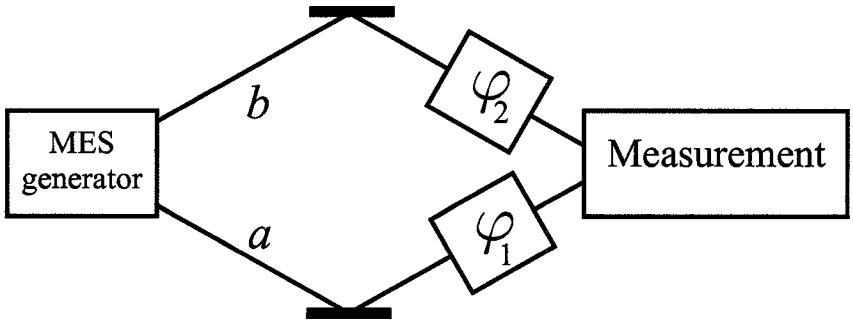

Figure 3.1: An interferometer to measure the phase φ.

have a device that is used to generate MES. We shall refer to this device as MES generator. Later we will discuss how we can realize MES generators. Right after the MES generator we have $|N :: 0\rangle_{a,b}^{\Phi}$.

Suppose we have phase shifts φ_1 and φ_2, as indicated in Fig. 3.1, that are described by the unitary transformation

$$\hat{U}_{\rm PS} = e^{i\varphi_1 \hat{a}^\dagger \hat{a}} e^{i\varphi_2 \hat{b}^\dagger \hat{b}} \tag{3.0.3}$$

as introduced in Chapter 2. The state right after the phase shifts is

$$\begin{aligned} \hat{U}_{\rm PS}|N :: 0\rangle_{a,b}^{\Phi} &= \frac{1}{\sqrt{2}}\left[|N\rangle_a|0\rangle_b + e^{i(N\varphi+\Phi)}|0\rangle_a|N\rangle_b\right] \\ &= |N :: 0\rangle_{a,b}^{N\varphi+\Phi}, \end{aligned} \tag{3.0.4}$$

where $\varphi = \varphi_2 - \varphi_1$ and the overall phase factor $e^{i\varphi_1}$ has been dropped. To see if such states are good candidates for phase measurement, we look at the phase distribution, which we found, using Eq. 2.1.30, to be

$$\mathcal{D}(\theta|\varphi) = \frac{1}{2\pi}\left(1 + \cos\left[N(\varphi - \theta) + \Phi\right]\right) \tag{3.0.5}$$

In Figs. 3.2 we plot the phase distributions $\mathcal{D}(\theta|0)$ for the states in Eq. 3.0.4 for (a) $N = 5$ and for (b) $N = 10$, where $\Phi = 0$. It is obvious that as N increases

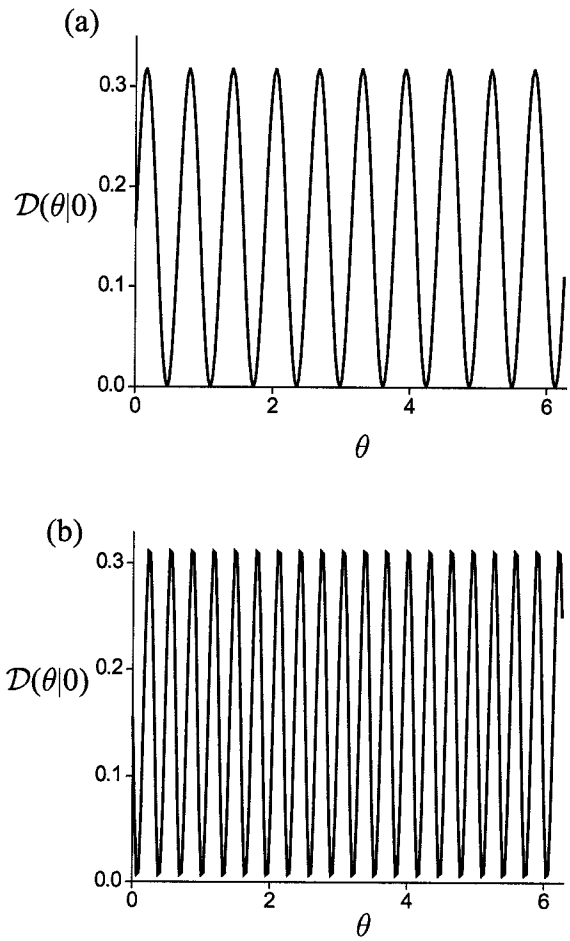

Figure 3.2: Phase difference distribution $\mathcal{D}(\theta|0)$ inside the interferometer of Fig. 3.1 versus the phase difference φ for the MES for (a) $N = 5$, (b) $N = 10$.

the distribution get more oscillatory with narrower peaks. The "frequency" of these "oscillations" is $2N$, so the peak-to-trough distance along the horizontal axis is as $1/2N$, approximately the Heisenberg limit of resolution. This property makes the MES an excellent candidate state for interferometry.

The question that we want to answer now is: what do we measure to determine φ?

To obtain the phase shift φ with these states, Kok *et al.* [7] have proposed the measurement of the following operator:

$$\hat{\Sigma}_N = |N,0\rangle\langle 0,N| + |0,N\rangle\langle N,0|. \tag{3.0.6}$$

It is easily found that $\left\langle \hat{\Sigma}_N \right\rangle = \cos(N\varphi + \Phi)$ for MES of Eq.3.0.4, and using error analysis as in Eq. 2.1.22 we obtain

$$\Delta\varphi = \frac{\Delta\hat{\Sigma}_N}{\left|\partial \left\langle \hat{\Sigma}_N \right\rangle / \partial\varphi\right|} \tag{3.0.7}$$

$$= \frac{\sqrt{1 - \left\langle \hat{\Sigma}_N \right\rangle^2}}{\left|\partial \left\langle \hat{\Sigma}_N \right\rangle / \partial\varphi\right|} = 1/N, \tag{3.0.8}$$

exactly the Heisenberg limit of sensitivity.

The question that one may ask now is: how can we physically realize any operator that yields the same result as $\hat{\Sigma}_N$? The answer turns out to be: photomixing with a 50:50 beam splitter followed by parity measurements in one of the output beams. Parity is determined by the operator $\hat{\Pi} = (-1)^{\hat{N}}$, if the measurements are carried out at the b mode we rewrite this operator as:

$$\hat{\Pi}_b = (-1)^{\hat{b}^\dagger \hat{b}}, \tag{3.0.9}$$

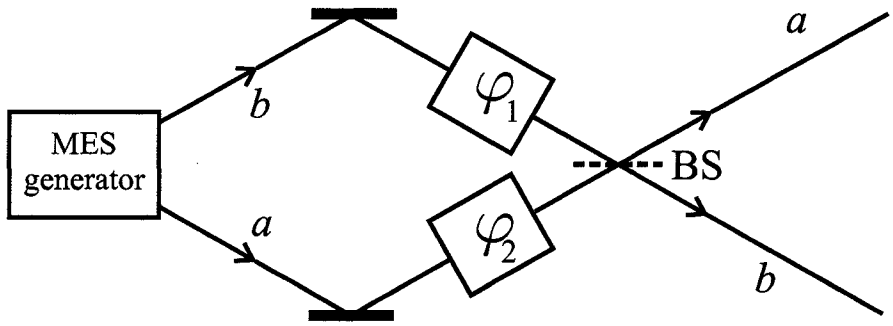

Figure 3.3: A Mach-Zehnder interferometer to measure the phase difference $\varphi = \varphi_2 - \varphi_1$ where the first beam splitter has been replaced by an MES generator.

which we can rewrite, for later simplification, using the formalism introduced in Appendix A as

$$\hat{\Pi}_b = (-1)^{\hat{b}^\dagger \hat{b}} = e^{i\pi(\hat{N}/2 - \hat{J}_3)}, \tag{3.0.10}$$

where

$$\hat{N} = \hat{a}^\dagger \hat{b} + \hat{a}\hat{b}^\dagger \tag{3.0.11}$$

$$\hat{J}_3 = \frac{1}{2}\left(\hat{a}^\dagger \hat{a} - \hat{b}^\dagger \hat{b}\right). \tag{3.0.12}$$

The method of measuring the parity is an adaptation of the scheme proposed by Bollinger *et al.* [9] in the context of atomic spectroscopy with N atoms. We shall discuss the issue of parity measurements further in Chapter 6.

Now, suppose we have a MES generator entirely replaces the first beam splitter in an otherwise ordinary MZI, as indicated in Fig. 3.3. In terms of the angular momentum operator, the transformation associated with the beam splitter BS in Fig. 3.3 has the form

$$\hat{U}_{\rm BS} = \exp\left(i\pi \hat{J}_1/2\right). \tag{3.0.13}$$

If the output states of the MES generator is given by Eq. 3.0.1, and if the result of the phase shifts by Eq. 3.0.4, then the output state of the MZI is

$$|\text{out}\rangle = \hat{U}_{\text{BS}}|N::0\rangle_{a,b}^{N\varphi+\Phi}. \tag{3.0.14}$$

The expectation value of the parity operator in the output b can be calculated as follows

$$\left\langle \hat{\Pi}_b \right\rangle = \langle \text{out}|\hat{U}_{\text{MZI}}^{\dagger}\hat{\Pi}_b\hat{U}_{\text{MZI}}|\text{out}\rangle \tag{3.0.15}$$

$$= {}_{a,b}^{N\varphi+\Phi}\langle N::0|\hat{U}_{\text{BS}}^{\dagger}\hat{\Pi}_b\hat{U}_{\text{BS}}|N::0\rangle_{a,b}^{N\varphi+\Phi} \tag{3.0.16}$$

$$= {}_{a,b}^{N\varphi+\Phi}\langle N::0|e^{-i\pi\hat{J}_1/2}e^{i\pi(\hat{N}/2-\hat{J}_3)}e^{i\pi\hat{J}_1/2}|N::0\rangle_{a,b}^{N\varphi+\Phi} \tag{3.0.17}$$

$$= {}_{a,b}^{N\varphi+\Phi}\langle N::0|e^{i\pi\hat{N}/2}e^{i\varphi\hat{J}_3}e^{i\pi\hat{J}_2}e^{-i\varphi\hat{J}_3}|N::0\rangle_{a,b}^{N\varphi+\Phi} \tag{3.0.18}$$

where we have used following identity

$$e^{-i\pi\hat{J}_1/2}e^{-i\pi\hat{J}_3}e^{i\pi\hat{J}_1/2} = -e^{i\pi\hat{J}_2}. \tag{3.0.19}$$

Expression in Eq. 3.0.18 can be simplified, using the identity in Eq. A.0.13, to this simple form

$$\left\langle \hat{\Pi}_b \right\rangle = \begin{cases} -\cos(\Phi + N\varphi), & N \text{ even}, \\ \sin(\Phi + N\varphi), & N \text{ odd}. \end{cases} \tag{3.0.20}$$

The phase uncertainty for N either even or odd, is found to be

$$\Delta\varphi = \frac{\Delta\hat{\Pi}_b}{\left|\partial\langle\Delta\hat{\Pi}_b\rangle/\partial\varphi\right|} \tag{3.0.21}$$

$$= \frac{1}{N} = \Delta\varphi_{HL}, \tag{3.0.22}$$

exactly the Heisenberg limit of sensitivity, where $\Delta\hat{\Pi}_b = (1 - \langle\Delta\hat{\Pi}_b\rangle^2)^{1/2}$ owing to the fact that $\hat{\Pi}_b^2 = \hat{I}$. Note that the result is independent of the phase difference φ.

Now let's consider a more general case: superposition of MES at the output of the MES generator. In particular we assume that we have an entangled coherent state given as

$$|\alpha :: 0\rangle_{a,b}^{\theta,\phi} \equiv \frac{1}{\sqrt{2}}\left(|\alpha\rangle_a|0\rangle_b + e^{i\theta}|0\rangle_a|e^{i\phi}\alpha\rangle_b\right) \tag{3.0.23}$$

$$= \sum_{N=0}^{\infty} c_N |N :: 0\rangle_{a,b}^{N\phi+\theta} \tag{3.0.24}$$

where

$$c_N = \exp\left(-|\alpha|^2/2\right)\frac{\alpha^N}{\sqrt{2N!}}. \tag{3.0.25}$$

We have introduced the symbol $|\alpha :: 0\rangle_{a,b}^{\theta,\phi}$ in an obvious way to represent the entanglement of a coherent state and the vacuum as defined by Eq. 4.0.1. In Chapter 4 we will discuss how to generate states in Eq. 3.0.24. In this section we assume that $\phi = \theta = 0$, without any loss of generality, so we drop the superscript. The phase shifts result in

$$\hat{U}_{\rm PS}|\alpha :: 0\rangle_{a,b} = |\alpha e^{i\varphi_1} :: 0\rangle_{a,b}^{0,\varphi}, \tag{3.0.26}$$

where $\hat{U}_{\rm PS}$ is the transformation associated with phase shifts and $\varphi = \varphi_2 - \varphi_1$ as before. Again we want to examine the phase-difference distribution of these states. It is easy to show that the phase distribution inside the interferometer with these states is given by

$$\mathcal{D}(\theta|\varphi) = \frac{1}{2\pi}\sum_{N=0}^{\infty}\frac{e^{-|\alpha|^2}|\alpha|^{2N}}{N!}\left[1+\cos\left[N(\varphi-\theta)\right]\right] \tag{3.0.27}$$

where we have used result in Eq. 2.1.30. In Fig. 3.4, we plot $\mathcal{D}(\theta|0)$. By comparing graphs (a) and (b) in Fig. 3.4 we can deduce that the envelop gets more localized and the oscillations inside are of a higher "frequency" as the average photon number

$|\alpha|^2$ gets larger. This makes the entangled coherent states very good candidates for interferometry. So, we now consider the phase uncertainty in the case of the entangled coherent state. In order to calculate ${}_{a,b}\langle\alpha :: 0|\hat{\Pi}_b|\alpha :: 0\rangle_{a,b}$, we need the following result:

$$\exp(i\pi\hat{N}/2)\exp(i\varphi\hat{J}_3)\exp(i\pi\hat{J}_2)\exp(i\varphi\hat{J}_3)|\alpha :: 0\rangle_{a,b}$$

$$= \frac{1}{\sqrt{2}}\left[|-\alpha e^{i\varphi}\rangle_a|0\rangle_b + i|0\rangle_a|i\alpha e^{-i\varphi}\rangle_b\right] \tag{3.0.28}$$

$$= |-\alpha e^{i\varphi} :: 0\rangle_{a,b}^{\pi/2,-2(\varphi+\pi/2)}, \tag{3.0.29}$$

where we have used identities in Eq. 3.0.19. We thus obtain

$$\left\langle\hat{\Pi}_b\right\rangle = {}_{a,b}^{\pi/2,-2(\varphi+\pi/2)}\langle\alpha :: 0|\hat{\Pi}_b|\alpha :: 0\rangle_{a,b}^{\pi/2,-2(\varphi+\pi/2)}$$

$$= e^{-\bar{N}}\left[1 + e^{\bar{N}\cos\varphi}\sin\left(\bar{N}\sin\varphi\right)\right], \tag{3.0.30}$$

where Eq. 3.0.15 has been used and $\bar{N} = |\alpha|^2$. Also we have

$$\frac{d\left\langle\hat{\Pi}_b\right\rangle}{d\varphi} = \bar{N}e^{-\bar{N}(1-\cos\varphi)}\cos(\varphi + \bar{N}\sin\varphi). \tag{3.0.31}$$

The phase uncertainty may again be calculated according to Eq. 3.0.21. This time $\Delta\varphi$ will clearly depend on φ. Suppose we take $\varphi \to 0$. In this case we find that

$$\left\langle\hat{\Pi}_b\right\rangle\Big|_{\varphi=0} = e^{-\bar{N}}$$

and

$$d\left\langle\hat{\Pi}_b\right\rangle/d\varphi\Big|_{\varphi=0} = \bar{N}$$

and thus

$$\Delta\varphi = \sqrt{1 - e^{-2\bar{N}}}/\bar{N}, \tag{3.0.32}$$

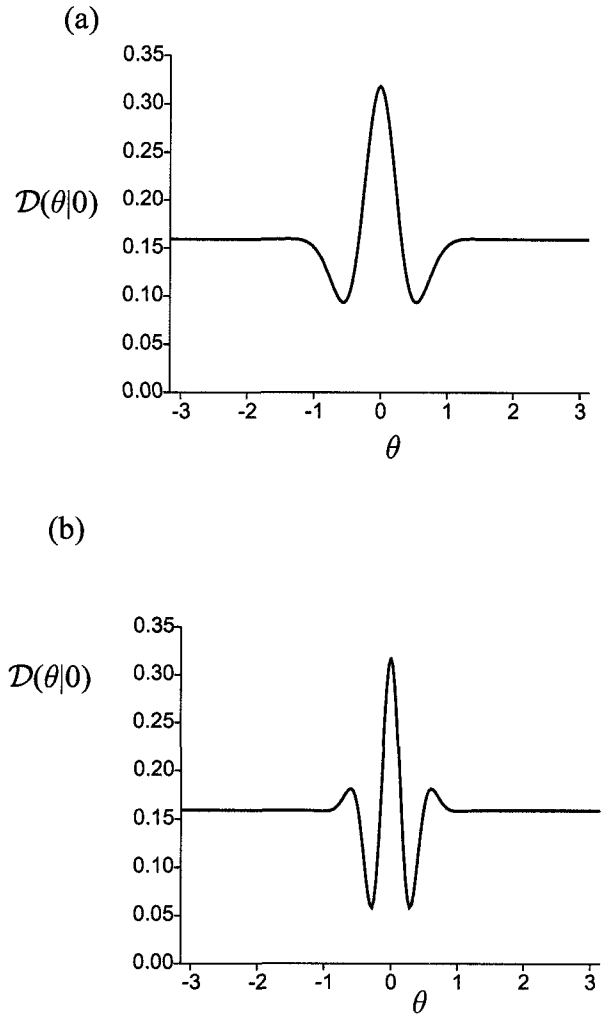

Figure 3.4: Phase difference distribution $\mathcal{D}(\theta|0)$ inside the interferometer of Fig. 3.3 for entangled coherent states for (a) $|\alpha|^2 = 5$, (b) $|\alpha|^2 = 10$.

which clearly goes over to $1/\bar{N}$ for large $\bar{N}$. (In fact, this result is valid for $\varphi = 2\pi k,\ k = 0,\ 1,\ 2, \ldots$.) But suppose φ deviates from zero by only a small amount $\delta \ll 1$ as anticipated for a weak signal in the interferometer. Letting $\varphi = \delta \ll 1$ we then have

$$\left\langle \hat{\Pi}_b \right\rangle \approx e^{-\bar{N}} + e^{-\bar{N}\delta^2/2} \sin(\bar{N}\delta). \tag{3.0.33}$$

If $\bar{N}$ is large but $\bar{N}\delta^2/2$ still small we have $\left\langle \hat{\Pi}_b \right\rangle \approx \sin(\bar{N}\delta)$ and thus $\Delta\varphi \approx 1/\bar{N}$. In Fig 3.5 we plot the exact phase uncertainty $\Delta\varphi$ (solid line) vs $\bar{N}$ for three values of φ a bit removed from zero: (a) $\varphi = \pi/45$, (b) $\varphi = \pi/18$, and (c) $\varphi = \pi/7$. For the sake of comparison we also include the curve for the Heisenberg limit, $\Delta\varphi_{\mathrm{HL}} = 1/\bar{N}$ (the dashed lines) and standard quantum limit given by $\Delta\varphi_{\mathrm{SQL}} = 1/\sqrt{\bar{N}}$ (the dot-dashed lines). We note from Fig 3.5 (a) for $\varphi = \pi/45$ that apart from the spikes at around $\bar{N} \approx 21$ and 69, the curve we obtain follows very closely that of the Heisenber-limit curve. The spikes occur simply because of the periodic functions in $\left\langle \hat{\Pi}_b \right\rangle$ and its derivative. In Fig. 3.5 (b) for the larger phase difference $\varphi = \pi/18$ we find more spikes but nevertheless the same general trend that for a wide range of $\bar{N}$ our curve is close to the Heisenberg limit and considerably below that of a standard quantum limit. For the phase difference as high as $\varphi = \pi/7$, however the correspondence to the Heisenberg limit breaks down and generally even exceeds that of the standard quantum limit as indicated in Fig. 3.5 (c). But as we have said this breakdown may be of no practical consequence if one starts with an interferometer calibrated to $\varphi = 0$, and if the expected signals are very weak causing only small disturbances. MES generator of this section will be discussed thoroughly in next chapter. We will see that it can be realized using interferometry and large nonlinear Kerr media.

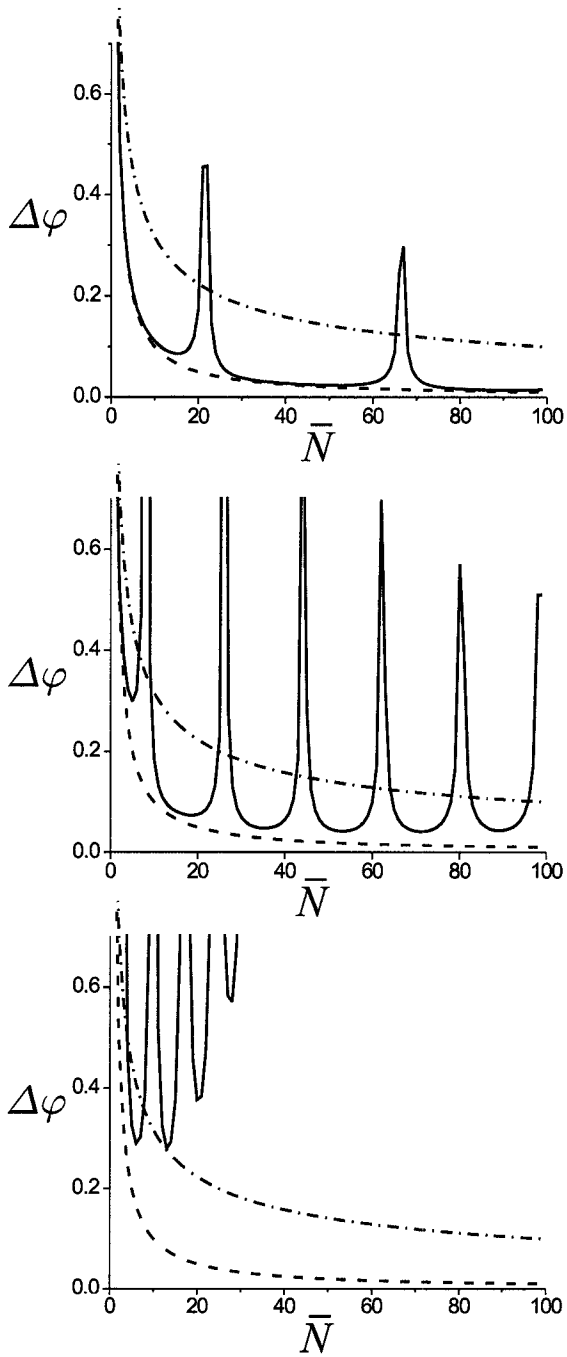

Figure 3.5: The phase uncertainty $\Delta\varphi$ versus the average photon number $\bar{N} = |\alpha|^2$ for an ECS inside the interferometer for (a) $\varphi = \pi/45$, (b) $\varphi = \pi/18$, and (c) $\varphi = \pi/7$. The solid line is our $\Delta\varphi$ obtained from Eqs. 3.0.30 and 3.0.31, the dashed line for the Heisenberg limit $\Delta\varphi_{HL} = 1/\bar{N}$, and the dot-dashed line is for the standard quantum limt $\Delta\varphi_{SQL} = 1/\sqrt{\bar{N}}$.

Chapter 4

Generation of Maximally Entangled States

Two-mode photonic MES are states consisting of a superposition of the photonic states in which all the photons are in one mode or all in the other mode. Their generic form as mentioned in Chap. 3 is

$$|N :: 0\rangle_{a,b}^{\Phi_N} \equiv \frac{1}{\sqrt{2}}(|N\rangle_a|0\rangle_b + e^{i\Phi_N}|0\rangle_a|N\rangle_b) \tag{4.0.1}$$

where a and b refer to the modes. Using beam splitter we construct MES for $N = 1$ and $N = 2$, as we will see in details. For $N > 2$, beam splitters, which are linear devices, cannot alone produce MES [10]. This suggests perhaps nonlinear devices may be used. MES can also be constructed using state reduction. But this is limited to low N. In this chapter we study more than one scheme to generate MES. First we review constructions of MES using just beam splitter and sources of single photon. Next we discuss a novel apparatus to generate MES for any N, should large nonlinear Kerr medium and N photon states be available. Then we study a scheme to construct MES for even N only using the nonlinear four-wave mixer, and its applications in interferometry.

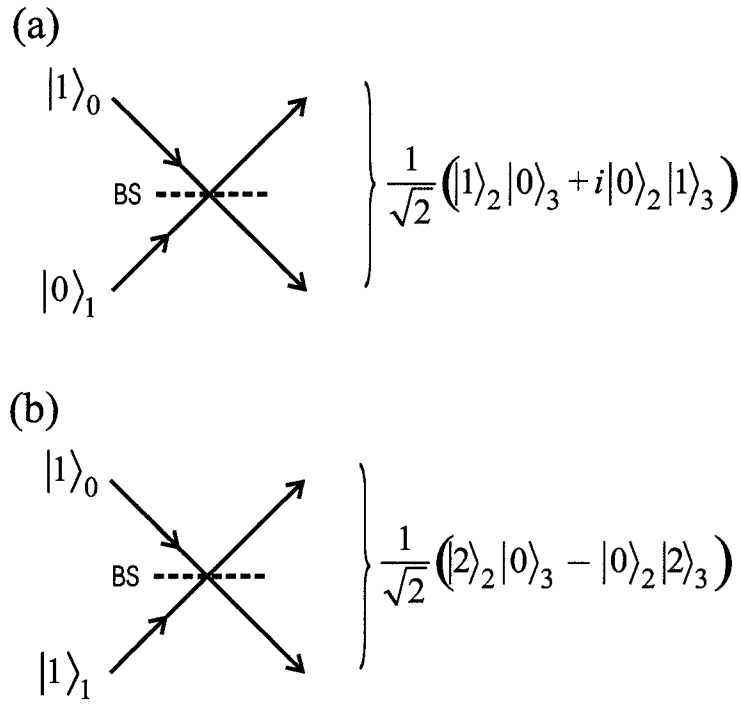

Figure 4.1: A beam splitter is injected by (a) a single photon and vacuum in the two input ports 0 and 1, respectively, result in the creation of MES for $N = 1$. (b) Two single-photons injected simultaneously at each port of the beam result in the creation of an MES for $N = 2$.

4.1 Beam splitters and MES

MES for $N = 1$ has been already produced using a beam splitter and and a source of one-single photon state. The same way in the case of $N = 2$, one can produce MES by injecting pairs of single-photon states, maybe obtained from nondegnerate down-conversion, simultaneously into the input ports of a 50:50 beam splitter. For simplicity, we start discussing schemes to generate MES with $N = 1$ and $N = 2$. States in 4.0.1 can be constructed in principle for $N = 1$ with a single photon and a 50/50 beam splitter, see Fig. 4.1 (a). Using the formalism developed in Appendix

A, it is easy to see how a single photon, $|1\rangle$, at one port and the vacuum, $|0\rangle$ at the other input port we can generate an MES for $N = 1$. Let the input state be

$$\begin{aligned} |\text{in}\rangle &= |1\rangle_0|0\rangle_1 \\ &= \hat{a}_0^\dagger|0\rangle_0|0\rangle_1, \end{aligned} \tag{4.1.1}$$

as it is depicted in Fig. 4.1, where $\hat{a}_i^\dagger$ is the creation operator related to input port i, $i = 0, 1$. The action of the beam splitter rotates the states into

$$\hat{U}_{BS}|\text{in}\rangle = \hat{U}_{BS}\hat{a}_0^\dagger\hat{U}_{BS}^\dagger\hat{U}_{BS}|0\rangle_0|0\rangle_1 \tag{4.1.2}$$

$$= \frac{1}{\sqrt{2}}\left(\hat{a}_2^\dagger + i\hat{a}_3^\dagger\right)|0\rangle_2|0\rangle_3 \tag{4.1.3}$$

$$= \frac{1}{\sqrt{2}}\left(|1\rangle_2|0\rangle_3 + i|0\rangle_2|1\rangle_3\right) \tag{4.1.4}$$

$$= |1::0\rangle_{2,3}^{\pi/2}, \tag{4.1.5}$$

where we have used the identity in Eq. A.0.27 and $\hat{U}_{BS}|0\rangle_0|0\rangle_1 = |0\rangle_2|0\rangle_3$.

Similarly, we can construct $|2::0\rangle_{2,3}^{\pi}$ by injecting a single photon at the port 0 and another single photon at the port 1 as depicted in Fig 4.1(b), so the input state this time is

$$\begin{aligned} |\text{in}\rangle &= |1\rangle_0|1\rangle_1 \\ &= \hat{a}_0^\dagger\hat{a}_1^\dagger|0\rangle_0|0\rangle_1. \end{aligned} \tag{4.1.6}$$

The action of the beams splitter leads to the following result

$$\hat{U}_{BS}|\text{in}\rangle = \hat{U}_{BS}\hat{a}_0^\dagger\hat{U}_{BS}^\dagger\hat{U}_{BS}\hat{a}_1^\dagger\hat{U}_{BS}^\dagger\hat{U}_{BS}|0\rangle_0|0\rangle_1 \tag{4.1.7}$$

$$= \frac{1}{\sqrt{2}}\left(\hat{a}_2^\dagger + i\hat{a}_3^\dagger\right)\left(i\hat{a}_2^\dagger + \hat{a}_3^\dagger\right)|0\rangle_2|0\rangle_3 \tag{4.1.8}$$

$$= \frac{-i}{\sqrt{2}}\left(|2\rangle_2|0\rangle_3 - |0\rangle_2|2\rangle_3\right) \tag{4.1.9}$$

$$= |2::0\rangle_{2,3}^{\pi}, \tag{4.1.10}$$

where $\hat{a}_i^\dagger$ is the creation operator related to the output port i; $i = 2, 3$. This is all we can do with only linear optics. In order to go beyond $N = 2$ one needs to use either states reduction, nonlinear optics, or both. In this work we address mainly the use of the nonlinear optics.

4.2 Nonlinear interferometer as resource for MES

Now we consider a way to generate MES using a device known as a nonlinear interferometer. We consider an asymmetric nonlinear interferometer (ANLI) which is characterized by the presence of a Kerr medium in just one arm (a symmetric nonlinear interferometer will be consider, for different purpose, in Chap. 6).

Fig. 4.2 depicts a sketch of an ANLI. It is a Mach-Zehnder interferometer with a Kerr medium in one arm. The beam splitters BS1 and BS2 are 50:50 $\hat{J}_1$ type, so the unitary transformation associated with them is $\hat{U}_{BS} = \exp(i\pi \hat{J}_1/2)$ as before. The Kerr effect interaction is described by the interaction Hamiltonian [11, 12]

$$\hat{H}_K = \hbar\chi \hat{a}^{\dagger 2}\hat{a}^2 = \hbar\chi \left[(\hat{a}^\dagger \hat{a})^2 - \hat{a}^\dagger \hat{a}\right], \tag{4.2.1}$$

where here χ is proportional to the third-order nonlinear $\chi^{(3)}$ of the medium. Many authors employ a truncated version where the term linear in the photon number operator is dropped [13, 14]. We will use this more realistic form but in order to more easily obtain our desired result we shall need to compensate for the effect of the linear term. This accounts for the presence of the phase shifter in the counterclockwise beam. Shortly we shall specify the required value of the phase shift ϕ_a. The unitary transformation associated with the Kerr interaction is

$$\hat{U}_{K,a} = \exp(-i\hat{H}_K t_K/\hbar) = \exp(-i\kappa(\hat{a}^\dagger \hat{a})^2) \exp(i\kappa \hat{a}^\dagger \hat{a}). \tag{4.2.2}$$

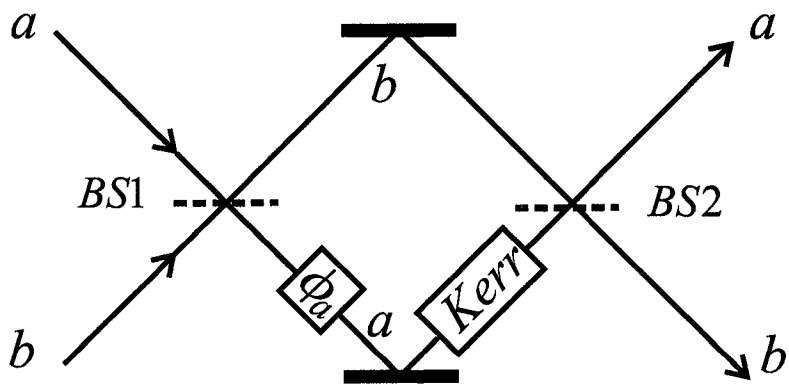

Figure 4.2: The asymmetric nonlinear interferometer.

Obviously $t_K = l/v_K$ is the time for light to cross the Kerr medium, l is the length of the medium, v_K is the velocity of light in the medium, and $\kappa = \chi l/v_K$. In what follows we assume that the third-order nonlinear susceptibility is large enough to maintain the condition $\kappa = \pi/2$, so for further simplification. There are prospects that such nonlinearities will eventually become available through the techniques of the electromagnetically induced transparency [15, 16, 17, 18]. It is perhaps worthwhile to recall here that many proposals for quantum nondemolition measurements of photon number require Kerr interactions, either self-interactions of the type in Eq. 4.2.1 [19] or cross-Kerr interactions between two modes [20, 21], with large nonlinear susceptibilities of the magnitude required in the present work.

For simplicity, let's assume we are injecting the interferometer depicted in figure 4.2 with an input coherent state in mode a and the vacuum in mode b. Later we can get the result for N-photon by projection. In any case the input state is given by:

$$|\text{in}\rangle = |\alpha\rangle_a|0\rangle_b. \tag{4.2.3}$$

It is convenient to write the last expression as

$$|\text{in}\rangle = \hat{D}_a(\alpha)|0\rangle_a|0\rangle_b, \tag{4.2.4}$$

where $\hat{D}_a(\alpha)$ is the Glauber displacement operator as defined in Eq. 2.1.5.

Just after the first beam splitter, we obtain

$$\hat{U}_{\text{BS1}}|\text{in}\rangle = e^{i\pi\hat{J}_1/2}e^{\alpha\hat{a}^\dagger+\alpha^*\hat{a}}e^{-i\pi\hat{J}_1/2}e^{i\pi\hat{J}_1/2}|0\rangle \tag{4.2.5}$$

$$= \hat{D}_a\left(\frac{\alpha}{\sqrt{2}}\right)\hat{D}_b\left(\frac{i\alpha}{\sqrt{2}}\right)|0\rangle \tag{4.2.6}$$

$$= \left|\frac{\alpha}{\sqrt{2}}\right\rangle_a\left|\frac{i\alpha}{\sqrt{2}}\right\rangle_b, \tag{4.2.7}$$

where we have used the identity in Eq. A.0.28. Notice that state in Eq. 4.2.7 is separable and the mode b picks a $\pi/2$ phase shift as one would expect for a classical-like light. The phase shifter transforms the state in Eq. 4.2.7 to

$$\hat{U}_{\text{PS}}\hat{U}_{\text{BS1}}|\text{in}\rangle = e^{i\phi_a\hat{a}^\dagger\hat{a}}\left|\frac{\alpha}{\sqrt{2}}\right\rangle_a\left|\frac{i\alpha}{\sqrt{2}}\right\rangle_b \tag{4.2.8}$$

$$= \left|\frac{\alpha e^{i\phi_a}}{\sqrt{2}}\right\rangle_a\left|\frac{i\alpha}{\sqrt{2}}\right\rangle_b. \tag{4.2.9}$$

We now apply the operator $\hat{U}_{K,a}$ of equation 4.2.2 for $\kappa = \pi/2$ to obtain the following result

$$\hat{U}_{K,a}\left(\frac{\pi}{2}\right)\hat{U}_{\text{BS1}}|\text{in}\rangle = e^{-i\frac{\pi}{2}(\hat{a}^\dagger\hat{a})^2}\left|\frac{\alpha e^{i(\phi_a+\frac{\pi}{2})}}{\sqrt{2}}\right\rangle_a\left|\frac{i\alpha}{\sqrt{2}}\right\rangle_b. \tag{4.2.10}$$

At this stage, we choose $\phi_a = -\frac{\pi}{2}$, and the identity

$$\exp\left(-i\frac{\pi}{2}(\hat{a}^\dagger\hat{a})^2\right)|\beta\rangle = \frac{1}{\sqrt{2}}\left(e^{-i\pi/4}|\beta\rangle + e^{i\pi/4}|-\beta\rangle\right), \tag{4.2.11}$$

which is a form of Schrödinger-cat state usually known as the Yurke-Stoler state [5]. Applying this result, we rewrite the state in Eq. 4.2.10 as

$$\frac{1}{\sqrt{2}}\left(e^{-i\pi/4}\left|\frac{\alpha}{\sqrt{2}}\right\rangle_a + e^{i\pi/4}\left|-\frac{\alpha}{\sqrt{2}}\right\rangle_a\right)\left|i\frac{\alpha}{\sqrt{2}}\right\rangle_b, \tag{4.2.12}$$

The second beam splitter performs the transformations

$$\hat{U}_{\rm BS2}\left|\frac{\alpha}{\sqrt{2}}\right\rangle_a\left|i\frac{\alpha}{\sqrt{2}}\right\rangle_b = |0\rangle_a|i\alpha\rangle_b, \tag{4.2.13}$$

and

$$\hat{U}_{\rm BS2}\left|-\frac{\alpha}{\sqrt{2}}\right\rangle_a\left|i\frac{\alpha}{\sqrt{2}}\right\rangle_b = |-\alpha\rangle_a|0\rangle_b, \tag{4.2.14}$$

therefore the output state, apart from an overall irrelevant $e^{i\pi/4}$ factor, reads:

$$|\text{out}\rangle = \frac{1}{\sqrt{2}}[|0\rangle_a|i\alpha\rangle_b + i|-\alpha\rangle_a|0\rangle_b] \tag{4.2.15}$$

$$\equiv i|-\alpha :: 0\rangle_{a,b}^{-\pi/2,-\pi/2}. \tag{4.2.16}$$

where the definition in Eq. 3.0.23 has been used. This is the same type of state we have used for interferometry in Chap. 3, apart from phases. In terms of the number states, the state in Eq. 4.2.16 can be expanded into

$$|\alpha :: 0\rangle_{a,b}^{-\pi/2,-\pi/2} = \frac{1}{\sqrt{2}}e^{-|\alpha|^2/2}\sum_{N=0}^{\infty}\frac{\alpha^N}{\sqrt{N!}}(-1)^N\left[|N\rangle_a|0\rangle_b + e^{i\Phi_N}|0\rangle_a|N\rangle_b\right], \tag{4.2.17}$$

where $\Phi_N = -(N+1)\pi/2$ and an irrelevant overall $e^{i\pi/2}$ factor has been dropped. Furthermore, it can be deduced from Eq. 4.2.17 that with an input state such as $|\text{in}\rangle = |N\rangle_a|0\rangle_b$ the output state will be the MES, up to a factor,

$$|\text{out}\rangle = (-1)^N|N :: 0\rangle_{a,b}^{\Phi_N}, \tag{4.2.18}$$

this being, apart from the phase factor $(-1)^N$, the same state we have mentioned in relation to the MES generator in Chap. 3. Of course, to obtain this ultimate result one must be able to generate number states $|N\rangle$, to inject into the NLI; and the higher N the better. Some progress has been made in that direction [22] but there is as yet no available source of optical number states for arbitrary N. In general an input state

of the form

$$|\text{in}\rangle = \sum_{N}^{\infty} c_N |N\rangle_a |0\rangle_b \tag{4.2.19}$$

will result an output state in the form of a superposition of MES's

$$|\text{out}\rangle = \frac{1}{\sqrt{2}} \sum_{N}^{\infty} c_N (-1)^N |N :: 0\rangle_{a,b}^{\Phi_N}. \tag{4.2.20}$$

For the sake of completeness we state the result of inputing arbitrary coherent states $|\alpha\rangle_a$ and $|\beta\rangle_b$ in modes a and b, respectively, i.e., $|\text{in}\rangle = |\alpha\rangle_a |\beta\rangle_b$. Retaining the choice of phase $\phi_a = -\pi/2$, it is straightforward to obtain the output state

$$|\text{out}\rangle = |\alpha :: \beta\rangle_{a,b} \equiv \frac{1}{\sqrt{2}} [|i\beta\rangle_a |i\alpha\rangle_b + i|-\alpha\rangle_a |\beta\rangle_b], \tag{4.2.21}$$

an entanglement of coherent states. Entangled coherent states have been much discussed in the literature, especially in connection with application in quantum information theory [13, 23, 24, 25, 26, 27, 28]. Expressed in terms of number states,

$$|\alpha :: \beta\rangle_{a,b} = e^{-(|\alpha|^2+|\beta|^2)/2} \sum_{N=0}^{\infty} \sum_{M=0}^{\infty} \frac{\alpha^N \beta^M}{\sqrt{M!N!}} (-1)^N |N :: M\rangle_{a,b}^{\Phi_{NM}} \tag{4.2.22}$$

where $\Phi_{NM} = -\pi(N-M+1)/2$ and where again an irrelevant overall $e^{i\pi/2}$ factor has been dropped. Thus we have a superposition of the entangled states $|N :: M\rangle_{a,b}^{\Phi_{NM}}$ of Eq. 3.0.2. From this result we deduce that for the input states $|N\rangle_a |M\rangle_b$ we obtain the output state $|N :: M\rangle_{a,b}^{\Phi_{NM}}$, apart from an irrelevant phase factor.

4.3 Nonlinear Four-wave Mixing as Resource for MES

Another possibility for generating MES involves a nonlinear four-wave mixer. This method is not as general as that discussed in the previous section, as it seems to work

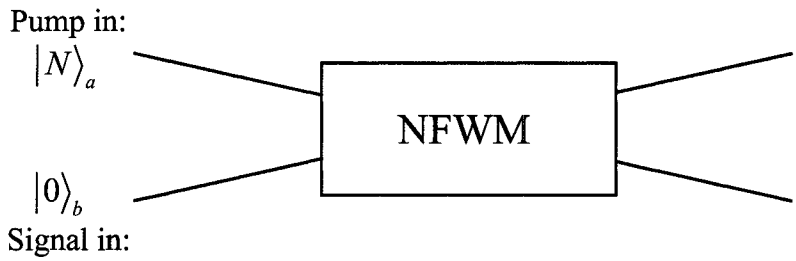

Figure 4.3: Nonlinear four-wave mixing with a vacuum in the signal input mode and a Fock state $|N\rangle_a$ at the pump mode.

only for even number states. The interaction Hamiltonian for a degenerate four-wave mixer (FWM) is given by [29]

$$\hat{H}^I_{FWM} = \hbar\frac{\Omega}{4}\left(\hat{a}^{\dagger 2}\hat{b}^2 + \hat{a}^2\hat{b}^{\dagger 2}\right), \tag{4.3.1}$$

where Ω is proportional to the nonlinear susceptibility $\chi^{(3)}_{FWM}$ of the four-wave mixing process in the medium. The Kerr interaction of the medium is given by [5]

$$\hat{H}^I_{Kerr} = \hbar\frac{K}{2}\hat{a}^\dagger\hat{a}\hat{b}^\dagger\hat{b}, \tag{4.3.2}$$

where the self-modulation terms of the form $(\hat{a}^\dagger\hat{a})^2$ and $(\hat{b}^\dagger\hat{b})^2$ can be dropped by choosing the resonances of the medium in an appropriate way [30], and K is proportional to the Kerr susceptibility $\chi^{(3)}_{Kerr}$. In the assumption that $\Omega = K$, maybe possible through the enhancement of Kerr nonlinearities using the electromagnetically induced transparency, as we have mentioned above. Then the complete interaction Hamiltonian for the medium takes the form

$$\hat{H}^I = \hbar\frac{\Omega}{4}(\hat{a}^{\dagger 2}\hat{b}^2 + \hat{a}^2\hat{b}^{\dagger 2}) + \hbar\frac{\Omega}{2}\hat{a}^\dagger\hat{a}\hat{b}^\dagger\hat{b} \tag{4.3.3}$$

This is the Hamiltonian for the NFWM as discussed by Yurke and Stoler [5]. It consists of two competing nonlinear process, four-wave mixer and cross-Kerr. Assuming

that modes a and b are degenerate with frequency ω, the Hamiltonian is

$$\hat{H} = \hbar\omega\left(\hat{a}^\dagger\hat{a} + \hat{b}^\dagger\hat{b}\right) + \hbar\frac{\Omega}{4}\left(\hat{a}^\dagger\hat{b} + \hat{b}^\dagger\hat{a}\right)^2. \tag{4.3.4}$$

In term of the angular momentum notation of Appendix A

$$\hat{H} = 2\omega\hbar\hat{J}_0 + \Omega\hbar\hat{J}_1^2. \tag{4.3.5}$$

With $|N\rangle_a$ and $|0\rangle_b$ as input states in pump and signal modes, we would obtain

$$|\text{out}\rangle = \exp\left(-i\kappa\hat{J}_1^2\right)|\text{in}\rangle. \tag{4.3.6}$$

From Eq. A.0.21 and the following identity

$$\exp\left(i\frac{\pi}{2}\hat{J}_2\right)\hat{J}_1\exp\left(-i\frac{\pi}{2}\hat{J}_2\right) = \hat{J}_3, \tag{4.3.7}$$

we can write

$$|\text{out}\rangle = \exp(i\frac{\pi}{2}\hat{J}_2)\sum_{m=-j}^{j}\exp\left(-i\kappa m^2\right)d_{m,j}^{(j)}\left(\frac{\pi}{2}\right)|j,m\rangle, \tag{4.3.8}$$

where $\kappa = \Omega t$ and

$$d_{m,j}^{(j)}(\theta) = \langle j,m|\exp(-i\theta\hat{J}_2)|j,j\rangle \tag{4.3.9}$$

for any angle θ. From now on we take $\kappa = \pi/2$. Further, we can modify equation 4.3.9 to

$$(-1)^m d_{m,j}^{(j)}(\theta) = \langle j,m|\exp\left(-i\pi\hat{J}_3\right)\exp\left(-i\theta\hat{J}_2\right)|j,j\rangle \tag{4.3.10}$$

for later simplifications. Now, let assume that N is even so j and m are integers. It can be shown that

$$\exp\left(i\frac{\pi}{2}m^2\right) = \frac{\exp\left(-i\pi/4\right) + \exp(i\pi/4)(-1)^m}{\sqrt{2}}, \tag{4.3.11}$$

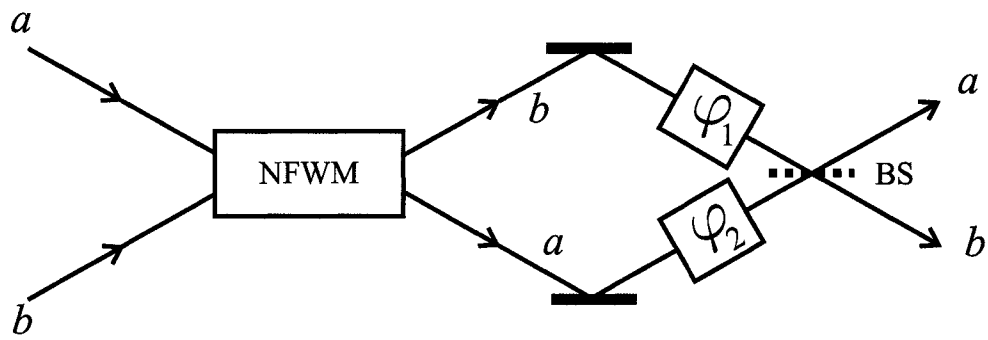

Figure 4.4: Modified Mach-Zehnder interferometer to measure the phase φ where the first beam splitter has been replaced by an nonlinear four-wave mixer operating under the conditions required to produce maximally entangled states for an even input state. Detection is performed only on the output b mode.

then equation (4.3.8) can be simplified [31, 32, 33] to

$$|\text{out}\rangle = \frac{1}{\sqrt{2}}[|j,j\rangle + \exp(-i\Phi_N)\,|j,-j\rangle], \tag{4.3.12}$$

which can be written as

$$|\text{out}\rangle = \frac{1}{\sqrt{2}}\left[|N\rangle|0\rangle + \exp(-i\Phi_N)\,|0\rangle|N\rangle\right], \tag{4.3.13}$$

where $j = N/2$.

In summary, for a Fock state $|N\rangle$ with N even, one can generate, in principle, a maximally entangled state of Eq. 4.0.1 at the output of the nonlinear four-wave mixer. It is straightforward to generalize it to the case where the input state is a superposition of even photon numbers. As this is a different superposition than the one discussed in Chap. 3, containing only even number states, we again study the phase uncertainty for these states.

In Fig. 4.4, we illustrate out prototype for interferometric measurements with a Mach-Zehnder interferometer device except where the first beam splitter has been replaced by an NFWM.

Now first we consider as input to the NFWM the more general state consisting of a superposition of only the even number states which we write as

$$|\text{in}\rangle = \sum_{m=0}^{\infty} C_{2m}|2m\rangle_a, \tag{4.3.14}$$

and for which the average photon number

$$\bar{N} = \sum_{m=0}^{\infty} 2m|C_{2m}|^2, \tag{4.3.15}$$

The output of the NFWM is now

$$|\text{out}\rangle_{NFWM} = \sum_{m=0}^{\infty} C_{2m}|2m :: 0\rangle_{a,b}^{\Phi}, \tag{4.3.16}$$

where we have used results derived in Eq. 4.3.13. And the expectation value of the operator $\hat{\Pi}_b$ of Eq. 3.0.10 is then

$$\left\langle \hat{\Pi}_b \right\rangle_{NFWM} = \sum_{m=0}^{\infty} |C_{2m}|^2(-1)^2 \cos(2m\varphi + \Phi_{2m}), \tag{4.3.17}$$

where this time $\Phi_{2m} = (2m+1)\pi/2$.

We consider two particular input states: the even coherent states and the squeezed vacuum states. For the former, the state is denoted $|z\rangle_{ECS}$ and the coefficients are [34]

$$C_{2m} = [\cosh(|z|)]^{-1/2} \frac{z^m}{\sqrt{(2m)!}}. \tag{4.3.18}$$

The average photon number is $\bar{N}_{ECS} = |z| \tanh(|z|)$. Recall that the photon number probability distribution is similar to that of the Poisson distribution but the important difference that all the odd number states have zero probabilities. The peak of the distribution is near $\bar{N}_{ECS}$. The parameter z is $0 \leq |z| < \infty$. The even coherent state may be written as a superposition of the usual coherent states as

$$|z\rangle_{ECS} = \frac{1}{\sqrt{2}}\left(1 + e^{-2|\alpha|^2}\right)(|\alpha\rangle + |-\alpha\rangle), \tag{4.3.19}$$

which is a form of Schrodinger cat state with $z = \alpha^2$. The output state in this case may be written as

$$|\text{out}\rangle_{NFWM} = \frac{1}{2}(|z\rangle_{ECS,a}|0\rangle_b - i|0\rangle_a|z\rangle_{ECS,b}), \tag{4.3.20}$$

an entanglement of the vacuum and even coherent states.

For the squeezed vacuum state, which we denote in the customary way as $|\xi\rangle_{SV}$, the coefficients are

$$c_{2m} = (\cosh r)^{-1/2}(-1)^m \frac{\sqrt{(2m)!}}{2^m m!}(e^{i\theta}\tanh r)^m, \tag{4.3.21}$$

where $\xi = e^{i\theta}\tanh r$, $0 \leq \theta < 2\pi$, $0 \leq r < \infty$, r being the squeeze parameter. The average photon number for this state is $\bar{N}_{SV} = \sinh^2 r$. The corresponding photon number probability distribution is similar to that of thermal light except that, again, all odd states are missing and, of course the squeezed vacuum states are pure states. In this case we have

$$|\text{out}\rangle_{NFWM} = \frac{1}{2}(|\xi\rangle_{SV,a}|0\rangle_b - i|0\rangle_a| - \xi\rangle_{SV,b}), \tag{4.3.22}$$

As it turns out, there exists closed form expressions for $\left\langle \hat{\Pi}_b \right\rangle$ for each of these states. For the even coherent states

$$\left\langle \hat{\Pi}_b \right\rangle_{ECS} = -\sinh(|z|\cos\varphi)\sin(|z|\sin\varphi)\cosh|z|, \tag{4.3.23}$$

and for the squeezed vacuum states

$$\left\langle \hat{\Pi}_b \right\rangle_{ECS} = -\sin(\Lambda/2)/\left(1+\sinh^2(2r)\sin^2\varphi\right)^{1/4}, \tag{4.3.24}$$

$$\Lambda = \tan^{-1}\left(\frac{-\sinh^2 r\sin(2\varphi)}{1+2\sinh^2 r\sin^2\varphi}\right). \tag{4.3.25}$$

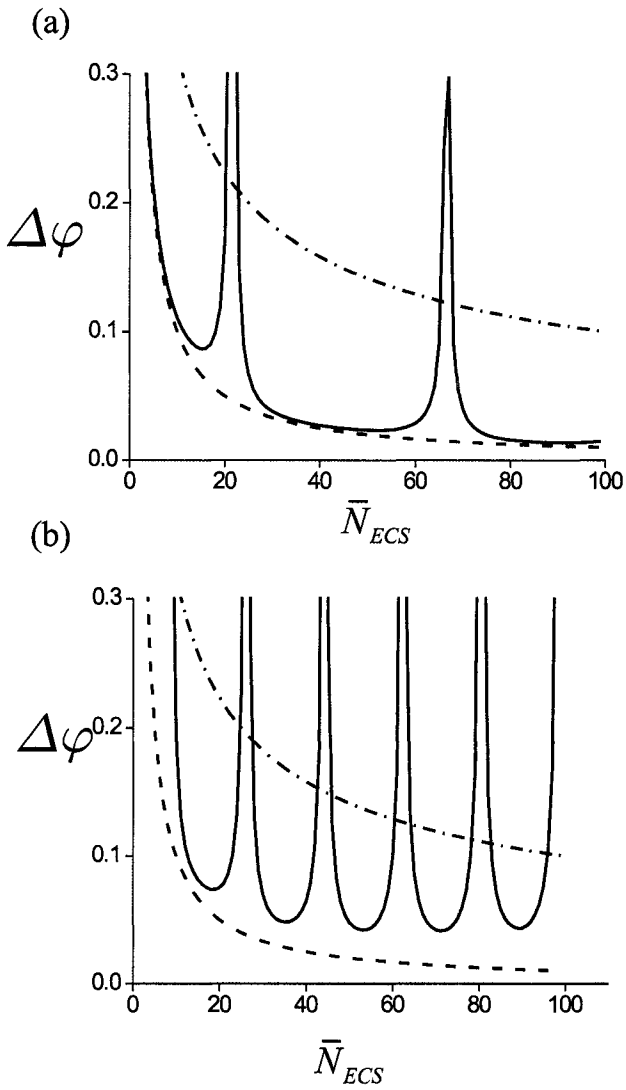

Figure 4.5: Phase difference uncertainty $\Delta\varphi$ for the input even coherent states (solid line) along with $\Delta\varphi_{SQL}$ (dot-dashed line) and $\Delta\varphi_{HL}$ (dashed line) for (a) $\varphi = \pi/45$, (b)$\varphi = \pi/18$. The dashed lines represent the Heisenberg limit $1/\bar{N}_{ECS}$ while the dot-dashed lines represent the standard quantum limit $1/\sqrt{\bar{N}_{ECS}}$.

For an MZI calibrated to $\varphi = 0$, it is easy to show that $\Delta\varphi = 1/\bar{N}$, $\bar{N}$ being either $\bar{N}_{ECS}$ or $\bar{N}_{SV}$. Thus for an interferometer with zero phase shift $\varphi = 0$, we obtain sensitivities at the Heisenberg limit in terms of the average photon number of the input even state. This procedure of using an even coherent state as an input, a state that is perhaps a challenge to generate in its own right, makes it possible to approach the Heisenberg limit of sensitivity without the need for generating an even number state for the input to the NFWM. But for the case of an MZI where $\varphi \neq 0$, the phase uncertainty will generally deviate from the Heisenberg limit but may still be improved over the corresponding standard quantum limit.

In Figs. 4.5 we plot the phase uncertainty versus average photon number for the input even coherent state. Fig. 4.5(a) is for $\varphi = \pi/45$ while Fig. 4.5(b) is for $\varphi = \pi/18$. The exact Heisenberg-limit curve $\Delta\varphi_{HL} = 1/\bar{N}$ and the standard quantum limit curve $\Delta\varphi_{HL} = 1/\sqrt{\bar{N}}$ are also shown. Aside from the periodic spikes the phase uncertainties closely follow the Heisenberg-limit curve, at least for small φ. We notice that, even when φ is large enough to cause significant deviations from the Heisenberg limit, the phase uncertainty is still lower than the standard quantum limit.

In Figs. 4.6 we plot the phase difference distribution $\mathcal{D}(\varphi|0)$ with even coherent input states for (a) $\bar{N} = 10$ and (b) $\bar{N} = 42$. The plots are dominated by a horizontal plateau with two envelops separated by π radians of "rapid" oscillations peaks. It is clear the larger the average photon number, greater the "frequency" of the oscillation and the more compact become the envelops.

But for the squeezed vacuum input, the situation is different. For φ only slightly different than zero, there are significant deviations from the Heisenberg limit as is shown in Fig. 4.7 for $\varphi = \pi/90$. It is evident that the phase uncertainty in this case

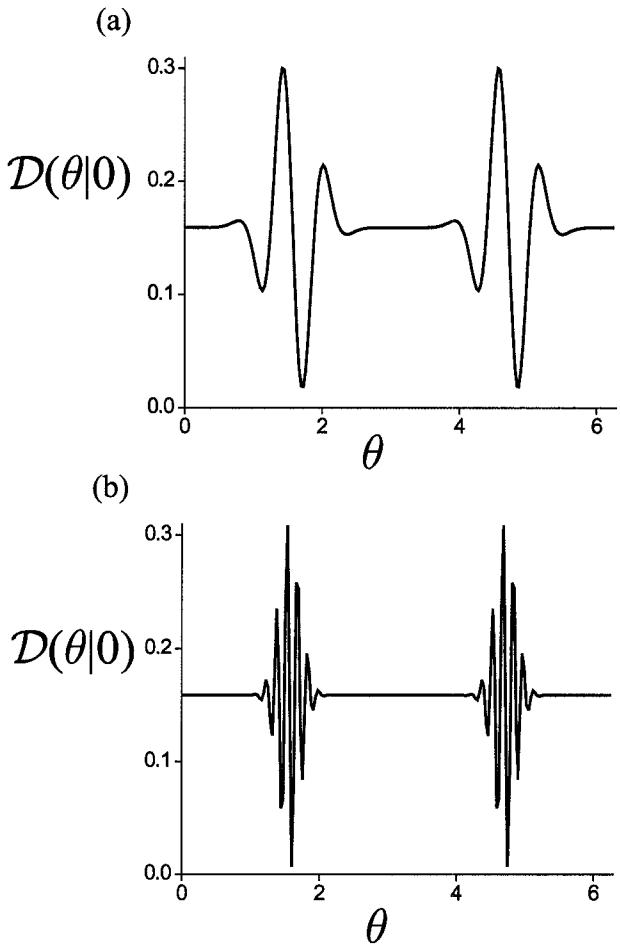

Figure 4.6: Phase difference distribution $\mathcal{D}(\theta|0)$ inside the MZI versus the phase difference between arms b and a for the input even coherent states for (a) $\bar{N}_{ECS} = 10$, (b)$\bar{N}_{ECS} = 42$.

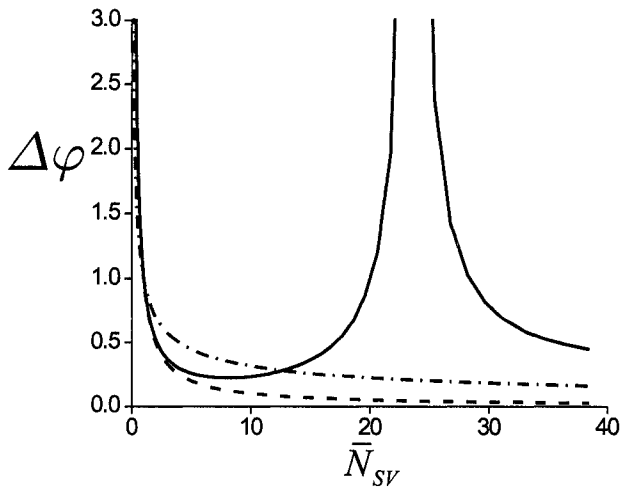

Figure 4.7: Phase difference uncertainty $\Delta\varphi$ for the input squeezed state (solid line) versus $\bar{N}_{SV}$ along with $\Delta\varphi_{SQL}$ (dot-dashed line) and $\Delta\varphi_{HL}$ (dashed line) for $\varphi = \pi/90$.

becomes markedly noisy as the average photon number increases, even exceeding that of the standard quantum limit. The difference in the results obtained for these two types of input states lies in the nature of the respective photon probability distributions. For the even coherent states, even though all odd number states are missing, the photon number distribution is peaked near the average photon number $\bar{N}_{ECS}$. For the squeezed vacuum the distribution is thermal-like and for increasing $\bar{N}_{SV}$ becomes extremely flat. This in turn means that a wide range of number states are contributing to the expectation value of the operator $\hat{\Pi}_b$. Clearly it is not enough just to have a superposition of even number states but rather there needs to be at least some degree of localization in the photon number distribution. Ideally it appears that the distribution should be sub-Poissonian. Recall that for an input even number state (a number state being the ultimate sub-Poissonian state) the phase uncertainty

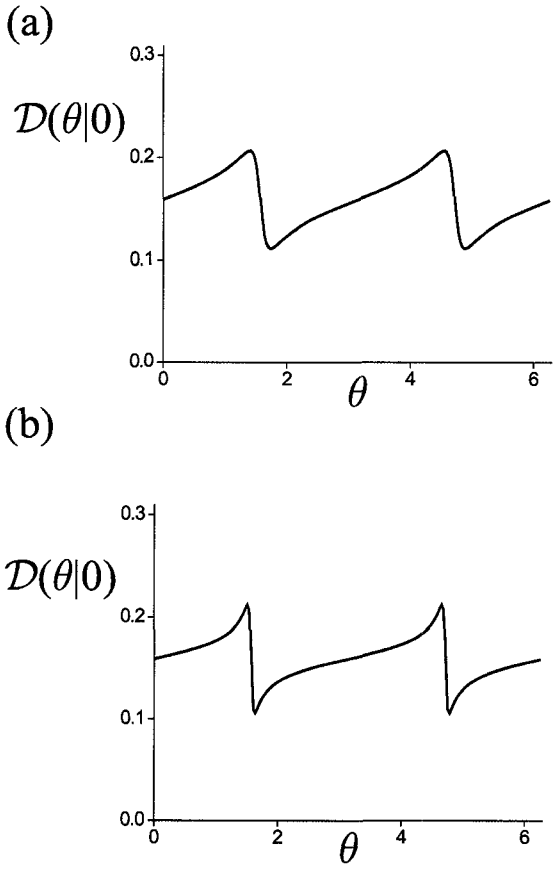

Figure 4.8: Phase difference distribution $\mathcal{D}(\theta|0)$ inside the MZI versus the phase difference between arms b and a for for the input squeezed vacuum states for (a) $\bar{N}_{SV} = 4.06$, (b)$\bar{N}_{SV} = 15$.

is exactly the Heisenberg limit with no dependence on the phase φ. But as it is well known, the squeezed vacuum states are super-Poissonian, just the opposite of the ideal input states.

In Figs. 4.8 we plot the phase difference distribution inside the interferometer for the squeeze vacuum input states for (a) $\bar{N}_{SV} = 4.06$ and (b) $\bar{N}_{SV} = 15$. These plots consist mainly of two peaks separated by π radians. A change in the average photon number does not create any more oscillation in the phase distribution except making the peaks slightly narrower, so this phase distribution lacks localization. This is in contrast to the case of the even coherent states. One concludes from this comparison that a well localized phase distribution inside the interferometer is a good indication in the precision of phase shift measurements when using the parity measurements on one of the output beams.

Chapter 5

Interferometry with Twin Fock States

Some years ago, Holland and Burnett [35] studied the problem of optical phase shift measurement with use of twin Fock states $|N\rangle_a|N\rangle_b$, where N photons are simultaneously injected into the output of a MZI. In a previous work [36], Holland and Burnett concluded that the phase measurement approaches the Heisenberg quantum limit asymptotically using the usual method of subtracting the photocurrents at the output beam splitter of the MZI. It turns out, that balanced detection is, in principle, not a functional method for interferometry with this class of input states, because, as in the case of MES, $\langle \hat{J}_3 \rangle = 0$. Hillery *et al.* reexamined the original detection method, pointing out that there are *two* narrow peaks separated by π radians. In Fig. 5.1, we picture a Mach-Zehnder interferometer with twin Fock states input $|N\rangle_a|N\rangle_b$, the

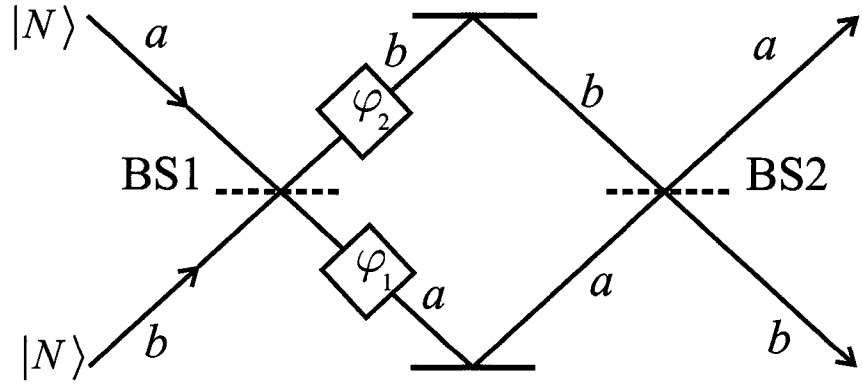

Figure 5.1: Mach-Zehnder interferometer with twin Fock state as an input state.

state inside the interferometer just after the BS1 is given by the expansion [10]

$$|\psi_{2N}\rangle = \hat{U}_{\mathrm{BS1}}|\mathrm{in}\rangle \tag{5.0.1}$$

$$= \hat{U}_{\mathrm{BS1}}\frac{\hat{a}^{\dagger N}\hat{b}^{\dagger N}}{N!}|0\rangle_a|0\rangle_b \tag{5.0.2}$$

$$= \frac{i^N}{2^N N!}\left[\left(\hat{a}^\dagger + i\hat{b}^\dagger\right)\left(\hat{a}^\dagger - i\hat{b}^\dagger\right)\right]^N |0\rangle_a|0\rangle_b \tag{5.0.3}$$

$$= \frac{i^N}{2^N N!}\left(\hat{a}^{\dagger 2} + \hat{b}^{\dagger 2}\right)^N |0\rangle_a|0\rangle_b \tag{5.0.4}$$

$$= \frac{i^N}{2^N}\sum_{q=0}^{N}\left[\binom{2q}{q}\binom{2N-2q}{2q}\right]^{1/2} |2q\rangle_a|2N-2q\rangle_b \tag{5.0.5}$$

where we have used results of Eq. A.0.27. We refer to the state in Eq.5.0.5 as the arcsine (AS) state. We assumed that the 50:50 beam splitter BS1 of Fig. 5.1 is of $\hat{J}_1$ type. The two photon ($N = 1$) version of this state is basically a MES

$$|\psi_2\rangle = |2::0\rangle_{a,b}^{\pi} = \frac{1}{\sqrt{2}}\left(|2\rangle_a|0\rangle_b - |0\rangle_a|2\rangle_b\right), \tag{5.0.6}$$

that has long been available in the laboratory [37]. The four-photon version ($N = 2$) given by

$$|\psi_4\rangle = \sqrt{\frac{3}{4}}|4::0\rangle_{a,b}^{\pi} - \frac{1}{2}|2\rangle_a|2\rangle_b, \tag{5.0.7}$$

was also detected in experiments by Ou *et al.* [38]. With the phase shift operator in the both modes (as in Fig. 5.1) represented by $\hat{U}_{\rm PS} = \exp(i\varphi\hat{J}_3)$, the state just prior to the second beam spitter BS2 is

$$\hat{U}_{\rm PS}\hat{U}_{\rm BS1}|{\rm in}\rangle = \frac{i^N}{2^N}\sum_{q=0}^{N} e^{i2\varphi(N-q)}\left[\begin{pmatrix} 2q \\ q \end{pmatrix}\begin{pmatrix} 2N-2q \\ 2q \end{pmatrix}\right]^{1/2} |2q\rangle_a|2N-2q\rangle_b. \tag{5.0.8}$$

Evidently, there are strong correlations between the photon number states of the two modes. Because of this, the only nonzero elements states of the joint photon number probability distribution are the joint probabilities for finding $2k$ photons in mode a and $2N-2k$ in mode b given by

$$P_{AS}(2k, 2N-2k) = |{}_a\langle 2k|{}_b\langle 2N-2k|\psi_{2N}\rangle|^2 \tag{5.0.9}$$

$$= \begin{pmatrix} 2k \\ k \end{pmatrix}\begin{pmatrix} 2N-2k \\ N-k \end{pmatrix}\left(\frac{1}{2}\right)^{2N} \tag{5.0.10}$$

forming a distribution known in probability theory as the fixed-multiplicative discrete arcsine law of order N [39]; hence the name for our state. This should be contrasted with the distribution for the MES of Eq. 3.0.1, which takes the form

$$P_{MES}(2k, 2N-2k) = \frac{1}{2}(\delta_{k,0} + \delta_{k,N}). \tag{5.0.11}$$

In Fig. 5.2 we plot (a) the elements of the joint number distribution $P_{MES}(2k, 2N-2k)$ and (b) the elements of the joint photon number distribution $P_{AS}(2k, 2N-2k)$ for $N = 10$. For the arcsine distribution we see the characteristic "bathtub" shape of

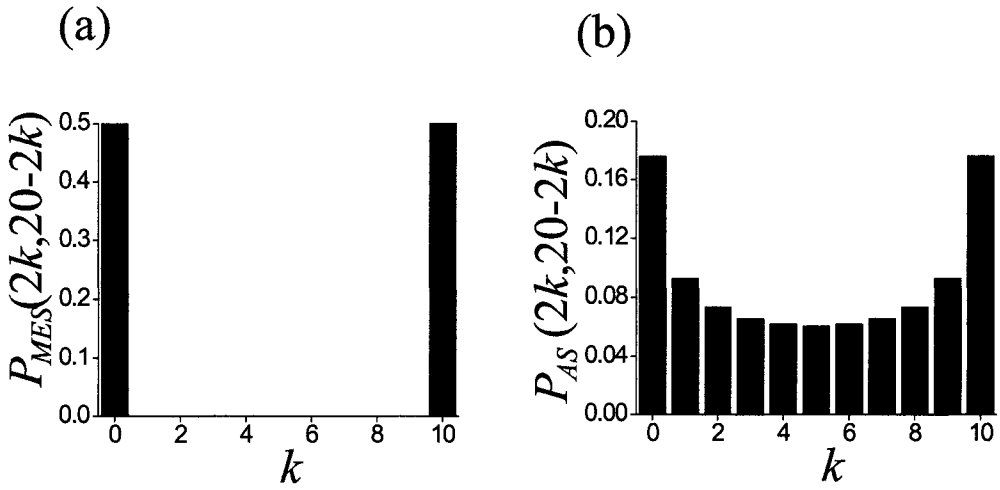

Figure 5.2: (a) Photon number distribution for the maximally entangled states for $2N = 20$; (b)the same for the arcsine state.

an arcsine distribution. Although it would seem from the pictured joint distribution, that the arcsine states represent a poor candidate for precision interferometry, they in fact provide an excellent approximation to the Heisenberg limit in selected ranges of phase difference, as we will see later.

Holland and Burnett [35] assumed that the measurement of the phase difference in the two arms of the MZI could be carried out in the usual way by subtracting the currents of the photodetectors placed at the output ports of the second beam splitter BS2, essentially measuring the operator $\hat{a}^\dagger\hat{a} - \hat{b}^\dagger\hat{b}$ at the output. But for states of the type of Eq. 5.0.8 inside a MZI, this difference will vanish, thus yielding no information on the relative path lengths. This is a result of the symmetry between the two modes of the states inside the MZI. Alternatively, as Hillery, Zou, and Buzek [8] pointed out, the phase-difference distribution just prior to BS2 consists of two narrows peaks, as shown in Fig. 5.3 and it is this double peaked structure that accounts for the vanishing

of the difference in the output fields at BS2. In any case, the photon number difference operator is not a useful measure of the phase difference φ for input twin Fock states.

We now illustrate the phase properties of these states. In Fig 5.3 we plot the phase difference distribution (a) $2N = 10$ and (b) $2N = 20$. The distributions consist mainly of two narrow peaks. Their widths go $\sim 1/2N$ for large N, similarly to the MES. This makes the AS states good candidates for the Heisenberg-limited interferometry, as we shall see below.

We consider a detector that is placed at one of the output beams, for instance, the b mode. Again we choose the parity operator $\hat{\Pi}_b = (-1)^{\hat{b}^\dagger \hat{b}} = \exp(i\pi \hat{b}^\dagger \hat{b})$. With the operator representation for the beam splitter BS2 [5, 10] as mentioned in Appendix B, $\hat{U}_{BS2} = \exp\left[-i\pi(\hat{a}^\dagger \hat{b} - \hat{a}\hat{b}^\dagger)/4\right]$, the expectation value of the parity operator is

$$\left\langle \hat{\Pi}_b \right\rangle = \langle \Psi_{2N}(\varphi) | \hat{U}^\dagger_{\mathrm{BS2}} \hat{\Pi}_b \hat{U}_{\mathrm{BS2}} | \Psi_{2N}(\varphi) \rangle \tag{5.0.12}$$

$$= \frac{1}{2^N} \sum_{q=0}^{N} e^{-i2\varphi(N-2q)} \begin{pmatrix} 2q \\ q \end{pmatrix} \begin{pmatrix} 2N-2q \\ 2q \end{pmatrix} \tag{5.0.13}$$

The imaginary part of the expression in Eq. 5.0.14 sums identically to zero as a sum of odd functions. The surviving part can be written in terms of Legendre polynomials [36]:

$$\left\langle \hat{\Pi}_b \right\rangle_N = P_N \left[\cos(2\varphi)\right]. \tag{5.0.14}$$

The phase uncertainty given from the error propagation as expressed in Eq. 3.0.21 is

$$\Delta\varphi = \frac{\Delta\hat{\Pi}_b}{\left|\partial \left\langle \hat{\Pi}_b \right\rangle / \partial\varphi\right|} \tag{5.0.15}$$

$$= \frac{|\sin(2\varphi)| \sqrt{1 - \left(P_N[\cos(2\varphi)]\right)^2}}{2N \left|\cos(2\varphi) P_N[\cos(2\varphi)] - P_{N-1}[\cos(2\varphi)]\right|} \tag{5.0.16}$$

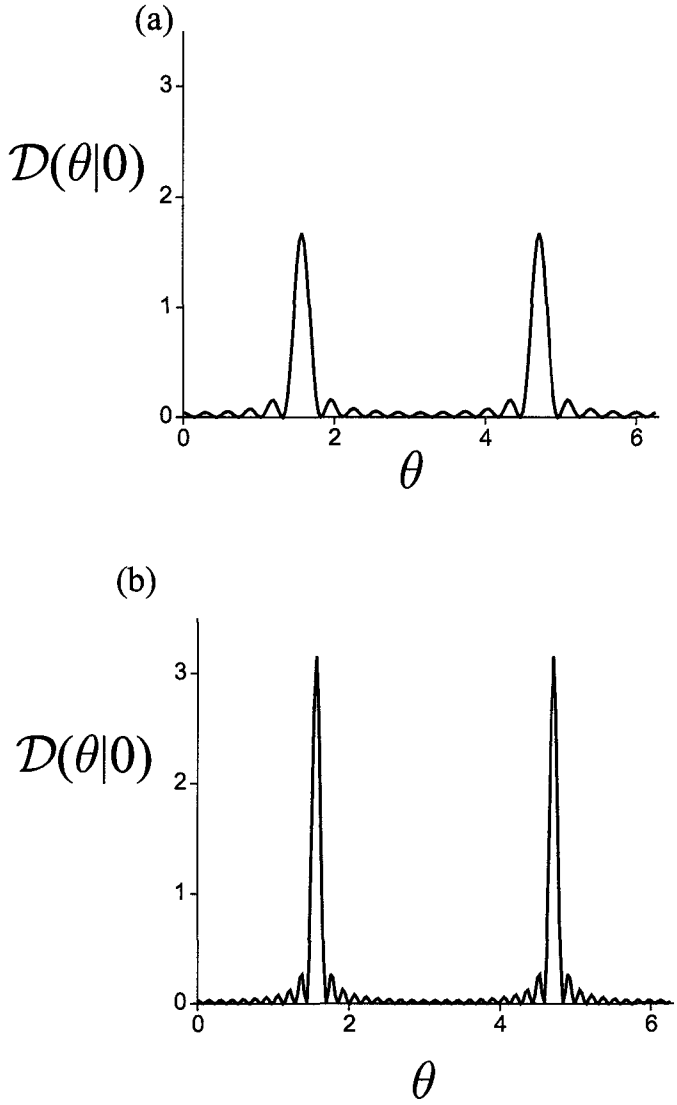

Figure 5.3: Phase difference distribution $\mathcal{D}(\theta|0)$ inside the MZI versus the phase difference between arms b and a for for the input twin Fock states for (a) $N = 5$, (b)$N = 10$.

where $\Delta\Pi_b = \sqrt{\langle\hat{\Pi}_b^2\rangle - \langle\hat{\Pi}_b\rangle^2} = \sqrt{1 - \langle\hat{\Pi}_b\rangle^2}$ as $\hat{\Pi}_b^2 = \hat{I}$. For $N = 1$ we have $\left\langle\hat{\Pi}_b\right\rangle_1 = \cos 2\varphi$ so that $\Delta\varphi = 1/2$, the Heisenberg limit for a total of $2N = 2$ photons. For $N = 2$ (the photomixing of the photons with two photons) we have $\left\langle\hat{\Pi}_b\right\rangle_2 = (3\cos^2 2\varphi - 1)/2 = (1 + 3\cos 4\varphi)/4$, from which we obtain, in the limit $\varphi \to 0$, $\Delta\varphi = 1/\sqrt{12} = 0.2886$, which is just above the Heisenberg limit of $\Delta\varphi_{HL} = 1/4 = 0.25$, and still considerably below the standard quantum limit of $\Delta\varphi_{SQL} = 1/\sqrt{4} = 0.5$, for a total of $2N = 4$ photons passing through the interferometer.

Assuming now that $\varphi = 0$, we plot in Fig. 5.4(a) the phase uncertainty $\Delta\varphi$ obtained from out states as a function of N along with $\Delta\varphi_{HL} = 1/2N$ (dashed line) and $\Delta\varphi_{SQL} = 1/\sqrt{2N}$ (dot-dashed line), where it is clear this is time that the total photon number inside the interferometer is $2N$. We notice that the phase uncertainty for the parity measurement very rapidly approaches the Heisenberg limit for increasing photon number $2N$ and is always much less that the standard quantum limit. In Fig. 5.4(b) we plot the phase uncertainty for $\varphi = \pi/90 = 0.0349$ rad from the origin. Evidently, for certain photon numbers, the phase uncertainty blows up due to periodic nature of $\langle\hat{\Pi}_b\rangle$, but then there are other photon numbers where the uncertainty is still below the standard quantum limit. Therefore the twin Fock states $|N\rangle_a|N\rangle_b$ may still be of use for interferometry for certain N even when the phase difference $\varphi \neq 0$. Of course, for very weak phase shifts, as are expected from gravity waves, and starting from an interferometer where $\varphi = 0$, we still can expect high-resolution phase measurements over a wide range of input phase numbers.

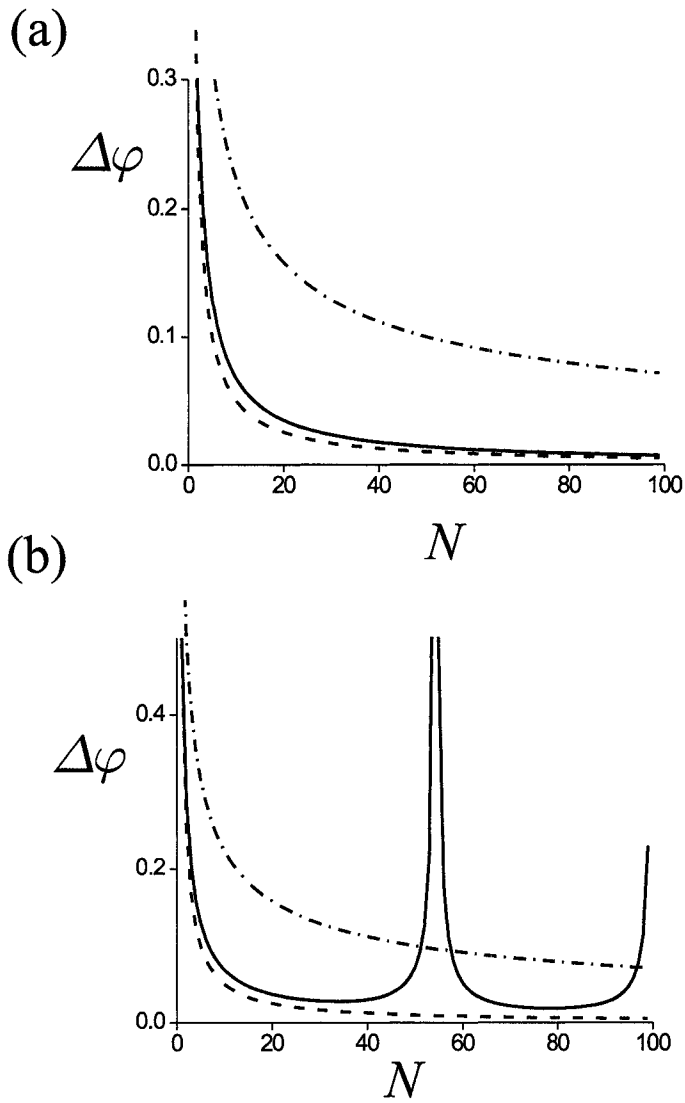

Figure 5.4: Phase difference uncertainty $\Delta\varphi$ (solid line) along with $\Delta\varphi_{SQL}$ (dot-dashed line) and $\Delta\varphi_{HL}$ (dashed line) for (a) $\varphi = 0$, (b)$\varphi = \pi/90$.

Chapter 6

Measurement of Parity

Parity measurements play a crucial role in this thesis. In principle, we can perform parity measurements by counting the number of photons precisely, so we can determine its parity. This method relies on the exact number of photons, then detectors capable of distinguishing photon numbers at a single one are required. Currently such detectors are not available. As an alternative, we suggest two methods that amount at determining parity of the number of photons without knowing the photon number. The first method, that we will discuss is based on a symmetric nonlinear interferometer (SNLI). We then discuss a quantum non-demolition approach to measuring parity.

6.1 Parity Measurements with the Symmetric Nonlinear Interferometer

In Fig. 6.1 we sketch the SNLI, an MZI with Kerr media in both arms. We follow through the case of the input state $|\text{in}\rangle = |\alpha\rangle_a |0\rangle_b$. After the first beam splitter we again have $\left|\alpha/\sqrt{2}\right\rangle_a \left|i\alpha/\sqrt{2}\right\rangle_b$. The phase shift operators $\exp(i\phi_a \hat{a}^\dagger \hat{a}) \exp(i\phi_b \hat{b}^\dagger \hat{b})$ produce $\left|\alpha e^{i\phi_a}/\sqrt{2}\right\rangle_a \left|i\alpha e^{i\phi_b}/\sqrt{2}\right\rangle_b$. With the choices $\phi_a = -\pi/2 = \phi_b$, the Kerr

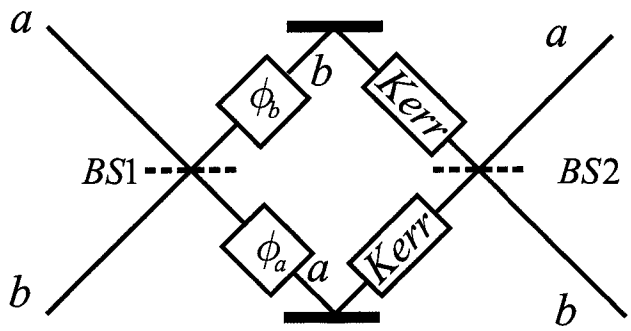

Figure 6.1: The symmetric nonlinear interferometer (SNLI). The required phase shift are $\phi_a = -\pi/2 = \phi_b$.

media, described by the operatorexp$(-i\kappa\hat{a}^{\dagger 2}\hat{a})^2 \exp(-i\kappa\hat{b}^{\dagger 2}\hat{b}^2)$, with $\kappa = \pi/2$, produce

$$\frac{1}{2}\left[e^{-i\pi/2}\left|\alpha/\sqrt{2}\right\rangle_a\left|i\alpha/\sqrt{2}\right\rangle_b + e^{i\pi/2}\left|-\alpha/\sqrt{2}\right\rangle_a\left|-i\alpha/\sqrt{2}\right\rangle_b\right. \tag{6.1.1}$$

$$\left. + \left|-\alpha/\sqrt{2}\right\rangle_a\left|i\alpha/\sqrt{2}\right\rangle_b + \left|\alpha/\sqrt{2}\right\rangle_a\left|-i\alpha/\sqrt{2}\right\rangle_b\right]. \tag{6.1.2}$$

Lastly, the second beam splitter produces the output state

$$|\text{out}\rangle = \frac{1}{2}\left[-i|0\rangle_a|i\alpha\rangle_b + i|0\rangle_a|-i\alpha\rangle_b + |-\alpha\rangle_a|0\rangle_b + |\alpha\rangle_a|0\rangle_b\right]. \tag{6.1.3}$$

We may rewrite this more transparently as

$$|\text{out}\rangle = \frac{1}{2}\left[-i|0\rangle_a(|i\alpha\rangle_b - |-i\alpha\rangle_b) + (|\alpha\rangle_a + |-\alpha\rangle_a)|0\rangle_b\right]. \tag{6.1.4}$$

Evidently, the symmetric NLI generates an entanglement of the vacuum with the even and odd coherent states, where even coherent states are already defined in Eq. 4.3.19, and odd coherent states are states of the form

$$\left(1 - e^{-|\alpha|^2/2}\right)^{-1/2}(|\alpha\rangle - |-\alpha\rangle) \tag{6.1.5}$$

Suppose a photodetector is placed in the output of mode a, with no detector in the output of mode b. If the vacuum is detected (i.e., a "no count" detection) in the

output a mode, the b mode is projected into the odd coherent state $|i\alpha\rangle - |-i\alpha\rangle$. Conversely, if the detector is placed in output mode b and if a vacuum state is detected then the a mode is projected into an even coherent state $|\alpha\rangle + |-\alpha\rangle$ (apart from the normalization). Notice that only one detector (in either output beam) is used to make these projections. So we have found yet another procedure for generating single-mode Schrödinger-cat states.

In terms of the number states the output state of Eq. 6.1.4 maybe written as

$$|\text{out}\rangle = e^{-|\alpha|^2/2}\left[-i\sum_{N,\text{odd}}^{\infty}\frac{(i\alpha)^N}{\sqrt{N!}}|0\rangle_a|N\rangle_b + \sum_{N,\text{even}}^{\infty}\frac{\alpha^N}{\sqrt{N!}}|N\rangle_a|0\rangle_b\right]. \tag{6.1.6}$$

The probability of detecting the vacuum in mode b is

$$\text{Prob}(|0\rangle_b) = \langle\text{out}|0\rangle_{bb}\langle 0|\text{out}\rangle = e^{-|\alpha|^2}\sum_{N,\text{even}}^{\infty}\frac{|\alpha|^{2N}}{N!}, \tag{6.1.7}$$

while the probability of detecting the vacuum in mode a is

$$\text{Prob}(|0\rangle_a) = \langle\text{out}|0\rangle_{aa}\langle 0|\text{out}\rangle = e^{-|\alpha|^2}\left(1+\sum_{N,\text{odd}}^{\infty}\frac{|\alpha|^{2N}}{N!}\right). \tag{6.1.8}$$

In this last expression the $+1$ appears in the parentheses because the vacuum state $|0\rangle_a$ appears not only correlated with all the odd number states of mode b, but also with the vacuum state $|0\rangle_b$. Of course, for large $|\alpha|$ that contribution is nil and to a good approximation $\text{Prob}(|0\rangle_a) \approx \frac{1}{2} \approx \text{Prob}(|0\rangle_b)$. From Eq. 6.1.6 we deduce that if the input to the SNLI is $|\text{in}\rangle = |N\rangle_a|0\rangle_b$ the output will be

$$|\text{out}\rangle = \begin{cases} |N\rangle_a|0\rangle_b, & N \text{ even} \\ -i^{N+1}|0\rangle_a|N\rangle_b, & N \text{ odd}. \end{cases} \tag{6.1.9}$$

Evidently, the SNLI acts as filter with respect to parity. All one needs to do is place photodetectors in *both* of the output modes, and by noting which detector fires (and/or which does not fire) the parity can be determined. It will not be necessary

to employ detectors with resolutions at the level of a single photon. The action of the SNLI is very similar to that of the nonlinear four-wave mixing device described by Yurke and Stoler [29], which produces essentially identical output states for the given inputs as the symmetric NLI. However, the former requires two competing nonlinear interactions, a cross-Kerr and four-wave mixing, while the later requires only single-mode Kerr interactions. Evidently, the symmetric NLI is capable of performing the parity measurements required for the interferometric measurements discussed previously.

For the sake of completeness, we state the output of the symmetric NLI with coherent state inputs in both modes. If $|\text{in}\rangle = |\alpha\rangle_a|\beta\rangle_b$ then

$$|\text{out}\rangle = \frac{1}{2}\left[-i|i\beta\rangle_a|i\alpha\rangle_b + i|-i\beta\rangle_a|-i\alpha\rangle_b + |\alpha\rangle_a|-\beta\rangle_b + |-\alpha\rangle_a|\beta\rangle_b\right]. \quad (6.1.10)$$

Thus we obtain a four-component entanglement of coherent states of the two modes. In terms of the number states we have

$$|\text{out}\rangle = \frac{1}{2}e^{-(|\alpha|^2+|\beta|^2)/2}\sum_{M=0}^{\infty}\sum_{N=0}^{\infty}\left\{i^{M+N+1}\left[-1+(-1)^{M+N}\right]|M\rangle_a|N\rangle_b + \left[(-1)^N+(-1)^M\right]|N\rangle_a|M\rangle_b\right\}. \quad (6.1.11)$$

Thus for input number state $|N\rangle_a|M\rangle_b$ we obtain the ouput state

$$|\text{out}\rangle = \frac{1}{2}\left\{i^{M+N+1}\left[-1+(-1)^{M+N}\right]|M\rangle_a|N\rangle_b + \left[(-1)^N+(-1)^M\right]|N\rangle_a|M\rangle_b\right\}. \quad (6.1.12)$$

If M and N are both even or both are odd, then apart from irrelevant phase factors we have $|N\rangle_a|M\rangle_b \xrightarrow{\text{SNLI}} |N\rangle_a|M\rangle_b$; the photons do not exchange modes. But if one of them is even and the other odd we have $|N\rangle_a|M\rangle_b \xrightarrow{\text{SNLI}} |M\rangle_a|N\rangle_b$; the photons collectively exchange modes. In this case it will not be possible to determine the parity of the

states of the individual modes, only that they are different. In summary, if either M or N is zero we can determine the parity; if they are nonzero we can determine if they have different or the same parity if they exchange modes or not. We cannot determine the parity of the individual number states except in the case where one of the input modes is in the vacuum.

6.2 Quantum Non-demolition Measurement of Parity

The notion of the quantum non-demolition measurement of photon number has been around for some time and was originally discussed by Imoto, Haus and Yamamoto [20] and subsequently discussed by other authors [40, 41, 42]. This approach utilizes a two-mode cross-Kerr and also requires a large nonlinear susceptibility $\chi^{(3)}$. Encouraged by the recent advances in EIT mentioned above, Munro *et al.* [43] have recently discussed a proposal for a high-efficiency quantum non-demolition single photon number resolving detector containing less than 1600 atoms embedded in a dielectric waveguide. A number state in the signal mode induces a phase shift on the coherent state in the probe mode, the phase shift, being dependent on the photon number, can be detected via homodyning on a quadrature of the probe field. The number state itself is not destroyed.

In this section, we go further and show that one can use a similar technique to measure the parity of optical fields non-destructively though without the need to perform quadrature measurements of the signal field to obtain the photon number itself. Our method does require a kind of homodying on the probe field but immediately yields even/odd as answers. In fact, photon measurements on the probe field can

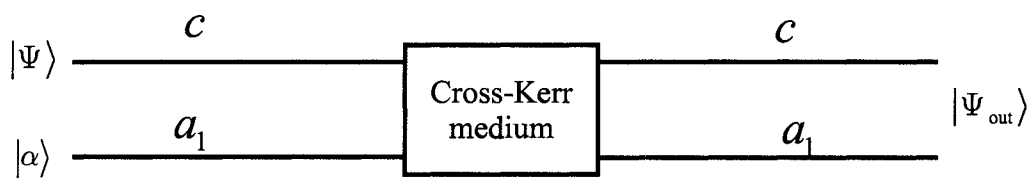

Figure 6.2: Cross-Kerr interaction with $|\Psi\rangle_c|\alpha\rangle_{a_1}$ as an input state and $|\Psi_{\text{out}}\rangle$ is the output state.

be entirely insensitive to photon number and one needs only to distinguish between there being some photons and none. We further show that the scheme we propose can not only measure parity but also be used the create, via von Neumann projective measurements, states of definite parity and states of a "higher order" parity that have been proposed as the basis of a scheme for quantum key distribution [44].

In Fig 6.2 we depict a proposed scheme for a device that measures parity. The scheme consists of a cross-Kerr interaction with two input ports and two output ports. Let assume we want to determine the parity of a general state

$$|\Psi\rangle = \sum_{n=0}^{\infty} c_n |n\rangle_c \tag{6.2.1}$$

that we inject in the input port c and where the coefficients c_n satisfy the usual normalization relation $\sum_{n=0}^{\infty} |c_n|^2 = 1$. With a coherent state $|\alpha\rangle_{a_1}$ in the second input port a_1, so that our input state can be written as

$$|\Psi_{\text{in}}\rangle = |\Psi\rangle|\alpha\rangle_{a_1} \tag{6.2.2}$$

$$= \sum_{n=0}^{\infty} c_n |n\rangle_c |\alpha\rangle_{a_1}, \tag{6.2.3}$$

where

$$|\alpha\rangle_{a_1} = e^{-|\alpha|^2/2} \sum_{n'=0}^{\infty} \frac{\alpha^{n'}}{\sqrt{n'!}} |n'\rangle_{a_1}. \tag{6.2.4}$$

The cross-Kerr interaction Hamiltonian can be described by the following expression

$$\hat{H}_K = \hbar\chi \hat{a}_1^\dagger \hat{a}_1 \hat{c}^\dagger \hat{c}, \tag{6.2.5}$$

where χ is proportional to the third order nonlinear susceptibility $\chi^{(3)}$, and $\hat{a}_1$ and $\hat{c}$ are the usual creation operators related to the modes a_1 and c, respectively. The output state of the cross interaction is obviously given by

$$|\Psi_{\text{out}}\rangle = e^{-i\hat{H}_K t/\hbar} |\Psi_{\text{in}}\rangle \tag{6.2.6}$$

$$= e^{-i\chi t \hat{a}_1^\dagger \hat{a}_1 \hat{c}^\dagger \hat{c}} |\Psi\rangle_c |\alpha\rangle_{a_1} \tag{6.2.7}$$

$$= \sum_{n=0}^{\infty} c_n |n\rangle_c |\alpha e^{-i\chi t n}\rangle_{a_1}. \tag{6.2.8}$$

Now we assume that we can set $\chi t = \pi$, thus we have

$$\begin{aligned} |\Psi_{\text{out}}\rangle &= \sum_{n=0}^{\infty} c_n |n\rangle_c \, |(-1)^n \alpha\rangle_{a_1} \\ &= \left(\sum_{n,\text{even}}^{\infty} c_n |n\rangle_c \right) |\alpha\rangle_{a_1} + \left(\sum_{n,\text{odd}}^{\infty} c_n |n\rangle_c \right) |-\alpha\rangle_{a_1} \\ &= |\Psi_e\rangle \, |\alpha\rangle_{a_1} + |\Psi_o\rangle \, |-\alpha\rangle_{a_1}, \end{aligned} \tag{6.2.9}$$

where $|\Psi_e\rangle$ and $|\Psi_o\rangle$ are defined as

$$|\Psi_e\rangle = \sum_{n,\text{even}}^{\infty} c_n |n\rangle_c \tag{6.2.10}$$

$$|\Psi_o\rangle = \sum_{n,\text{odd}}^{\infty} c_n |n\rangle_c. \tag{6.2.11}$$

The two-mode state of Eq. 6.2.9 is an entangled state. Clearly if one detects $|\alpha\rangle_{a_1}$ in mode a_1 the state in mode c becomes $|\Psi_e\rangle_c$, and if one detects $|-\alpha\rangle_{a_1}$ the projected state in mode c is $|\Psi_e\rangle_c$. The question that one may ask is: how do we detect the states $|\alpha\rangle_{a_1}$ and $|-\alpha\rangle_{a_1}$? The answer is: homodying detection. To that direction,

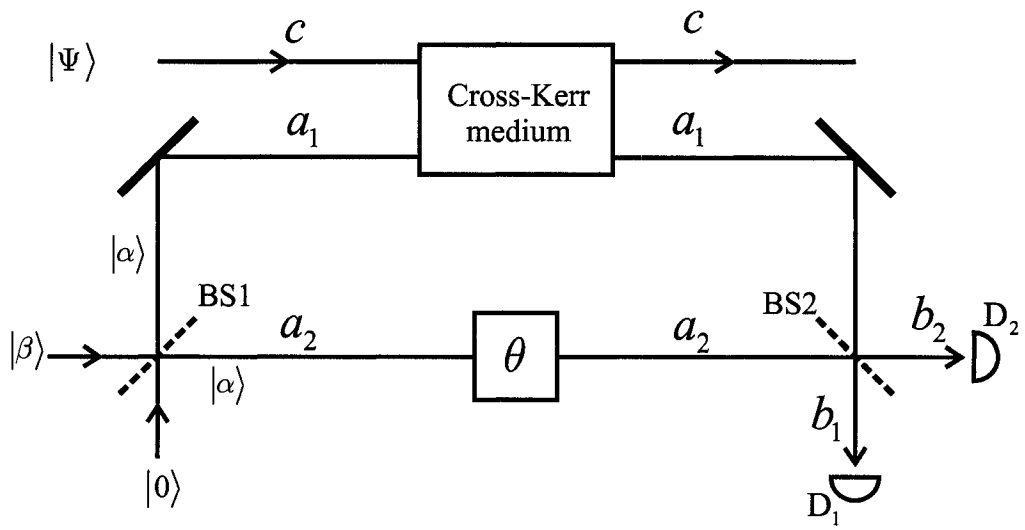

Figure 6.3: Schematic for performing non-demolition parity measurements. See text for details.

we propose the schematic depicted in Fig. 6.3. With an input state $|\Psi\rangle_c|\beta\rangle_{a_1}|0\rangle_{a_2} = |\Psi\rangle_c\left|\sqrt{2}\alpha\right\rangle_{a_1}|0\rangle_{a_2}$ we obtain $|\Psi\rangle_c|\alpha\rangle_{a_1}|\alpha\rangle_{a_2}$ right after the BS1, given that BS1 is a 50:50 $\hat{J}_2$-type beam splitter. Using Eq. 6.2.9, the state right after the cross-Kerr media is of the form

$$|\Psi_e\rangle_c|\alpha\rangle_{a_1}|\alpha\rangle_{a_2} + |\Psi_o\rangle_c|\alpha\rangle_{a_1}|-\alpha\rangle_{a_2}. \tag{6.2.12}$$

The beam splitter BS2 is a 0:50 $\hat{J}_2$-type, so the unitary transformation associated with it is given as

$$\hat{U}_{\rm BS} = \exp\left(i\pi\hat{J}_2/2\right). \tag{6.2.13}$$

We can write the output annihilation operators associated with the output ports of BS2 as

$$\hat{b}_1 = \hat{U}_{\rm BS2}\hat{a}_1\hat{U}^{\dagger}_{\rm BS2} = \frac{1}{\sqrt{2}}\left(\hat{a}_1 + \hat{a}_2\right)$$
$$\hat{b}_2 = \hat{U}_{\rm BS2}\hat{a}_2\hat{U}^{\dagger}_{\rm BS2} = \frac{1}{\sqrt{2}}\left(-\hat{a}_1 + \hat{a}_2\right). \qquad (6.2.14)$$

Now at the second beam splitter we have the following transformations

$$\hat{U}_{\rm BS2}|\alpha\rangle_{a_1}|\alpha\rangle_{a_2} = \left|\sqrt{2}\alpha\right\rangle_{b_1}|0\rangle_{b_2} \qquad (6.2.15)$$
$$\hat{U}_{\rm BS2}|-\alpha\rangle_{a_1}|\alpha\rangle_{a_2} = |0\rangle_{b_1}\left|\sqrt{2}\alpha\right\rangle_{b_2},$$

where we have used Eq. 6.2.14.

The three-mode output state just before the detectors D_1 and D_2 is

$$|\Psi\rangle_{\rm out} = |\Psi_e\rangle_c\left|\sqrt{2}\alpha\right\rangle_{b_1}|0\rangle_{b_2} + |\Psi_o\rangle_c|0\rangle_{b_1}\left|\sqrt{2}\alpha\right\rangle_{b_2}, \qquad (6.2.16)$$

a three-mode entangled state. So if any photons are detected in b_1-mode, but none in b_2, we have detected even parity. If any are detected in b_2-mode but none in b_1-mode, we have detected odd parity. For instance, let assume that $|\Psi\rangle = |N\rangle$. State in Eq. 6.2.16 becomes a separable state of the following form

$$|\Psi\rangle_{\rm out} = \begin{cases} |N\rangle_c\left|\sqrt{2}\alpha\right\rangle_{b_1}|0\rangle_{b_2} & N \text{ even} \\ |N\rangle_c|0\rangle_{b_1}\left|\sqrt{2}\alpha\right\rangle_{b_2} & N \text{ odd.} \end{cases} \qquad (6.2.17)$$

In the case of an even N, D_1 will click and D_2 will not, and only D_2 clicks in the case of an odd N. More importantly, notice none of the detected states in mode c is demolished in either case, even or odd state. Before we discuss the general case, where we may have a state with odd and even photon number sates we want to show another important use of the proposed scheme. In fact, for the particular case where we assume that

$$|\Psi\rangle = |\beta\rangle = e^{-|\beta|^2/2}\sum_{n=0}^{\infty}\frac{\beta^n}{\sqrt{n!}}|n\rangle,$$

so the corresponding even and odd states, properly normalized are the usual even and odd cat states

$$|\Psi_e\rangle = \mathcal{N}_e(|\beta\rangle + |-\beta\rangle) \equiv |\beta_+\rangle$$
$$|\Psi_o\rangle = \mathcal{N}_o(|\beta\rangle - |-\beta\rangle) \equiv |\beta_-\rangle, \tag{6.2.18}$$

where

$$\mathcal{N}_e = \frac{1}{\sqrt{2}}\left(1 + e^{-2|\alpha|^2}\right)^{-1/2}, \tag{6.2.19}$$
$$\mathcal{N}_o = \frac{1}{\sqrt{2}}\left(1 - e^{-2|\alpha|^2}\right)^{-1/2}. \tag{6.2.20}$$

This time any detection of photons at detector D_1 and none at D_2 signals the presence of even-cat state in mode c. And if detector D_2 clicks and D_1 does not detect any photon, we know that the original state in mode c is projected into an odd-cat state.

In the general case, we assume that we have a state consisting of both even and odd photon numbers. This time we represent the light in mode c by the density operator

$$\hat{\rho}_c = \sum_{m=0}^{\infty}\sum_{n=0}^{\infty} \rho_{n,m}|n\rangle_c\ {}_c\langle m|, \tag{6.2.21}$$

and the same way we can express the mode a_1 by

$$\hat{\rho}_c = |\alpha\rangle_{a_1}\ {}_{a_1}\langle\alpha|. \tag{6.2.22}$$

The input density operator is basically a direct product of modes c and a_1. We can write this as

$$\hat{\rho}(0) = \hat{\rho}_c \otimes \hat{\rho}_{a_1} \tag{6.2.23}$$

Right after the cross-Kerr interaction the density operator is described by

$$\hat{\rho}(t) = e^{-i\hat{H}_K t/\hbar}\hat{\rho}(0)e^{i\hat{H}_K t/\hbar}, \tag{6.2.24}$$

where t is the time of interaction. Again, we set $\chi t = \pi$ and we end up by the following expression for the density operator

$$\hat{\rho}(\pi/\chi) = e^{-i\hat{H}_K t/\hbar}\hat{\rho}(0)e^{i\hat{H}_K t/\hbar} \tag{6.2.25}$$

$$= \sum_{m=0}^{\infty}\sum_{n=0}^{\infty}\rho_{n,m}\left(|n\rangle_c\,|(-1)^n\alpha\rangle_{a_1}\right)\left({}_c\langle m|_{a_1}\,\langle(-1)^m\alpha|\right) \tag{6.2.26}$$

$$= \hat{\rho}_{++}|\alpha\rangle_{a_1\ a_1}\langle\alpha| + \hat{\rho}_{--}|-\alpha\rangle_{a_1\ a_1}\langle-\alpha|$$

$$+ \hat{\rho}_{+-}|\alpha\rangle_{a_1\ a_1}\langle-\alpha| + \hat{\rho}_{-+}|-\alpha\rangle_{a_1\ a_1}\langle\alpha| \tag{6.2.27}$$

where

$$\hat{\rho}_{++} = \sum_{m,\text{even}}^{\infty}\sum_{n,\text{even}}^{\infty}\rho_{n,m}|n\rangle_{c\ c}\langle m| \tag{6.2.28}$$

$$\hat{\rho}_{--} = \sum_{m,\text{odd}}^{\infty}\sum_{n,\text{odd}}^{\infty}\rho_{n,m}|n\rangle_{c\ c}\langle m| \tag{6.2.29}$$

$$\hat{\rho}_{+-} = \sum_{m,\text{even}}^{\infty}\sum_{n,\text{odd}}^{\infty}\rho_{n,m}|n\rangle_{c\ c}\langle m| \tag{6.2.30}$$

$$\hat{\rho}_{-+} = \sum_{m,\text{odd}}^{\infty}\sum_{n,\text{even}}^{\infty}\rho_{n,m}|n\rangle_{c\ c}\langle m|. \tag{6.2.31}$$

Now at the second beam splitter we have the following transformations

$$|\alpha\rangle_{a_1\ a_1}\langle\alpha| \otimes |\alpha\rangle_{a_2\ a_2}\langle\alpha| \longrightarrow \left(\left|\sqrt{2}\alpha\right\rangle_{b_1}|0\rangle_{b_2}\right)\left({}_{b_1}\left\langle\sqrt{2}\alpha\right|{}_{b_2}\langle 0|\right) \tag{6.2.32}$$

$$|-\alpha\rangle_{a_1\ a_1}\langle-\alpha| \otimes |\alpha\rangle_{a_2\ a_2}\langle\alpha| \longrightarrow \left(|0\rangle_{b_1}\left|\sqrt{2}\alpha\right\rangle_{b_2}\right)\left({}_{b_1}\langle 0|_{b_2}\left\langle\sqrt{2}\alpha\right|\right) \tag{6.2.33}$$

$$|\alpha\rangle_{a_1\ a_1}\langle-\alpha| \otimes |\alpha\rangle_{a_2\ a_2}\langle\alpha| \longrightarrow \left(\left|\sqrt{2}\alpha\right\rangle_{b_1}|0\rangle_{b_2}\right)\left({}_{b_1}\langle 0|_{b_2}\left\langle\sqrt{2}\alpha\right|\right) \tag{6.2.34}$$

$$|-\alpha\rangle_{a_1\ a_1}\langle-\alpha| \otimes |\alpha\rangle_{a_2\ a_2}\langle\alpha| \longrightarrow \left(|0\rangle_{b_1}\left|\sqrt{2}\alpha\right\rangle_{b_2}\right)\left({}_{b_1}\left\langle\sqrt{2}\alpha\right|{}_{b_2}\langle 0|\right) \tag{6.2.35}$$

where Eqs. 6.2.15 have been used. So after the beam splitter, just before the detectors, we have

$$\hat{\rho} = \hat{\rho}_{++} \left(|\gamma\rangle_{b_1}|0\rangle_{b_2}\right) \left({}_{b_1}\langle\gamma|_{b_2}\langle 0|\right) + \hat{\rho}_{--} \left(|0\rangle_{b_1}|\gamma\rangle_{b_2}\right) \left({}_{b_1}\langle 0|_{b_2}\langle\gamma|\right) \tag{6.2.36}$$

$$+ \hat{\rho}_{+-} \left(|\gamma\rangle_{b_1}|0\rangle_{b_2}\right) \left({}_{b_1}\langle 0|_{b_2}\langle\gamma|\right) + \hat{\rho}_{-+} \left(|0\rangle_{b_1}|\gamma\rangle_{b_2}\right) \left({}_{b_1}\langle\gamma|_{b_2}\langle 0|\right), \tag{6.2.37}$$

where we define $\gamma = \sqrt{2}\alpha$.

If we measure photon in b_1 and vacuum in b_2, we project the state onto $|\gamma\rangle_{b_1}|0\rangle_{b_2}$. Then we have the collapse to the non-normalized state vector:

$$\hat{\rho} \longrightarrow {}_{b_1}\langle\gamma|_{b_2}\langle 0|\hat{\rho}|\gamma\rangle_{b_1}|0\rangle_{b_2}. \tag{6.2.38}$$

If γ is large enough so that $\langle\gamma|0\rangle = 0$, we shall have $\hat{\rho} \longrightarrow \hat{\rho}_{++}$. This needs to be normalized, which we write as

$$\hat{\tilde{\rho}}_{++} = \left(\sum_{n \text{ even}}^{\infty} \rho_{nn}\right)^{-1} \sum_{n,m \text{ even}}^{\infty} \rho_{nm}. \tag{6.2.39}$$

In the same way, if $|0\rangle_{b_1}|\gamma\rangle_{b_2}$ is detected then we have the collapse

$$\hat{\rho} \longrightarrow {}_{b_1}\langle 0|_{b_2}\langle\gamma|\hat{\rho}|0\rangle_{b_1}|\gamma\rangle_{b_2} = \hat{\rho}_{--}. \tag{6.2.40}$$

The corresponding normalized state is

$$\hat{\tilde{\rho}}_{--} = \left(\sum_{n \text{ odd}}^{\infty} \rho_{nn}\right)^{-1} \sum_{n,m \text{ odd}}^{\infty} \rho_{nm}. \tag{6.2.41}$$

These exhaust all possibilities for measurement.

Chapter 7

Parity Measurements in an All or Nothing Test of Quantum Mechanics

In this chapter we discuss an application of parity measurement to something other than interferometer. In particular, we apply it to a possible large-scale test of quantum mechanics versus the predictions of local hidden variable theories.

Some years ago, Greenberger, Horne, and Zeilinger (GHZ) [45], proposed a new form of Bell's theorem [46] whereby contradictions between quantum mechanics and local realistic theories can be exposed, not in the statistical manner of the original formulation of Bell [46], but in one set of measurements from a single run of an experiment, this test being an "all or nothing test of quantum mechanics". The GHZ approach requires entangled states of three or more "particles". A typical GHZ state for three spin-1/2 particles has the simple form

$$|\Psi_{\rm GHZ}\rangle = \frac{1}{\sqrt{2}}\left(|+\rangle_1|+\rangle_2|+\rangle_3 - |-\rangle_1|-\rangle_2|-\rangle_3\right), \tag{7.0.1}$$

where $|\pm\rangle$ are spin up or down along some axis, usually taken to be the z-axis. In cases where the "particles" are photons, the GHZ states considered are typically

polarization entangled single photon states of the form

$$|\Psi_{\rm GHZ}\rangle = \frac{1}{\sqrt{2}}\left(|H\rangle_1|H\rangle_2|H\rangle_3 - |V\rangle_1|V\rangle_2|V\rangle_3\right), \tag{7.0.2}$$

where $|H\rangle_1$ is the state of a horizontally polarized single photon in mode 1 while $|V\rangle_1$ is the state of a vertically polarized single photon in the same mode, etc. Zeilinger *et al.* [47] have experimentally realized such a state and have used it to demonstrate violations of local realistic theories.

A few years ago, Gerry [48] proposed, in the context of cavity QED, a method to generate a three-mode entanglement of coherent states of the form

$$|\Psi_{\rm GHZ}\rangle = \frac{1}{\sqrt{2}}\left(|\alpha\rangle_1|\alpha\rangle_2|\alpha\rangle_3 - |-\alpha\rangle_1|-\alpha\rangle_2|-\alpha\rangle_3\right), \tag{7.0.3}$$

a GHZ state featuring distinguishable coherent states, the coherent states given by

$$|\alpha\rangle = \exp -|\alpha|^2/2)\sum_{n=0}^{\infty}\frac{\alpha^n}{\sqrt{n!}}|n\rangle, \tag{7.0.4}$$

as long as α, which we assume real, is large enough in a sense the we shall describe below. The modes in each case are cavity modes in three separated cavities. This state formally exhibits violations of local realism with respect to parity measurements performed by atoms and selective field ionization. However, in the context of cavity QED, there is no possibility for the space-like separation of the measurement events as the cavities must be adjacent. In this present work, we propose a method of generating states of the form of Eq. 7.0.3 and a test of local realistic theories against quantum mechanics in the optical regime where space-like separations of the measurement events are possible. Further, we examine the effect of field decoherence. Our proposed production method is based on an extension of a method previously put forward [49] for the generation of single-mode optical Schrödinger cat states of the form $|\alpha\rangle \pm |\alpha\rangle$.

Before discussing the proposed production method, we first review the analogy between the coherent states $|\alpha\rangle$ and $|-\alpha\rangle$ and their superpositions, to a two-level system, such as that of a spin one-half particle in a magnetic field. We consider the states

$$|\alpha_{\pm}\rangle = \mathcal{N}_{\pm}(|\alpha\rangle \pm |-\alpha\rangle), \tag{7.0.5}$$

where

$$\mathcal{N}_{\pm} = \frac{1}{\sqrt{2}}\left(1 \pm e^{-2|\alpha|^2}\right)^{-1/2} \tag{7.0.6}$$

are the respective normalization factors. These are the usual Schrödinger cat states mentioned in Eqs. 6.2.18. For large, the states $|\alpha\rangle$ and $|-\alpha\rangle$ are orthogonal. Actually, α need not be all that large. For example, for $\alpha = 2$ we have $\exp(-|\alpha|^2) \simeq 0.00035$ and thus the states $|\alpha = 2\rangle$ and $|-\alpha = -2\rangle$ are practically orthogonal. We do not yet make the assumption of large α, however. The states $|\alpha_{\pm}\rangle$ are eigenstates of the parity operator $\hat{\Pi} = (-1)^{\hat{N}} = \exp(i\pi\hat{N})$, where is the number operator for the relevant mode, such that

$$\hat{\Pi}|\alpha_{\pm}\rangle = \pm|\alpha_{\pm}\rangle. \tag{7.0.7}$$

From Eq. 7.0.5, it is easy to see that the states $|\alpha_{\pm}\rangle$ contain only even or odd photon number states, respectively. An alternative way of writing the parity operator is

$$\hat{\Pi} = \hat{\Sigma}_z = |\alpha_+\rangle\langle\alpha_+| - |\alpha_-\rangle\langle\alpha_-| \tag{7.0.8}$$

thus indicating that even and odd parity is analogous to spin up and spin down states for a spin one-half particle. The operator $\hat{\Sigma}_z$ is a Pauli operator, the label z representing a fictitious quantization axis, and we can define two more operators to

get the complete set of Pauli operators

$$\begin{aligned}\hat{\Sigma}_x &= |\alpha_+\rangle\langle\alpha_-| + |\alpha_-\rangle\langle\alpha_+| \\ \hat{\Sigma}_y &= i(|\alpha_+\rangle\langle\alpha_-| - |\alpha_-\rangle\langle\alpha_+|) \\ \hat{\Sigma}_z &= |\alpha_+\rangle\langle\alpha_+| - |\alpha_-\rangle\langle\alpha_-|\end{aligned} \tag{7.0.9}$$

which satisfy the Pauli spin algebra

$$\begin{aligned}\left[\hat{\Sigma}_i, \hat{\Sigma}_j\right] &= 2i\epsilon_{ijk}\hat{\Sigma}_k \\ \left\{\hat{\Sigma}_i, \hat{\Sigma}_j\right\} &= 2i\delta_{ij}\end{aligned} \tag{7.0.10}$$

where $\{,\}$ is an anti-commutator. Thus we have shown that parity states $|\alpha_\pm\rangle$ and the set of non-commuting operators of Eq. 7.0.10 are isomorphic to the spin up and spin down states, $|\pm\rangle$, of a spin one-half particle and the attendant algebra of the Pauli spin matrices, respectively. The eigenstates of the operator $\hat{\Sigma}_x$ are

$$\begin{aligned}|\alpha_{x+}\rangle &= \frac{1}{\sqrt{2}}(|\alpha_+\rangle + |\alpha_-\rangle) = \frac{1}{2\sqrt{2}}\left[\left(\frac{1}{\mathcal{N}_+} + \frac{1}{\mathcal{N}_-}\right)|\alpha\rangle + \left(\frac{1}{\mathcal{N}_+} - \frac{1}{\mathcal{N}_-}\right)|-\alpha\rangle\right] \\ |\alpha_{x-}\rangle &= \frac{1}{\sqrt{2}}(|\alpha_+\rangle - |\alpha_-\rangle) = \frac{1}{2\sqrt{2}}\left[\left(\frac{1}{\mathcal{N}_+} - \frac{1}{\mathcal{N}_-}\right)|\alpha\rangle + \left(\frac{1}{\mathcal{N}_+} + \frac{1}{\mathcal{N}_-}\right)|-\alpha\rangle\right]\end{aligned} \tag{7.0.11}$$

with eigenvalues ± 1 respectively. Thus we can write $\hat{\Sigma}_x$ as

$$\begin{aligned}\hat{\Sigma}_x &= |\alpha_{x+}\rangle\langle\alpha_{x+}| - |\alpha_{x-}\rangle\langle\alpha_{x-}| \\ &= \frac{1}{2}\left[(\mathcal{N}_+ + \mathcal{N}_-)^2 - (\mathcal{N}_+ - \mathcal{N}_-)^2\right](|\alpha\rangle\langle\alpha| - |-\alpha\rangle\langle-\alpha|)\end{aligned} \tag{7.0.12}$$

where we have used Eqs. 7.0.5. Evidently, in the case where α is large, the eigenstates of $\hat{\Sigma}_x$ go over according to $|\alpha_{x\pm}\rangle \rightarrow |\pm\alpha\rangle$and the operator itself goes over to the form

$$\hat{\Sigma}_x \rightarrow |\alpha\rangle\langle\alpha| - |-\alpha\rangle\langle-\alpha|. \tag{7.0.13}$$

The eigenstates of $\hat{\Sigma}_y$ are

$$|\alpha_{y+}\rangle = \frac{1}{\sqrt{2}}(|\alpha_+\rangle + i|\alpha_-\rangle),$$
$$|\alpha_{y-}\rangle = \frac{1}{\sqrt{2}}(|\alpha_+\rangle - i|\alpha_-\rangle), \tag{7.0.14}$$

with respective eigenvalues ± 1. Of course, we can write

$$\hat{\Sigma}_y = |\alpha_{y+}\rangle\langle\alpha_{y+}| - |\alpha_{y-}\rangle\langle\alpha_{y-}| \to i(|\alpha\rangle\langle -\alpha| - |-\alpha\rangle\langle\alpha|). \tag{7.0.15}$$

where the right hand side is the expression in the limit of large α. All of this is isomorphic to the description of a spin one-half particle.

One can extend these considerations to the case of two- and three-mode fields. For example, the set of two-mode entangled states

$$|\Psi_z^{\pm}\rangle = \frac{1}{\sqrt{2}}(|\alpha_+\rangle_1|\beta_-\rangle_2 \pm |\alpha_-\rangle_1|\beta_+\rangle_2)$$
$$|\Phi_z^{\pm}\rangle = \frac{1}{\sqrt{2}}(|\alpha_+\rangle_1|\beta_+\rangle_2 \pm |\alpha_-\rangle_1|\beta_-\rangle_2) \tag{7.0.16}$$

where β is sufficiently large, are entirely analogous to the Bell states [50]. Another Bell type state, recently named quasi-Bell states [51], are those of the form

$$|\Psi_x'^{\pm}\rangle = \frac{1}{\sqrt{2}}(|\alpha\rangle_1|-\beta\rangle_2 \pm |-\alpha\rangle_1|\beta\rangle_2)$$
$$|\Phi_x'^{\pm}\rangle = \frac{1}{\sqrt{2}}(|\alpha\rangle_1|\beta\rangle_2 \pm |-\alpha\rangle_1|-\beta\rangle_2) \tag{7.0.17}$$

where the quantization "direction" is now along the fictitious x axis. The magnitudes of α and β are assumed large. In extending to three modes, one possible state is the GHZ state

$$|\Phi_{\mathrm{GHZ}(z)}\rangle = \frac{1}{\sqrt{2}}(|\alpha_+\rangle_1|\beta_+\rangle_2|\gamma_+\rangle_3 - |\alpha_-\rangle_1|\beta_-\rangle_2|\gamma_-\rangle_3) \tag{7.0.18}$$

which is analogous to the state of Eq. 7.0.1 in that the states involved are eigenstates of the $\hat{\Sigma}_z$ operators for each mode. But one can just as easily deal with a GHZ state constructed out of the $\hat{\Sigma}_x$ eigenstates of the three modes:

$$\left|\Phi_{\mathrm{GHZ}(x)}\right\rangle = \frac{1}{\sqrt{2}}(|\alpha_{x+}\rangle_1|\beta_{x+}\rangle_2|\gamma_{x+}\rangle_3 - |\alpha_{x-}\rangle_1|\beta_{x-}\rangle_2|\gamma_{x-}\rangle_3) \tag{7.0.19}$$

which to a good approximation, for large enough α, β, and γ is equivalent to

$$\left|\Phi_{\mathrm{GHZ}(x)}\right\rangle = \frac{1}{\sqrt{2}}(|\alpha\rangle_1|\beta\rangle_2|\gamma\rangle_3 \pm |-\alpha\rangle_1|-\beta\rangle_2|-\gamma\rangle_3) \tag{7.0.20}$$

More generally, we can write

$$\left|\Phi_{\mathrm{GHZ}(x)}\right\rangle = \mathcal{N}(|\alpha\rangle_1|\beta\rangle_2|\gamma\rangle_3 \pm |-\alpha\rangle_1|-\beta\rangle_2|-\gamma\rangle_3) \tag{7.0.21}$$

where

$$\mathcal{N} = \frac{1}{\sqrt{2}}\left[1 - \exp(-2|\alpha|^2 - 2|\beta|^2 - 2|\gamma|^2)\right]^{-1/2} \tag{7.0.22}$$

is the normalization factor which obviously goes over to $1/\sqrt{2}$ for large enough α, β, and γ. For simplicity, and with no loss of generality, we may take these parameters to be identical so that we have now

$$\left|\Phi_{\mathrm{GHZ}(x)}\right\rangle = \mathcal{N}(|\alpha\rangle_1|\alpha\rangle_2|\alpha\rangle_3 \pm |-\alpha\rangle_1|-\alpha\rangle_2|-\alpha\rangle_3) \tag{7.0.23}$$

where

$$\mathcal{N} = \frac{1}{\sqrt{2}}\left[1 - \exp(-6|\alpha|^2)\right]^{-1/2} \tag{7.0.24}$$

Obviously, for large enough $|\alpha|$, and this need not be very large at all, we have

$$\left|\Phi_{\mathrm{GHZ}(x)}\right\rangle \approx \frac{1}{\sqrt{2}}(|\alpha\rangle_1|\alpha\rangle_2|\alpha\rangle_3 \pm |-\alpha\rangle_1|-\alpha\rangle_2|-\alpha\rangle_3) \tag{7.0.25}$$

Local realistic theories may be tested against quantum mechanics using the state of Eq. 7.0.23 as follows [52]: The state $\left|\Phi_{\mathrm{GHZ}(x)}\right\rangle$ is an eigenstate of the commuting operator products

$$\hat{\Sigma}_z^{(1)}\hat{\Sigma}_y^{(2)}\hat{\Sigma}_y^{(3)},\ \hat{\Sigma}_y^{(1)}\hat{\Sigma}_z^{(2)}\hat{\Sigma}_y^{(3)},\ \hat{\Sigma}_y^{(1)}\hat{\Sigma}_y^{(2)}\hat{\Sigma}_z^{(3)}, \tag{7.0.26}$$

where the superscript refers to the mode label. All have eigenvalue $+1$. In a local realistic theory, all six quantities $\hat{\Sigma}_z^{(1)}$, $\hat{\Sigma}_y^{(2)}$, $\hat{\Sigma}_y^{(3)}$, $\hat{\Sigma}_y^{(1)}$, $\hat{\Sigma}_z^{(2)}$, and $\hat{\Sigma}_z^{(3)}$, have definite values $m_z^{(1)}$, $m_y^{(2)}$, $m_y^{(3)}$, $m_y^{(1)}$, $m_z^{(2)}$, and $m_z^{(3)}$, each being $\pm$, whether measured or not. From this assumption it follows that all the products $m_z^{(1)}m_y^{(2)}m_y^{(3)}$, $m_y^{(1)}m_z^{(2)}m_y^{(3)}$, and $m_y^{(1)}m_y^{(2)}m_z^{(3)}$, are all $+1$. Thus the product

$$\left(m_z^{(1)}m_y^{(2)}m_y^{(3)}\right)\left(m_y^{(1)}m_z^{(2)}m_y^{(3)}\right)\left(m_y^{(1)}m_y^{(2)}m_z^{(3)}\right) = \left(m_z^{(1)}m_z^{(2)}m_z^{(3)}\right)\left(m_y^{(2)}\right)^2\left(m_z^{(2)}\right)^2 = 1 \tag{7.0.27}$$

which implies that $m_z^{(1)}m_z^{(2)}m_z^{(3)} = +1$. However, the product of the corresponding operators leads to

$$\left(\hat{\Sigma}_z^{(1)}\hat{\Sigma}_y^{(2)}\hat{\Sigma}_y^{(3)}\right)\left(\hat{\Sigma}_y^{(1)}\hat{\Sigma}_z^{(2)}\hat{\Sigma}_y^{(3)}\right)\left(\hat{\Sigma}_y^{(1)}\hat{\Sigma}_y^{(2)}\hat{\Sigma}_z^{(3)}\right) = -\left(\hat{\Sigma}_z^{(1)}\hat{\Sigma}_z^{(2)}\hat{\Sigma}_z^{(3)}\right) \tag{7.0.28}$$

where the minus sign arises as the result of an anti-commutation. The operator product $\hat{\Sigma}_z^{(1)}\hat{\Sigma}_z^{(2)}\hat{\Sigma}_z^{(3)}$ on the right hand side of Eq. 7.0.28 commutes with all the operators in Eq. 7.0.26, thus it must have $\left|\Phi_{\mathrm{GHZ}(x)}\right\rangle$ as a common eigenstate. But the eigenvalue, in contradiction to the prediction of a local realistic theory, is -1 instead of $+1$. As the product $\hat{\Sigma}_z^{(1)}\hat{\Sigma}_z^{(2)}\hat{\Sigma}_z^{(3)}$ is equivalent to the product of the parity operators for each mode

$$\hat{\Sigma}_z^{(1)}\hat{\Sigma}_z^{(2)}\hat{\Sigma}_z^{(3)} = \hat{\Pi}_1\hat{\Pi}_2\hat{\Pi}_3, \tag{7.0.29}$$

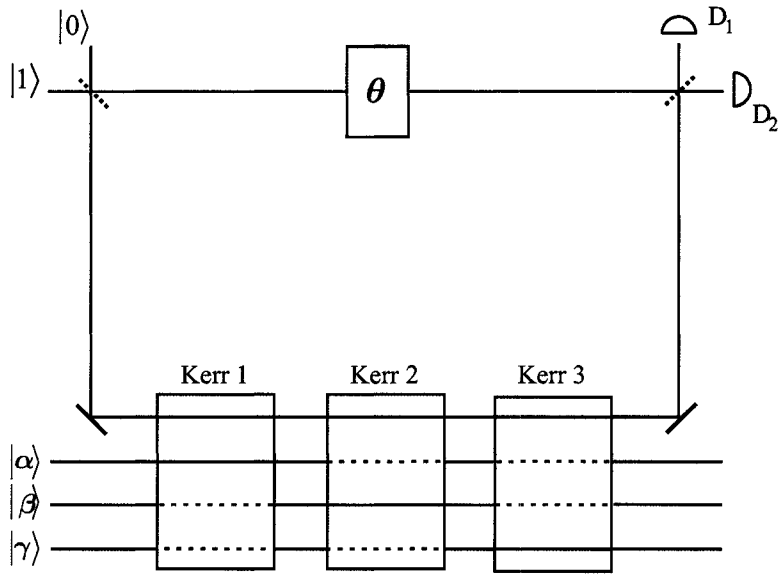

Figure 7.1: Schematic diagram of the device proposed for generating the three-mode GHZ state. All three Kerr media are coupled to the interferometer whereas the external beams initially containing coherent states are coupled to only one Kerr medium each, the dashed lines indicating a bypass of the medium. A single photon state is injected into interferometer and state reductive measurements are performed with the detectors D_1 and D_2 as described in the text.

all one need do is perform parity measurements, at space-like separations, on each of the beams and the product of the measurements, according to quantum mechanics, should be -1 :

$$\hat{\Sigma}_z^{(1)}\hat{\Sigma}_z^{(2)}\hat{\Sigma}_z^{(3)}\left|\Phi_{\mathrm{GHZ}(x)}\right\rangle = -\left|\Phi_{\mathrm{GHZ}(x)}\right\rangle . \tag{7.0.30}$$

Thus it is possible to falsify local realistic theories with a single run of the experiment.

We now describe a method for generating our optical GHZ states. Our proposal is an extension of a proposal previously given for generating optical Schrdinger-cat states [49]. In Fig. 7.1 is pictured the proposed experimental arrangement. The

Mach-Zehnder interferometer (MZI) contains a succession of three Kerr media in one arm. All the Kerr media are couple to the interferometer but each is separately coupled to an external mode initially containing a coherent state. We denote the external modes by the operators $\hat{a}_i, \hat{a}_i^\dagger$, $i = 1, 2, 3$, and the initial coherent states in these modes as $|\alpha\rangle_1$, $|\beta\rangle_2$, and $|\gamma\rangle_3$, respectively. We let $\hat{c}$ represent the clockwise interferometer path. If we let $\hat{d}$ represent the counter-clockwise beam of the MZI, then the mutual cross-Kerr interactions between that mode and each of three Kerr media is represented by the interaction Hamiltonian

$$\hat{H}_{\mathrm{CK}}^i \hbar K \hat{d}^\dagger \hat{d} \hat{a}_i^\dagger \hat{a}_i, \quad i = 1, 2, 3. \tag{7.0.31}$$

The constant K is proportional to a third order nonlinear susceptibility $\chi^{(3)}$. Self-modulation terms have been ignored here as can be justified if the resonances of the Kerr media in an appropriate manner, as discussed by Imoto *et al.* [20] Finally, a single photon is injected into the MZI as indicated in Fig. 7.1. Just after the first beam splitter, assumed to be 50:50, the state of the system is given by

$$|\Psi_0\rangle = \frac{1}{\sqrt{2}}(|1\rangle_c|0\rangle_d + i|0\rangle_c|1\rangle_d)|\alpha\rangle_1|\beta\rangle_2|\gamma\rangle_3. \tag{7.0.32}$$

In the clockwise arm, an adjustable phase shift θ is picked up such that $|1\rangle_c|0\rangle_d \rightarrow e^{i\theta}|0\rangle_c|1\rangle_d$. In the counter clockwise arm, the Kerr interactions, represented by the unitary operators

$$\hat{U}_k^i = \exp\left(-i\varphi_i \hat{d}^\dagger \hat{d} \hat{a}_i^\dagger \hat{a}_i\right), \quad i = 1, 2, 3, \tag{7.0.33}$$

operate successively on each of the coherent states. Because the interactions are not simultaneous, we must add additional phase shifts to account for free evolution that occurs in each mode. We incorporate all these phase shifts in the counter clockwise

arm into the phase factor $e^{i\Phi}$. Thus the state vector just before the second beam splitter is

$$|\Psi_1\rangle = \frac{1}{\sqrt{2}}\left(e^{i\theta}|1\rangle_c|0\rangle_d|\alpha\rangle_1|\beta\rangle_2|\gamma\rangle_3 + ie^{i\Phi}|0\rangle_c|1\rangle_d\left|\alpha e^{-i\varphi_1}\right\rangle_1\left|\beta e^{-i\varphi_2}\right\rangle_2\ \left|\gamma e^{-i\varphi_3}\right\rangle_3\right). \tag{7.0.34}$$

At the second beam splitter, also assumed 50:50, we have the transformations

$$\begin{aligned} |1\rangle_c|0\rangle_d &\to \frac{1}{\sqrt{2}}(|1\rangle_c|0\rangle_d + i|0\rangle_c|1\rangle_d) \\ |0\rangle_c|1\rangle_d &\to \frac{1}{\sqrt{2}}(|0\rangle_c|1\rangle_d + i|1\rangle_c|0\rangle_d) \end{aligned} \tag{7.0.35}$$

and thus the state after the beam splitter is

$$\begin{aligned} |\Psi_2\rangle =& \frac{1}{2}\left[e^{i\theta}(|1\rangle_c|0\rangle_d + i|0\rangle_c|1\rangle_d)|\alpha\rangle_1|\beta\rangle_2|\gamma\rangle_3\right. \\ &\left. + ie^{i\Phi}(|0\rangle_c|1\rangle_d + i|1\rangle_c|0\rangle_d)\left|\alpha e^{-i\varphi_1}\right\rangle_1\left|\beta e^{-i\varphi_2}\right\rangle_2\ \left|\gamma e^{-i\varphi_3}\right\rangle_3\right] \\ =& \frac{1}{2}\left[|1\rangle_c|0\rangle_d\left(e^{i\theta}|\alpha\rangle_1|\beta\rangle_2|\gamma\rangle_3 - e^{i\Phi}\left|\alpha e^{-i\varphi_1}\right\rangle_1\left|\beta e^{-i\varphi_2}\right\rangle_2\ \left|\gamma e^{-i\varphi_3}\right\rangle_3\right)\right. \\ &\left. + i|0\rangle_c|1\rangle_d\left(e^{i\theta}|\alpha\rangle_1|\beta\rangle_2|\gamma\rangle_3 + e^{i\Phi}\left|\alpha e^{-i\varphi_1}\right\rangle_1\left|\beta e^{-i\varphi_2}\right\rangle_2\ \left|\gamma e^{-i\varphi_3}\right\rangle_3\right)\right] \end{aligned} \tag{7.0.36}$$

If the detector D_1 clicks and D_2 does not, then the state $|0\rangle_c|1\rangle_d$ is detected and the fields are projected onto the state

$$|\Psi_{10}\rangle \sim e^{i\theta}|\alpha\rangle_1|\beta\rangle_2|\gamma\rangle_3 - e^{i\Phi}\left|\alpha e^{-i\varphi_1}\right\rangle_1\left|\beta e^{-i\varphi_2}\right\rangle_2\ \left|\gamma e^{-i\varphi_3}\right\rangle_3. \tag{7.0.37}$$

Of course, if only D_2 clicks signaling the detection of the state $|1\rangle_c|0\rangle_d$, the fields are projected into the state

$$|\Psi_{01}\rangle \sim e^{i\theta}|\alpha\rangle_1|\beta\rangle_2|\gamma\rangle_3 + e^{i\Phi}\left|\alpha e^{-i\varphi_1}\right\rangle_1\left|\beta e^{-i\varphi_2}\right\rangle_2\ \left|\gamma e^{-i\varphi_3}\right\rangle_3. \tag{7.0.38}$$

Henceforth we consider only $|\Psi_{10}\rangle$ and we take $\varphi_i = \pi$ $(i = 1, 2, 3)$. We further assume that $\exp(i\theta) = \exp(i\Phi)$ and thus up to an irrelevant overall phase factor we obtain

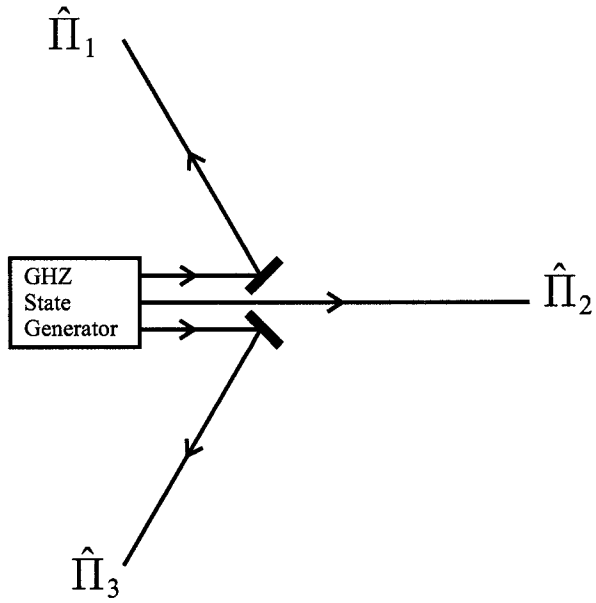

Figure 7.2: Parity measurements are performed on each of the beams. The beams are directed to achieve maximum space-like separation of the of the measurements.

the GHZ state of Eq. 7.0.21 which in the limit of large and equal amplitudes for the coherent states goes over to the state of Eq. 7.0.23.

The crucial element in the generation of our GHZ states is the action of the Kerr media for generating the required phase shifts $\varphi_i = \pi$. Commonly available Kerr media cannot produce phase shifts this large. However, there has been considerable progress of late in the use of the techniques of electromagnetically induced transparency as we have mentioned before.

We assume that the beams can be directed in such a way as to allow space-like separation of the parity measurements to be performed on each of the beams, as pictured in Fig.7.2. But we are then faced with the question of the decoherence of our state vector $\left|\Phi_{\mathrm{GHZ}(x)}\right\rangle$ of Eq. 7.0.23 into a statistical mixture. A simple way to

approach the problem is to assume that each mode of the GHZ state travels through a noisy channel where the losses are due to scattering and that the effect on the mode of interest may be characterized by the "beam splitter" transformation [53, 54]

$$|\alpha\rangle_i|0\rangle_{E,i} \rightarrow |\alpha\sqrt{\eta}\rangle_i \left|\alpha\sqrt{1-\eta}\right\rangle_{E,i}, \tag{7.0.39}$$

where the second state models the state of the environment of that mode and where η is the noise parameter, $0 \leq \eta \leq 1$. Our GHZ state becomes

$$\left|\Psi_{\mathrm{GHZ}(x)}\right\rangle |0\rangle_{E,1}|0\rangle_{E,2}|0\rangle_{E,3} \rightarrow \left|\Psi_{\mathrm{GHZ}(x)+E}\right\rangle \tag{7.0.40}$$

where

$$\left|\Psi_{\mathrm{GHZ}(x)+E}\right\rangle = \mathcal{N}_\alpha(|\beta|\gamma\rangle_{\mathrm{E}} - |-\beta\rangle|-\gamma\rangle_{\mathrm{E}}) \tag{7.0.41}$$

and where we have introduced the shorthand notation $|\beta\rangle \equiv |\beta\rangle_1|\beta\rangle_2|\beta\rangle_3$, $|\gamma\rangle \equiv |\gamma\rangle_{\mathrm{E},1}|\gamma\rangle_{\mathrm{E},2}|\gamma\rangle_{\mathrm{E},3}$, $\beta = \alpha\sqrt{\eta}$ and $\gamma = \alpha\sqrt{1-\eta}$. After tracing over the environmental degrees of freedom, the reduced density operator for the 1,2,3 modes is given by

$$\hat{\rho}_{1,2,3}(\eta) = |\mathcal{N}_\alpha|^2 \left[|\beta\rangle\langle\beta| + |-\beta\rangle\langle-\beta| - e^{-6|\gamma|^2}(|\beta\rangle\langle-\beta| + |-\beta\rangle\langle\beta|)\right]. \tag{7.0.42}$$

Because $|\gamma|^2 = |\alpha|^2(1-\eta)$, the "off diagonal" terms undergo a relatively rapid exponential decay, decreasing more rapidly than the coherent state field amplitudes $\beta = \alpha\sqrt{\eta}$ as η decreases from the value 1. This is the essence of decoherence. A relevant measure of the amount of entanglement that survives such that our state remains useful for a GHZ test of local realism is to take the expectation value of $\hat{\rho}_{1,2,3}$with the amplitude decayed GHZ state given by

$$\left|\Psi_{\mathrm{GHZ}(x)}\right\rangle = \mathcal{N}_\beta[|\beta\rangle - |-\beta\rangle] \tag{7.0.43}$$

to obtain the fidelity

$$F(\eta) = \left\langle \Psi_{\mathrm{GHZ}(x)}(\eta) \right| \hat{\rho}_{1,2,3} \left| \Psi_{\mathrm{GHZ}(x)}(\eta) \right\rangle$$
$$= \frac{\left[2 + 2e^{-12|\alpha|^2\eta} - 4e^{-6|\alpha|^2} - 4e^{-6|\alpha|^2\eta} + 2e^{-6|\alpha|^2(1-\eta)} + 2e^{-6|\alpha|^2(1+\eta)}\right]}{\left(2 - 2e^{-6|\alpha|^2}\right)\left(2 - 2e^{-6|\alpha|^2\eta}\right)} \quad (7.0.44)$$

Note that and, with the help of the L'Hospital rule, $F(\eta \to 0) = 0$. On the other hand, the expectation value of the product of the parity operators taken with the state of Eq. 7.0.41 is easily found to be

$$\left\langle \hat{\Pi}_1 \hat{\Pi}_2 \hat{\Pi}_3 \right\rangle (\eta) = -\frac{e^{-6|\alpha|^2(1-\eta)} - e^{-6|\alpha|^2\eta}}{1 - e^{-6|\alpha|^2}} = -\frac{\sinh\left[3|\alpha|^2(2\eta - 1)\right]}{\sinh\left(3|\alpha|^2\right)} \quad (7.0.45)$$

Note that for $\eta = 1$ the expectation value is -1 as it should be. In the Appendix C, we show that by starting with the usual master equation, identical results are obtain provided we make the identification $\eta = \exp(-\kappa t)$. Thus we can write the above results as functions of time:

$$F(\eta) = \frac{\left[2 + 2e^{-12\bar{N}e^{-\kappa t}} - 4e^{-6\bar{N}} - 4e^{-6\bar{N}e^{-\kappa t}} + 2e^{-6\bar{N}(1-e^{-\kappa t})} + 2e^{-6\bar{N}(1+e^{-\kappa t})}\right]}{\left(2 - 2e^{-6\bar{N}}\right)\left(2 - 2e^{-6\bar{N}e^{-\kappa t}}\right)} \quad (7.0.46)$$

and

$$\left\langle \hat{\Pi}_1 \hat{\Pi}_2 \hat{\Pi}_3 \right\rangle (\eta) = -\frac{e^{-6|\alpha|^2(1-e^{-\kappa t})} - e^{-6\bar{N}e^{-\kappa t}}}{1 - e^{-6\bar{N}}} = -\frac{\sinh\left[3\bar{N}(2e^{-\kappa t} - 1)\right]}{\sinh\left(3\bar{N}\right)} \quad (7.0.47)$$

where $\bar{N} = |\alpha|^2$ is the average photon number of one of the coherent state input beams.

As we are mainly interested in short time evolution for the expectation value of the product of the parity operators, we expand the right hand side of Eq. 7.0.49 to first order in time to obtain

$$\left\langle \hat{\Pi}_1 \hat{\Pi}_2 \hat{\Pi}_3 \right\rangle (\eta) \approx -1 + 6\bar{N}\kappa t \coth(3\bar{N}). \quad (7.0.48)$$

One would like to have

$$6\bar{N}\kappa t \coth(3\bar{N}) \ll 1. \tag{7.0.49}$$

If the distance d of the beam propagation is of the order of a few meters, then we may take $t = d/c \sim 10^{-8}$s, where c is the speed of light. If $\bar{N}$ is large enough such that $\coth(3\bar{N}) \approx 1$ (even for and for $\bar{N} = 0.5$, $\coth(3\bar{N}) = 1.1048$ and for $\bar{N} = 1$, $\coth(3\bar{N}) = 1.1050$) we have the condition on the decay rate that $\kappa \ll 10^8/(6\bar{N})\text{s}^{-1}$. This requirement may not be too stringent as long as $\bar{N}$ is not *too* high. The decay rate κ could be determined by a measurement of the photon number counting statistics for a single mode field prepared in a coherent state $|\alpha\rangle$ which, upon propagation for a time $t = d/c$, becomes the reduced amplitude coherent state $|\alpha e^{-\kappa t/2}\rangle$ having the photon probability distribution $P_n(\bar{N}, t) = \exp(-\bar{N}e^{-\kappa t})\bar{N}^n e^{-n\kappa t}/n!$, where the average photon number is $\langle \hat{a}^\dagger \hat{a} \rangle = \bar{N}e^{-\kappa t}$ and where $\bar{N} = |\alpha|^2$.

In Fig. 7.3 we plot the expectation values of the product of the parity operators and the fidelity as functions of $\bar{N}$ for various values of η close to unity. We note that only for small (mesoscopic) $\bar{N}$ and/or for very small deviations of $\bar{\eta}$ from unity do we find the expectation value of the product of the parity operators remaining close to -1. Of course, the smaller κt the larger (e.g. macroscopic) may be $\bar{N}$. If the experiment is done in such a way that the beams propagate through the vacuum, we would expect essentially no decoherence of the GHZ state and $\bar{N}$ could be arbitrarily large. Note also that the distance d can be made small as the requirement for space-like separation of the parity measurements can always be maintained if the adjacent beams emerge at 120^o as pictured in Fig. 7.2.

In Fig.7.4 we plot, for the case where $\bar{N} = 4$, the expectation value of the product of the parity operators and the fidelity as functions of $1 - \eta$ for the entire range

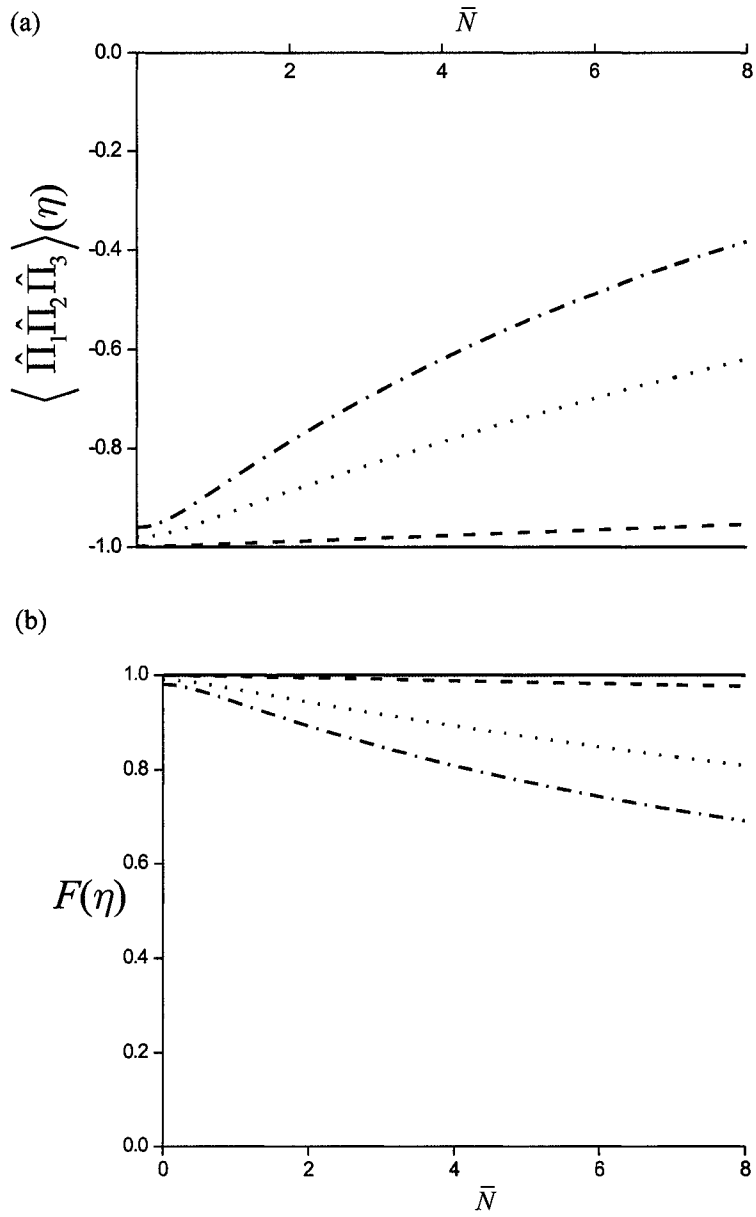

Figure 7.3: (a) Expectation value of the product of the parity operators as a function of $\bar{N}$ for $\eta = 0.999$ (dashed line), $\eta = 0.99$ (dotted line), and $\eta = 0.98$(dot-dashed line). (b) Fidelity versus $\bar{N}$ for the same values of η.

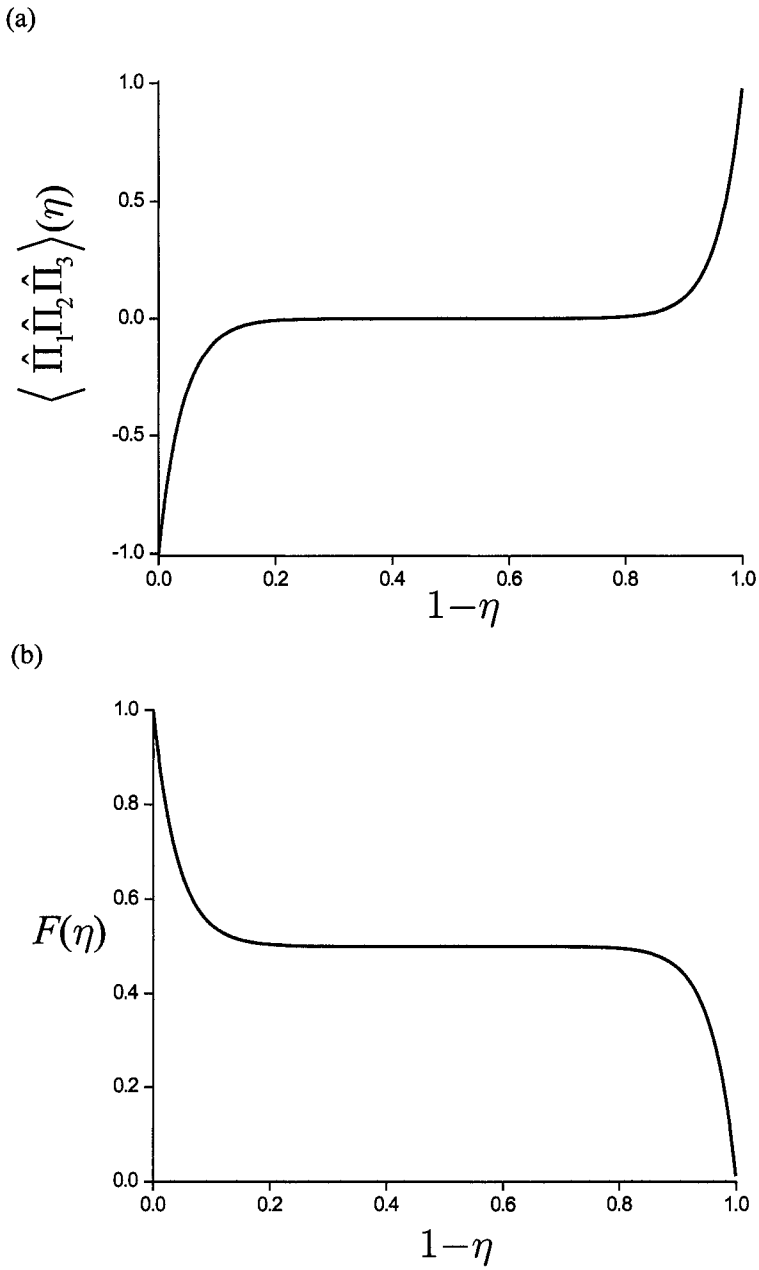

Figure 7.4: For $\bar{N} = 4$ (a) plot of the expectation value of the product of the parity operators and (b) of the fidelity as functions of $1 - \eta$. Note the broad plateau over which the results are those for a mixed state. As $\eta \to 0$ the state becomes a three mode vacuum state $|0\rangle_1|0\rangle_2|0\rangle_3$ for which the expectation value product of the parity operators in unity, and where there is zero overlap of the state of the form of Eq. 7.0.43, that state not containing the vacuum nor any even photon number states.

$\eta : 1 \rightarrow 0$. Note that over much of this range, where the expectation value of the parity vanishes, the photonic state is a statistical mixture, as expected.

In conclusion, we have discussed a method of performing a GHZ test of quantum mechanics against local realistic theories where the GHZ state is a three-mode entanglement of coherent states and where the observables are the parities of the three modes. The coherent field may need to be kept small (mesoscopic) if there is significant decoherence due to scattering but, in principle, can be large (macroscopic) if the experiment can be done in a scattering-free environment, such as in a vacuum system. The main obstacle in performing such a test is the requirement of Kerr media with sufficiently large nonlinearities needed for state preparation. In addition to providing a means of testing local realistic theories, the GHZ state produced in the manner described, could have applications in other areas of quantum information processing, such as quantum secret sharing [55] and dense coding [56].

Chapter 8

Conclusions

In this thesis, we have shown that the parity operator can be used as a relevant observable in order to achieve high resolution phase-shift measurements with sensitivity at the Heisenberg limit, and to test quantum mechanics against local realistic theories. We have shown that interferometry with certain nonclassical states can not be performed using the usual photocounting, subtracting and averaging as in the case of standard quantum-limited interferometry, simply because the difference of the photoncounts is insensitive to the phase difference in the case of these highly quantum mechanical states.

In fact, we have shown that maximally entangled states inside the Mach-Zehnder interferometer yields phase-difference uncertainty at the Heisenberg limit of sensitivity, if parity measurements at one of the output beams of the interferometer are performed. We have extended the same technique to study interferometry with entangled coherent states. We have found that there are some advantages to use entangled coherent states over the use of maximally entangled states of a definite photon number. The advantage is to the difficulties encountered in the construction of the the maximally entangled of definite number states.

Construction of maximally entangled state plays a crucial role in this thesis. Given that linear optical devices and state reduction limit the number of photons that can be placed in maximally entangled states, we have suggested the use of nonlinear optics. In fact we have proposed two schemes, an antisymmetric nonlinear interferometer (ANLI) with a Kerr medium in one arm and the second using nonlinear four-wave mixing. With the ANLI we show how to generate maximally entangled states for any N photon number deterministically, should we have the Fock state with N photons available to inject at one of the inputs. But there is as yet no source for arbitrary N, so we consider coherent state as input states in the ANLI to generate entangled coherent states. In the case of the nonlinear four-wave mixing, we can generate maximally entangled states only for even photon numbers, so we consider even coherent states and squeezed vacuum states.

In another setup, we have used parity measurements to study the uncertainties in optical phase measurements obtained in a Mach-Zehnder interferometer with twin Fock as input states. We found that the phase sensitivity approaches the Heisenberg quantum limit for large N. Our approach is an alternative the method studied by Holland and Burnett, because we noticed that photocounts difference is insensitive to the phase shift.

We have studied two methods of performing parity measurements that include the symmetric nonlinear interferometer (SNLI) and by quantum non-demolition measurements. The SNLI acts as a filter where odd numbers of photons exit in one output port and even numbers of photons exit in the other output port. We have shown that with this method, we do not need detectors of 100% efficiency in contrast to the measurements of parity by determining photon numbers precisely. We also discussed

the quantum non-demolition method of measuring parity and showed that it does not require 100% efficient detectors either. Another advantage of this method is that one can determine the parity of a well defined parity quantum state without destroying it. The only disadvantage is the requirement of large nonlinear media, as is also the case for the SNLI.

We have also studied the parity measurements to test quantum mechanics against local realistic theories using a GHZ state, where the GHZ state is a three-mode entanglement of coherent states. The coherent field may need to be kept small (mesoscopic) if there is significant decoherence due to scattering but, in principle, can be large (macroscopic) if the experiment can be done in a scattering-free environment, such as in a vacuum system. The main obstacle in performing such a test is again the requirement of Kerr media with sufficiently large nonlinearities needed for state preparation. It is worth mentioning that there are some prospects in building such media with the advancements of the electromagnetically induced transparencies.

Appendix A

Beam Splitters

A beam splitter is an essential element of the Mach-Zehnder interferometer, as we have discussed previously. Beam splitters can be treated either classically or quantum mechanically. For our purposes we treat them as quantum mechanical devices. In this Appendix we review transformations associated with two types of the beam splitters, using the Schwinger angular momentum realization. Beam splitters are passive devices that can split beams of light but not photons within the beam. These devices can be constructed to transmit and reflect any desired fraction of the incident flux density [57]. When the intensities of the transmitted and reflected beams are equal, the beam splitter is said to be 50 : 50. There are two types of beam splitters, J_1 and J_2 types for reasons that will be explained shortly. Quantum mechanical beam splitters have two input and two output ports as depicted in Fig. A.1. Boson operators associated with the four ports of the beam splitter obey the usual commutation rule

$$\left[\hat{a}_i, \hat{a}_j^\dagger\right] = \delta_{ij}, \tag{A.0.1}$$

and

$$[\hat{a}_i, \hat{a}_j] = \left[\hat{a}_i^\dagger, \hat{a}_j^\dagger\right] = 0, \tag{A.0.2}$$

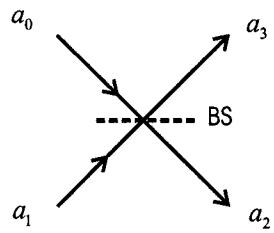

Figure A.1: A descriptive scheme for a quantum mechanical beam splitter.

where $(i, j = 0, 1, 2, 3)$, 0 and 1 refer to the two input ports, and 2 and 3 to the two output ports, as indicated in Fig. A.1. The input and output modes are related according to [58]

$$\begin{pmatrix} \hat{a}_2 \\ \hat{a}_3 \end{pmatrix} = \begin{pmatrix} U_{11} & U_{12} \\ U_{21} & U_{22} \end{pmatrix} \begin{pmatrix} \hat{a}_0 \\ \hat{a}_1 \end{pmatrix}. \tag{A.0.3}$$

The elements of the U matrix must obey the following conditions in order that the Boson commutation relations in equations A.0.1 and A.0.2 to hold:

$$|U_{11}|^2 + |U_{12}|^2 = 1, \tag{A.0.4}$$

$$|U_{21}|^2 + |U_{22}|^2 = 1, \tag{A.0.5}$$

and

$$U_{11}U_{21}^* + U_{12}U_{22}^* = 0. \tag{A.0.6}$$

The most general beam splitter transformation matrix satisfying the previous equations [10] is:

$$U = e^{i\phi_0} \begin{pmatrix} \cos\theta e^{i\phi_\tau} & \sin\theta e^{i\phi_\rho} \\ -\sin\theta e^{-i\phi_\rho} & \cos\theta e^{-i\phi_\tau} \end{pmatrix}, \tag{A.0.7}$$

where θ is related to the transmittance τ of the beam splitter, $\theta = \arccos(\tau^{1/2})$, and ϕ_τ, ϕ_ρ are just the phases related to the transmittance and reflection, respectively,

and ϕ_0 is an overall phase factor. In what follows, we are interested in two cases of the beam splitter transformation matrices

$$\hat{U}_1(\theta) = \begin{pmatrix} \cos(\theta/2) & -i\sin(\theta/2) \\ -i\sin(\theta/2) & \cos(\theta/2) \end{pmatrix}, \tag{A.0.8}$$

and

$$\hat{U}_2(\theta) = \begin{pmatrix} \cos(\theta/2) & -\sin(\theta/2) \\ \sin(\theta/2) & \cos(\theta/2) \end{pmatrix}, \tag{A.0.9}$$

which correspond to $\phi_\tau = \pi/2$ and $\phi_\tau = \pi$, respectively, and with $\phi_\rho = 0$ for both cases. The matrix $\hat{U}_1(\theta)$ describes a beam splitter for which the reflect beam picks a $\pi/2$ phase shift, and $\hat{U}_2(\theta)$ with a π phase shift. In the case of a beam splitter that is 100% reflective we have $\theta = \pi$ so the associating matrix becomes

$$\hat{U}_2(\pi) = \begin{pmatrix} 0 & -1 \\ 1 & 0 \end{pmatrix}. \tag{A.0.10}$$

This matrix transform the input boson operators as follows

$$\hat{U}_2(\pi)\hat{a}_0\hat{U}_2^\dagger(\pi) = -\hat{a}_3 \tag{A.0.11}$$

$$\hat{U}_2(\pi)\hat{a}_1\hat{U}_2^\dagger(\pi) = \hat{a}_2 \tag{A.0.12}$$

from which it follows that

$$\hat{U}_2(\pi)|M\rangle_0|N\rangle_1 = (-1)^M|N\rangle_2|M\rangle_3 \tag{A.0.13}$$

This identity has been used in the derivation of Eq. 3.0.20.

It is convenient to introduce the Schwinger realization [59] of the angular momentum operators in terms of the set of Bose operators. In terms of the a-mode and b-mode operators, the angular momentum operators are

$$\hat{J}_0 = \frac{1}{2}(\hat{a}^\dagger \hat{a} + \hat{b}^\dagger \hat{b}) = \hat{N}/2 \tag{A.0.14}$$

$$\hat{J}_1 = \frac{1}{2}(\hat{a}^\dagger \hat{b} + \hat{a}\hat{b}^\dagger), \tag{A.0.15}$$

$$\hat{J}_2 = \frac{1}{2i}(\hat{a}^\dagger \hat{b} - \hat{a}\hat{b}^\dagger), \tag{A.0.16}$$

$$\hat{J}_3 = \frac{1}{2}(\hat{a}^\dagger \hat{a} - \hat{b}^\dagger \hat{b}), \tag{A.0.17}$$

where $\hat{J}_1$, $\hat{J}_2$, and $\hat{J}_3$ satisfy the su(2) algebra

$$[\hat{J}_i, \hat{J}_j] = i\varepsilon_{ijk}\hat{J}_k, \text{ for } i,j,k = 1,2,3 \tag{A.0.18}$$

and

$$[\hat{J}_0, \hat{J}_i] = 0, \text{ for } i = 1,2,3. \tag{A.0.19}$$

The number states $|M\rangle_a|M\rangle_b$ correspond to the usual angular momentum states $|j,m\rangle$.

$$|M\rangle_a|M'\rangle_b \longrightarrow |j,m\rangle, \tag{A.0.20}$$

where

$$j = \frac{1}{2}(M + M'), \tag{A.0.21}$$

and

$$m = \frac{1}{2}(M - M'). \tag{A.0.22}$$

With these realization the fact that j and m are eigenvalues of $\hat{J}_0$ and $\hat{J}_3$ operators respectively, we can easily derive the following

$$\hat{J}_0|j,m\rangle = j|j,m\rangle \Rightarrow \hat{J}_0|M\rangle_a|M'\rangle_b = \frac{1}{2}(M + M')|M\rangle_a|M'\rangle_b \tag{A.0.23}$$

$$\hat{J}_3|j,m\rangle = m|j,m\rangle \Rightarrow \hat{J}_3|M\rangle_a|M'\rangle_b = \frac{1}{2}(M - M')|M\rangle_a|M'\rangle_b. \tag{A.0.24}$$

The beam splitter matrix transformation $\hat{U}_1$ transforms the angular momentum operators according to

$$\begin{pmatrix} \hat{J}_1 \\ \hat{J}_2 \\ \hat{J}_3 \end{pmatrix}_{\text{out}} = \begin{pmatrix} 1 & 0 & 0 \\ 0 & \cos\theta & -\sin\theta \\ 0 & \sin\theta & \cos\theta \end{pmatrix} \begin{pmatrix} \hat{J}_1 \\ \hat{J}_2 \\ \hat{J}_3 \end{pmatrix}_{\text{in}}, \tag{A.0.25}$$

which also can be expressed as

$$\begin{pmatrix} \hat{J}_1 \\ \hat{J}_2 \\ \hat{J}_3 \end{pmatrix}_{\text{out}} = e^{i\theta\hat{J}_1} \begin{pmatrix} \hat{J}_1 \\ \hat{J}_2 \\ \hat{J}_3 \end{pmatrix} e^{-i\theta\hat{J}_1}. \tag{A.0.26}$$

Beam splitters with this transformation are known as $\hat{J}_1$ type beams splitter. To illustrate how 50:50 beams splitter of type $\hat{J}_1$ transforms the creation operators associated with the input ports into their output counterparts

$$\begin{aligned} \hat{U}_1(\pi/2)\hat{a}_0\hat{U}_1^{\dagger}(\pi/2) &= e^{i\pi\hat{J}_1/2}\hat{a}_0 e^{-i\pi\hat{J}_1/2} = \frac{1}{\sqrt{2}}(\hat{a}_2 + i\hat{a}_3) \\ \hat{U}_1(\pi/2)\hat{a}_0\hat{U}_1^{\dagger}(\pi/2) &= e^{i\pi\hat{J}_1/2}\hat{a}_1 e^{-i\pi\hat{J}_1/2} = \frac{1}{\sqrt{2}}(i\hat{a}_2 + \hat{a}_3). \end{aligned} \tag{A.0.27}$$

As an application of these results, we can easily show how a 50:50 $\hat{J}_1$ type beam splitter transforms Glauber displacement operator. We derive the result as follows:

$$\begin{aligned} e^{i\pi\hat{J}_1/2}\hat{D}_{a_0}(\alpha)e^{-i\pi\hat{J}_1/2} &= e^{i\pi\hat{J}_1/2}e^{\alpha\hat{a}^{\dagger}-\alpha^*\hat{a}}e^{-i\pi\hat{J}_1/2} \\ &= \exp\left[\frac{\alpha}{\sqrt{2}}(\hat{a}_2^{\dagger} - i\hat{a}_3^{\dagger}) - \frac{\alpha^*}{\sqrt{2}}(\hat{a}_2 + i\hat{a}_3)\right] \\ &= \hat{D}_{a_2}\left(\frac{\alpha}{\sqrt{2}}\right)\hat{D}_{a_3}\left(\frac{i\alpha}{\sqrt{2}}\right), \end{aligned} \tag{A.0.28}$$

where we have use Eq. 2.1.5.

On the other hand, the beam splitter matrix transformation $\hat{U}_2$ transforms the

angular momentum operators according to

$$\begin{pmatrix} \hat{J}_1 \\ \hat{J}_2 \\ \hat{J}_3 \end{pmatrix}_{\text{out}} = \begin{pmatrix} \cos\theta & 0 & \sin\theta \\ 0 & 1 & 0 \\ -\sin\theta & 0 & \cos\theta \end{pmatrix} \begin{pmatrix} \hat{J}_1 \\ \hat{J}_2 \\ \hat{J}_3 \end{pmatrix}_{\text{in}}, \tag{A.0.29}$$

which can be expressed as

$$\begin{pmatrix} \hat{J}_1 \\ \hat{J}_2 \\ \hat{J}_3 \end{pmatrix}_{\text{out}} = e^{i\theta\hat{J}_2} \begin{pmatrix} \hat{J}_1 \\ \hat{J}_2 \\ \hat{J}_3 \end{pmatrix} e^{-i\theta\hat{J}_2}. \tag{A.0.30}$$

Beam splitters with the transformation in Eq. A.0.30 are known as $\hat{J}_2$ type beams splitter.

Appendix B

Quantum Phase Formalism

Since the astonishing success of the quantum elecrodynamics, the nature of the quantized field phase operator has been a source of heated discussions. Dirac had tried to define a Hermitian phase operator by decomposing the annihilation operator into an exponential operator where the exponent is the phase operator [60]. He assumed that the latter operator has a canonical counterpart, namely the photon number operator, but his approach failed because this phase operator turned to be not Hermitian. Since then it has been accepted that a well-behaved Hermitian phase operator does not exist. However, many different approaches have been taken. The most well known ones are those taken by Susskind and Glogower [61] and by Pegg and Barnett[62]. Here we follow the approach of Susskind and Glogower to define phase states and then determine phase distributions with these states for any field state of interest [63].

Susskind and Glogower [61] suggested a decomposition of the annihilation operator, $\hat{a}$, into a product of $\sqrt{\hat{n}+1}$ and $\hat{E}$, namely

$$\hat{E} = \frac{1}{\sqrt{\hat{n}+1}}\hat{a}, \tag{B.0.1}$$

where $\hat{E}$ is analogous to $\widehat{e^{i\Phi}}$, and similarly we can write

$$\hat{E}^{\dagger} = \hat{a}^{\dagger}\frac{1}{\sqrt{\hat{n}+1}}. \tag{B.0.2}$$

In the number basis those operators can be expanded as

$$\hat{E} = \sum_{n=0}^{\infty} |n\rangle\langle n+1|, \tag{B.0.3}$$

and

$$\hat{E}^{\dagger} = \sum_{n=0}^{\infty} |n+1\rangle\langle n|. \tag{B.0.4}$$

Some simple, but important, results can be derived from equations B.0.3 and B.0.1:

$$\hat{E}\hat{E}^{\dagger} = 1, \tag{B.0.5}$$

and

$$\hat{E}^{\dagger}\hat{E} = 1 - |0\rangle\langle 0|. \tag{B.0.6}$$

It is clear that $\hat{E}$ is not a unitary operator. Sometimes it is called one sided unitary. The previous two equations can be combined into

$$\left[\hat{E}, \hat{E}^{\dagger}\right] = |0\rangle\langle 0|. \tag{B.0.7}$$

For quantum states $|\Psi\rangle$ for which $\bar{N}$ is large $\left\langle \left[\hat{E}, \hat{E}^{\dagger}\right] \right\rangle = 0$. However, the SG operator has eigenstates of the form

$$|\phi\rangle = \sum_{n=0}^{\infty} e^{-in\phi}|n\rangle. \tag{B.0.8}$$

Notice that the states $|\phi\rangle$ are not normalized. Nevertheless these states resolve the identity in the following fashion

$$\frac{1}{2\pi}\int_{-\pi}^{\pi} d\phi |\phi\rangle\langle\phi| = 1. \tag{B.0.9}$$

For any state $|\psi\rangle$, the phase distribution $\mathcal{P}(\phi)$ is simply the squared absolute value of the overlap of the state $|\psi\rangle$ and the phase eigenstate $|\phi\rangle$

$$\mathcal{P}(\phi) = \frac{1}{2\pi}|\langle\phi|\psi\rangle|^2. \tag{B.0.10}$$

Generalizing the last formalism to more than one mode is straightforward. We overlap the state with two phase eigenstates $|\phi_1\rangle$ and $|\phi_2\rangle$ to get the phase distribution as follows

$$\mathcal{P}(\phi_1, \phi_2) = \frac{1}{(2\pi)^2}|\langle\phi_1|\langle\phi_2|\psi_{a,b}\rangle|^2. \tag{B.0.11}$$

Most of the time we are interested in the probability distribution of the phase difference $\theta = (\phi_2 - \phi_1)/2$. To that end, we introduce another quantity $\theta_s = (\phi_2 + \phi_1)/2$ along which we integrate:

$$\mathcal{D}(\varphi) = \int_0^{2\pi} d\theta \left|\langle(\theta - \theta_s)/2|\,\langle(\theta + \theta_s)/2|\,\psi_{a,b}\rangle\right|^2. \tag{B.0.12}$$

Eq. 2.1.30 is used to determine the phase difference distribution inside the interferometers studied in this work.

Appendix C

Master Equation Approach

In this Appendix we sketch a derivation of the expectation value of the parity operator as a function of time using a master equation approach to the dissipative interactions of the environment.

We consider first a single mode field where the relevant zero temperature master equation is given by

$$\frac{\partial\hat{\rho}}{\partial t} = \frac{1}{2}\kappa\left(2\hat{a}\hat{\rho}\hat{a}^{\dagger} - \hat{a}^{\dagger}\hat{a}\hat{\rho} - \hat{\rho}\hat{a}^{\dagger}\hat{a}\right) \tag{C.0.1}$$

where κ is the mode decay constant. If the initial state of the field is a coherent state such that it is easy to show that the solution at later times is $\hat{\rho}(t) = |\alpha e^{-\kappa t}\rangle\langle\alpha e^{-\kappa t}|$. Thus a coherent state remains a coherent state but one whose energy decays as $e^{-\kappa t}$. To obtain this solution, one can use the iterative form of the general solution in the number basis given by [64]

$$\rho_{mn}(t) = \exp\left(-\frac{\kappa t(m+n)}{2}\right)\sum_{l}^{\infty}\left(\frac{(m+l)!(n+l)!}{m!n!}\right)^{1/2}\frac{(1-\exp(-\kappa t))^{l}}{l!}\rho_{m+l,n+l}(0) \tag{C.0.2}$$

where $\rho_{mn}(t) = \langle m|\hat{\rho}(t)|n\rangle$.

For the case of the three-mode field, the density operator will be determined by the zero temperature master equation

$$\frac{\partial\hat{\rho}}{\partial t} = \frac{1}{2}\kappa\sum_{i=1}^{3}\left(2\hat{a}_i\hat{\rho}\hat{a}_i^{\dagger} - \hat{a}_i^{\dagger}\hat{a}_i\hat{\rho} - \hat{\rho}\hat{a}_i^{\dagger}\hat{a}_i\right) \tag{C.0.3}$$

where we have assumed the same decay rate for each mode. The exact solution can be represented by the iterative form in the three-mode number basis as

$$\begin{aligned}\rho_{nmq,n'm'q'}(t) =& \exp\left[-\frac{\kappa t(m+m'+n+n'+q+q')}{2}\right] \\ & \sum_{l}^{\infty}\sum_{k}^{\infty}\sum_{j}^{\infty}\left[\frac{(n+l)!(n'+l)!(m+k)!(q+j)!(q'+j)!}{m!m'!n!n'!j!j'!}\right]^{1/2} \\ & \frac{(1-\exp(-\kappa t))^{l+k+j}}{l!k!j!}\rho_{n+l,m+k,q+j;n'+l,m'+k,q'+j}(0)\end{aligned} \tag{C.0.4}$$

where

$$\rho_{nmq,n'm'q'}(t) = {}_1\langle n|_2\langle m|_3\langle q|\hat{\rho}(t)|n'\rangle_1|m'\rangle_2|q'\rangle_3.$$

The density operator at time $t = 0$ for the state of Eq. 7.0.23 is given by

$$\begin{aligned}&\rho_{n+l,n'+k,n''+j;m+l,m'+k,m''+j}(0) = |\mathcal{N}|^2 e^{-3|\alpha|^2} \\ &\times \frac{|\alpha|^{2(l+k+j)}\alpha^{n+n'+n''}(\alpha^*)^{m+m'+m''}}{\sqrt{(n+l)!(n'+k)!(n''+j)!(m+l)!(m'+k)!(m''+j)!}} \\ &\times\left[1+(-1)^{n+n'+n''+m+m'+m''} - (-1)^{l+k+j}\left((-1)^{n+n'+n''+(-1)^{m+m'+m''}}\right)\right].\end{aligned} \tag{C.0.5}$$

The iteration yields the density operator matrix elements

$$\begin{aligned}&\rho_{n,n',n'';m,m',m''}(t) = |\mathcal{N}|^2 e^{\frac{\kappa t}{2}(n+n'+n''+m+m'+m'')}e^{-3|\alpha|^2} \\ &\times \frac{|\alpha|^{2(l+k+j)}\alpha^{n+n'+n''}(\alpha^*)^{m+m'+m''}}{} \\ &\left[\left(1+(-1)^{n+n'+n''+m+m'+m''}\right)e^{3|\alpha|^2(1-e^{-\kappa t})} - \left((-1)^{n+n'+n''}+(-1)^{m+m'+m''}\right)e^{3|\alpha|^2(1-e^{-\kappa t})}\right].\end{aligned} \tag{C.0.6}$$

The expectation value of the product of the parity operators is given, after some manipulations, by

$$\left\langle \hat{\Pi}_1 \hat{\Pi}_2 \hat{\Pi}_3 \right\rangle (t) = \mathrm{Tr}_{1,2,3} \left[\hat{\rho}(t) \hat{\Pi}_1 \hat{\Pi}_2 \hat{\Pi}_3 \right] \tag{C.0.7}$$

$$= -\frac{e^{-6|\alpha|^2(1-e^{-\kappa t})} - e^{-6|\alpha|^2 e^{-\kappa t}}}{1 - e^{-6|\alpha|^2}} \tag{C.0.8}$$

in agreement with Eq. 7.0.45.

Bibliography

[1] B. Han, Ph.D. thesis, Hunter College, City University of New York, 1998.

[2] C. M. Caves, Phys. Rev. Lett. **45**, 75 (1981).

[3] D. F. Wall and G. J. Milburn, *Quantum Optics*, first edition ed. (Springer, Springer-Verlag Berlin Heidelberg, 1995).

[4] C. M. Caves, Phys. Rev. D **23**, 1693 (1981).

[5] B. Yurke and D. Stroler, Phys. Rev. Lett. **57**, 13 (1986).

[6] M. Xiao, L.-A. Wu, and H. J. Kimble, Phys. Rev. Lett. **59**, 278 (1987).

[7] P. Kok, H. Lee, and J. P. Dowling, Phys. Rev. A **65**, 052104 (2002).

[8] M. Hillery, M. Zou, and V. Bužek, Quantum Semiclassic. Opt. **8**, 1041 (1996).

[9] J. J. Bollinger, W. M. Itano, D. J. Wineland, and D. J. Heizen, Phy. Rev. A **54**, 4649 (1996).

[10] R. A. Campos, B. E. A. Saleh, and M. C. Teich, Phys. Rev. A **40**, 1371 (1989).

[11] M. Kitagawa and Y. Yamamoto, Phys. Rev. A **34**, 3974 (1986).

[12] M. Shirasaki, H. A. Haus, and D. L. Wong, J. Opt. Soc. Am. B **6**, 82 (1989).

[13] B. C. Sanders, Phys. Rev. A **45**, 6811 (1992).

[14] G. J. Milburn, Phys. Rev. A **33**, 647 (1986).

[15] H. Schmidt and A. Imamoglu, Opt. Lett. **21**, 1936 (1996).

[16] L. Deng, M. G. Payne, and W. R. Garret, Phys. Rev. A **64**, 023807 (2000).

[17] H. Hang and Y.Zhu, Phys. Rev. Lett. **91**, 093601 (2003).

[18] D. A. Braje, V. Balič, G. Y. Yin, and S. E. Harris, Phys. Rev. A **68**, R041801 (2003).

[19] A. N. Chaba, M. J. Collett, and D. F. Walls, Phys. Rev. A **53**, 1499 (1985).

[20] N. Imoto, H. A. Haus, and Y. Yamamoto, Phys. Rev. A **32**, 2287 (1985).

[21] H. A. Haus and F. X. Kärtner, Phys. Rev. A **53**, 3785 (1996).

[22] B. T. H. Varcoe, S. Brattke, M. Weidinger, and H. Walther, Nature(London) **403**, 743 (2000).

[23] D. A. Rice, G. Jaeger, and B. C. Sanders, Phys. Rev. A **62**, 012101 (2000).

[24] J. C. Howell and J. A. Yeazell, Phys. Rev. A **62**, 012102 (2000).

[25] A. Dragan and K. Banszek, Phys. Rev. A **63**, 062102 (2001).

[26] H. Jeong, M. S. Kim, and J. Lee, Phys. Rev. A **64**, 052308 (2001).

[27] X. Wang and B. C. Sanders, Phys. Rev. A **65**, 012303 (2001).

[28] X. Wang, Phys. Rev. A **64**, 022302 (2001).

[29] B. Yurke and D. Stroler, Phys. Rev. A **35**, 4846 (1987).

[30] N. Imoto, H. A. Haus, and Y. Yamamto, Phys. Rev. A **32**, 2287 (1985).

[31] C. C. Gerry, A. Benmoussa, and R. A. Campos, Phys. Rev. **A 66**, 033804 (2002).

[32] C. C. Gerry, Phys. Rev. A **61**, 048311 (2000).

[33] C. C. Gerry, A. Benmoussa, and R. A. Campos, Phys. Rev. A **66**, 013804 (2002).

[34] C. C. Gerry and E. E. Hach III, J. Mod. Opt. **40**, 1053 (1993).

[35] M. J. Holland and B. K, Phys. Rev. Lett. **71**, 1355 (1993).

[36] R. A. Campos, C. C. Gerry, and A. Benmoussa, Phys. Rev. A **68**, 023810 (2003).

[37] C. K. Hong, Z. Y. Ou, and L. Mandel, Phys. Rev. Lett. **59**, 2044 (1987).

[38] Z. Y. Ou, J.-K. Rhee, and L. J. Wang, Phys. Rev. Lett. **83**, 959 (1999).

[39] W. Feller, *An Introduction to Probability Theory and Its Applications* (Wiley, New York, 1968).

[40] F. X. Kärtner and H. A. Haus, Phys. Rev. A **47**, 4585 (1993).

[41] H. A. Haus and F. X. Kärtner, Phys. Rev. A **53**, 3785 (1996).

[42] J. C. Howell and J. A. Yeazell, Phys. Rev. A **62**, 032311 (2000).

[43] W. J. Munro, K. Nemoto, R. G. Beausoleil, and T. P. Spiller, quant-ph/ 0310066 (2004).

[44] B. Huttner, N. Imoto, N. Gisin, and T. Mor, Phys. Rev. A **51**, 1863 (1995).

[45] D. M. Greenberger, M. Horne, and A. Zeilinger, *Bell's Theorem, Quantum Theory, and Conceptions of the Universe* (Kluwer, Dorecht, 1989).

[46] J. S. Bell, Physics (Long Island) City, N.Y. **1**, 195 (1964).

[47] J.-W. Pan, D. Bouwmeester, M. Weinfurter, and A. zeilinger, Nature **103**, 515 (2000).

[48] C. C. Gerry, Phys. Rev. A. **54**, R2529 (1996).

[49] C. C. Gerry, Phys. Rev. A. **59**, 4095 (1999).

[50] M. B. Plenio and V. Vedral, Contemp. Phys. **39**, 431 (1998).

[51] O. Hirota and Sasaki, quant-ph/ 0101018 .

[52] D. Mermin, Physics Today **43**, 9 (1990).

[53] S. J. van Enk and O. Hirota, Phys. Rev. A **64**, 022313 (2001).

[54] S. Glancy, H. M. Vasconcelos, and T. C. Ralph, Phys. Rev. A **70**, 022317 (2004).

[55] M. Hillery, V. Bužel, and A. Berthiaume, Phys. Rev. A **59**, 1829 (1999).

[56] J.-C. Hao, C.-F. Li, and G.-C. Guo, Phys. Rev. A **63**, 054301 (2001).

[57] E. Hecht, *Optics*, third edition ed. (Addison-Wesley, University Press, YEAR), p. 126.

[58] B. Yurke, S. L. McCall, and J. R. Klauder, Phys. Rev. A **33**, 4033 (1986).

[59] J. Schwinger, *Quantum Theory of Angular Momentum* (Academic, New York, 1965).

[60] P. A. M. Dirac, Proc. Roy. Soc. A 243 (1927).

[61] L. Susskind and J. Glogower, Physics **1** 49 (1964).

[62] D. T. Pegg and S. M. Barnett, Phys. Rev. A **39**, 1665 (1989).

[63] G. S. Agarwal, S. Chaturvedi, K. Tara, and V. Srinivasan, Phys. Rev. A **45**, 4904 (1992).

[64] M. Hillery and J. Škvarček, J. Mod. Opt. **45**, 1717 (1998).